# THREE-DIMENSIONAL REGIONALIZATION AND MODELING FOR SEDIMENTARY BASIN ANALYSIS: THE ZENITH OIL FIELD, I

J. Harff, J.C. Davis, R.A. Olea, W.L. Watney,
J.H. Doveton, G.C. Bohling, K.D. Newell, C.D. McElwee,
P. Hoth, B. Lewerenz, J. Springer, R.J. Sampson,
J.C. Wong and K.J. Cunningham

KGS OFR 91-41

Kansas Geological Survey — The University of Kansas
1930 Constant Avenue, Lawrence, KS, 66047, USA
1991

# THREE-DIMENSIONAL REGIONALIZATION AND MODELING FOR SEDIMENTARY BASIN ANALYSIS: THE ZENITH OIL FIELD, I

J. Harff,[1]
J.C. Davis,[2]
R.A. Olea,[2]
W.L. Watney,[3]
J.H. Doveton,[2]
G.C. Bohling,[2]
K.D. Newell,[3]
C.D. McElwee,[2]
P. Hoth,[1]
B. Lewerenz,[1]
J. Springer,[1]
R.J. Sampson,[2]
J.C. Wong,[3]
K.J. Cunningham[3]

[1] Mathematical Geology Department, Central Institute for Physics of the Earth, Potsdam, FRG.

[2] Mathematical Geology Section, Kansas Geological Survey, The University of Kansas, Lawrence, Kansas 66047, USA.

[3] Petroleum Research Section, Kansas Geological Survey, The University of Kansas, Lawrence, Kansas 66047, USA.

Kansas Geological Survey
Open-file Report

*Disclaimer*

The Kansas Geological Survey does not guarantee this document to be free from errors or inaccuracies and disclaims any responsibility or liability for interpretations based on data used in the production of this document or decisions based thereon. This report is intended to make results of research available at the earliest possible date, but is not intended to constitute final or formal publication.

## Table of Contents

# THREE-DIMENSIONAL REGIONALIZATION AND MODELING FOR SEDIMENTARY BASIN ANALYSIS: THE ZENITH OIL FIELD, I

J. Harff,[1] J.C. Davis,[2] R.A. Olea,[2] W.L. Watney,[3]
J.H. Doveton,[2] G.C. Bohling,[2] K.D. Newell,[3] C.D. McElwee,[2]
P. Hoth,[1] B. Lewerenz,[1] J. Springer,[1]
R.J. Sampson,[2] J.C. Wong,[3] K.J. Cunningham[3]

*Two-dimensional regionalization (Harff and Davis, 1990) can be extended to three dimensions by regarding a sedimentary basin fill as a stack of stratigraphically correlated layers, each of which is treated as a two-dimensional unit. The result is a subdivision of three-dimensional space into homogeneous three-dimensional subunits. Petrophysical parameters can be assigned to each homogeneous unit, producing a generalized layered model of the basin fill that can be used for backstripping to reconstruct the geological history of the basin.*

*The same geometric modeling procedures can be applied to stratigraphic entities that are much smaller than a sedimentary basin, such as a petroleum reservoir. The resulting three-dimensional regionalization yields an initial model of reservoir geometry that can be used as input to a reservoir fluid-flow simulator. The model produced by three-dimensional regionalization will conform to the known stratigraphic relationships within the reservoir, and the number and shape of the three-dimensional homogeneous subunits will reflect the available information. Thus, reservoir heterogeneity can be modeled without resorting to speculations about sedimentary genesis and diagenetic or structural evolution. The concept is applied to the Zenith oil field in central Kansas and proves the practical value of the method.*

KEY WORDS: regionalization, sedimentary, basin analysis, three–dimensional modeling, petroleum, reservoir.

[1] Mathematical Geology Department, Central Institute for Physics of the Earth, Potsdam, FRG.

[2] Mathematical Geology Section, Kansas Geological Survey, The University of Kansas, Lawrence, Kansas 66047, USA.

[3] Petroleum Research Section, Kansas Geological Survey, The University of Kansas, Lawrence, Kansas 66047, USA.

## PREFACE

This report presents preliminary results of the first period of collaborative work (scheduled for 1991–1995) between the Mathematical Geology and Petroleum Research Sections of the Kansas Geological Survey, USA, and the Mathematical Geology Department of the Central Institute for Physics of the Earth (Zentral Institut für Physik der Erde—ZIPE), Potsdam, FRG. Research reported here was accomplished during March–September 1991 in Lawrence, Kansas.

Dr. J. Harff served for a half-year as Visiting Research Scientist at the Kansas Geological Survey (KGS), beginning in March 1991. After the collapse of the German Democratic Republic in 1990, ZIPE was granted a continuation by the government of the Federal Republic until the end of 1991. The team was joined in September 1991 for a month by Dr. J. Springer, P. Hoth, and B. Lewerenz. Financial resources for travel by the German team and for living expenses for Springer, Hoth, and Lewerenz were provided by the Federal German Science Foundation.

The research program is a direct continuation of a concept developed at the KGS by Dr. J.C. Davis and Harff during the latter's stay in Lawrence in 1989. This concept, called "regionalized classification" (Harff and Davis, 1990), links the theories of "classification of geological objects" developed in the East (Voronin, 1967; Rodionov, 1981) and "regionalized variables," developed in the West (Matheron, 1962; Journel and Huijbregts, 1978). Regionalization is a statistical procedure for subdividing units of the Earth's crust into spatially homogeneous, distinct subsets according to the general geological concept of discretization of space and time. This concept was described two-dimensionally by Harff and Davis (1990) in a regional case study of western Kansas using data from exploratory wells.

Current work is aimed at generalized application of regionalization to the third spatial dimension and indirectly to the temporal dimension. This extension is demonstrated by a case study of the Zenith oil field in western Kansas. Regionalization provides a three-dimensional generalized model of the field which is displayed on an interactive workstation for reconstruction of the geological history of the field, using basin analysis models, and serves as the starting point for reservoir modeling.

At the end of 1991, ZIPE was replaced by the new organization, GeoForschungsZentrum Potsdam (GFZ). Harff and other members of the mathematical geology team were appointed to the project group "Modeling of Geoprocesses," headed by Harff, and to the "Geothermics" group under direction of former ZIPE director, Dr. E. Hurtig. Cooperation between the KGS and the newly established GFZ continues.

# 1. REGIONALIZATION AND MODELING

**J. Harff, J.C. Davis, and G. Bohling**

Computer simulations of large dynamic earth systems, such as the flow of heat and fluids within sedimentary basins or the movement of masses of liquids through aquifers and petroleum reservoirs traditionally require that three-dimensional space be discretized into regular cells that can be represented as numerical arrays. A series of such arrays are necessary to represent successive increments of time. Resolution becomes a major problem with this approach, because studies must either be restricted to small volumes of space and time, or the dimensions of the simulation must be discretized into very coarse steps. Constraints imposed by the available computer memory restrict simulation studies even when using supercomputers, and are critical when using lesser machines. Ironically, geological simulations usually are based on very limited data, so most of the cells in a simulation are filled with extrapolated values. In a very real sense, most computer simulations of earth systems are severely overdetermined.

Davis, Harff, and Watney (1990) have proposed to simplify the starting point for dynamic modeling by "regionalizing" the models into a relatively small number of homogeneous units, appropriate for the amount of data available. Regionalization is a statistical process that attempts to subdivide a volume of space into regions that are as uniform as possible in their properties, while simultaneously the regions are as contiguous and compact as possible in space. It is then possible to treat each volume as an individual entity, inserting the average value for the properties into each cell. Regionalization is a hierarchical and iterative process; Harff and Davis (1990) have published the statistical background for the process, with a two-dimensional application to basin modeling.

In a dynamic simulation of heat or fluid flow through a basin, aquifer, or petroleum reservoir, deterministic equations are used to model transfers from node to node within a regular three-dimensional array, using conventional finite difference methods. The structure of the array does not conform with the natural configuration of the geologic body, which is determined in the vertical dimension by bedding and in the horizontal dimensions by lithofacies variation, all of which are modified by subsequent structural deformation. We propose that a model be first subdivided into lithostratigraphic units, and the resulting intervals further subdivided by regionalization. After regionalization has been performed, the nodes within an interval can be represented by regional averages, since the regions are homogeneous in their properties. The advantage for geological modeling consists of a data model which reflects the natural variability of input data

and a much smaller number of parameters which must be specified initially. In effect, this new approach will yield model resolutions that are completely appropriate for the complexities of the processes and the number of observations available to provide inputs. It will not be necessary to synthesize inputs in order to satisfy the symmetry requirements of traditional modeling approaches.

### 1.1 The Stochastic Regionalization Model

The regionalization concept presupposes a vertical subdivision of a basin fill into different layers, each of which can be investigated separately. The features of the layers projected on a subsurface datum $R_l$, $l \in \{1, \ldots, L\}$ can be described as a model by a random function

$$X(r) = m(r) + Y(r), \ \forall r \in R_l$$

where $X$ is an $n$-dimensional random variable describing the geological properties; $m(r)$ represents its deterministic and $Y(r)$ its stochastic components. The covariance matrix is

$$\Sigma(r) = E\big[\big(X(r) - m(r)\big)\big(X(r) - m(r)\big)'\big], \ \forall r \in R_l.$$

Each layer is subdivided into homogeneous parts. For each of these, the expected value function $m$ is assumed to be constant, as is the covariance matrix. That is, $m(r) = m_i$ and $\Sigma(r) = \Sigma_i$, $\forall r \in R_{li}$ where $m_i \in M$, $M = \{m_1, \ldots, m_K\}$ and $\Sigma_i \in C$, $C = \{\Sigma_1, \ldots, \Sigma_K\}$, and $R_{li}$ represents the subunits of the projected areas $R_l, l \in \{1, \ldots, L\}$. This means each random field $X(r)$ is stationary within each subregion $R_{li}$.

### 1.2 The Data Model

The basin to be studied is penetrated by $N$ wells, each of which is described by a sequence of data vectors taken from wireline logs. Each data vector describes the properties of the rock intervals as the smallest intervals to be studied. A model for the data from a rock interval $j$ of well $k$ can be given as

$$b'_{kj} := (x, r, \tau)_{kj}, \ k \in \{1, \ldots, N\}, \ j \in \{1, \ldots, N_k\}. \tag{1}$$

Here $x$ stands for an $n$-dimensional vector of measurements, $r$ gives the $x - y$ coordinates of a drill hole and the depth of the center of the rock interval, and $\tau$ is the depth to the top of the interval.

The three-dimensional data model is constructed iteratively by a sequence of procedures:

a) *Typification*

Hierarchical classification procedures are used to place the data $b'_{kj}$ into classes $B_i, i \in I,\ I = \{1, \ldots, K\}$, each of which represents a lithotype occurring within the basin. From the observations, the sets $M^* = \{m_i^*, i \in I\}$ and matrices $S = \{S_i, i \in I\}$ can be determined by standard statistical methods as estimations of the set of expected value vectors $\mathbf{M}$ and the set $\mathbf{C}$ of covariance matrices. For each lithotype,

$$B_i := (m_i^*, S_i) \tag{2}$$

serves as a model.

b) *Zonation*

Zonation begins by subdividing a reference well-log profile. By petrophysical interpretation of the wireline traces, this profile is subdivided into $L$ subunits representing bed sets or beds, in the terminology of sequence-stratigraphy (Van Wagoner *et al.*, 1990). Intervals $j$ that have similar measured values are merged to form seqences $b_{sl} := \{b'_{sj},\ j \in Z_l\}$ with

$$Z_l = \left\{1 + \sum_{a=1}^{l-1} N_{sa}, \ldots, \sum_{a=1}^{l} N_{sa}\right\}$$

where $N_{sa}$ is the number of intervals merged to form a zone $a$ in well $s$

$$\left(\sum_{a=1}^{L} N_{sa} = N_s\right).$$

The data model which describes a zone can be expressed by

$$b_{sl} := \left(\{x_{sj},\ j \in Z_l\}, \{r_{sj},\ j \in Z_l\}, \tau_{sl}\right),\ l \in \{1, \ldots, L\}. \tag{3}$$

The index $s$ marks the reference profile, $x_{sj}$ describes the sequence of measurement vectors assigned to points $r_{sj}$, and $\tau_{sl}$ is the top of the uppermost interval within the sequence. The zonation can be extended to neighboring wells by lithostratigraphic correlation using a process of automated cross-correlation described by Chapter 4.1.1 in this report and by Olea (1988). As a result of correlation, each of the $N$ wells is subdivided into $L$ zones.

An average vector $\bar{x}$ is calculated from the data within each zone in each well and this average

$$\bar{b}_{kl} := (\bar{x}, r, \tau)_{kl},\ k \in \{1, \ldots, N\},\ l \in \{1, \ldots, L\}. \tag{4}$$

serves as a *reduced model* of the characteristics of each zone. Here $r$ indicates the center of the zone and $\tau$ stands for the top of the zone.

c) *Discrimination*

Based on the classification of the original wells, the matrix $\mathbf{B}$ of unstandardized discriminant coefficients and the vector $a$ of associated constants is determined (Fisher, 1936; Tatsuoka, 1971). New variables can be derived from the data model in (4) by the transformation:

$$f(r_{kl}) = \bar{x}(r_{kl})\mathbf{B} + a. \tag{5}$$

For a given classification, mean vectors $C^* = \{c_i^*,\ i \in I\}$ and experimental intraclass covariance matrices $D = \{D_i,\ i \in I\}$ of these variables can be estimated. Using Bayes' formula, the probability of membership in each class within each zone can be calculated:

$$p[\bar{b}_{kl} \in B_i | \bar{x}(r_{kl})] = \frac{p_i' |D_i|^{-1/2} \exp(-\chi_{ikl}^2/2)}{\sum_j p_j' |D_j|^{-1/2} \exp(-\chi_{jkl}^2/2)}, \tag{6}$$

where $p_i'$ denotes the *a priori* probability of membership in class $B_i$ and

$$\chi_{ikl}^2 = \big(f(r_{kl}) - c_i^*\big)' D^{-1} \big(f(r_{kl}) - c_i^*\big). \tag{7}$$

For reasons of simplification, we write

$$p_i(r_{kl}) = p[\bar{b}_{kl} \in B_i | \bar{x}(r_{kl})].$$

A zone is allocated to one of the classes by determining the maximum probability:

$$\bar{b}_{kl} \rightarrow B_i \Leftrightarrow p_i(r_{kl}) = \max_j\ p_j(r_{kl}). \tag{8}$$

By this allocation to a class $B_i$, an experimental mean vector $m_i^*$ is also assigned to $\bar{b}_{kl}$. A *generalized model* can now be given for each of the zones

$$\bar{\bar{b}}_{kl} := (p_1, \ldots, p_K, c, m_c^*, r, \tau)_{kl}, \tag{9}$$

where the character $c$ indicates the class to which $\bar{b}_{kl}$ is allocated, and $r_1 \ldots, r_K$ denote the probabilities of eq. (6).

d) *Interpolation*

For each zone, an elevation grid $R_l'$ is determined $\big(R_l' \subset R,\quad l \in \{1, \ldots, L\}\big)$. The grid nodes are indicated as

$$r_{lst} \in R_l', \quad s \in \{1, \ldots, C\}, \quad t \in \{1, \ldots, T\}.$$

A grid of subsurface elevations for each zone can be determined by interpolation using elevations $\tau_l$ of zone $l$ as measured on well log traces in a neighborhood $J$. Then

$$\tau^*(r_{lst}) = \sum_{j \in J} \lambda_j \tau(r_{jl}) \tag{10}$$

where optimal parameters $\lambda_j$ can be found by kriging (Journel and Huijbregts, 1978) or the inverse distance weighting method (Sampson, 1988) can be used for interpolation. The $\tau^*(r_{lst})$ form vertices of three–dimensional cells or prisms, each defined by vertical faces $F_v$, a top face $F_t$, and a bottom face $F_b$.

The centers of the prisms are given by points $\{r_{lst}\}$, $l \in \{1, \ldots, L\}$, $s \in \{1, \ldots, C-1\}$, $t \in \{1, \ldots, T-1\}$.The Bayesian probabilities of class membership can be estimated at these centers by interpolation:

$$p_i^*(r_{lst}^*) = \sum_{j \in J} \lambda_j p_i(r_{jl}), \tag{11}$$

where $p_i(r_{jl})$ denotes a value for zone $l$ in well $j$, in the vicinity of $r_{lst}^*$.

Using the discrimination based on maximum probability (8), the cell can be classified and a class index $c$ and a mean value $m_c^*$ can be determined. The *generalized model* of the cells is

$$\bar{\bar{b}}_{lst} := (p_i^*, \ldots, p_K^*, c, m_c^*, r, F_v, F_t, F_b)_{lst}. \tag{12}$$

A three-dimensional model which fills the basin can be constructed hierarchically using these cell models. A *layered model* can be developed by combining all cells that share common vertical faces

$$B_l^L = \left\{ \bar{\bar{b}}_{lst},\ s \in \{1, \ldots, C-1\},\ \tau \in \{1, \ldots, T-1\} \right\}. \tag{13}$$

A *generalized layered model* for a basin is given by the sequence of layers

$$B = \left\{ B_l^L,\ l \in \{1, \ldots, L\} \right\}. \tag{14}$$

Facies units that are the desired homogeneous volumes are formed by those cells which belong to the same class and which share a face.

The model describes the present structure and geological properties of the basin fill and is appropriate for modeling of fluid flow within the basin. For modeling the geological history of the basin, both the model structure and the parameters of the model must be regarded as nonstationary and interrelated. The relationship must accord with known physical laws. Initial

conditions and boundary conditions for simulation of geological processes must be determined by backstripping and conceptual geological modeling.

### 1.3 Zenith Field Case Study

Although this introduction has been expressed in terms of modeling a geological basin, the same approach can be applied to any spatially contiguous geological body. In the remainder of this report, the steps in modeling will be demonstrated by an application to a petroleum reservoir, the Zenith field in central Kansas (Figure 1.1 ). This case study was selected because a well-organized set of data exists for the Zenith field, an extensive conventional geological analysis has just been completed, and dynamic simulations of fluid flow are about to be made. This provides the opportunity to compare the geologic model produced by regionalization with a model created by more conventional means.

The Zenith field was discovered in 1937; its original reserves in place have been estimated at 100 million barrels of oil. Production accounts for one-fourth of the original reserves in place, which puts the primary recovery below the 33% global average reported for all oil fields in Kansas. Two attempts to revitalize production through water flooding during the last 25 years have added only 1 million barrels to the cumulative production.

Production in the Zenith field comes from five different reservoirs: the Misener sandstone, Misener limestone (both Upper Devonian–Lower Mississippian), Maquoketa dolomite (Upper Ordovician), and three Viola Limestone reservoirs (Middle Ordovician). Geologists have a clear understanding of correlations and the geology of the Viola, but the stratigraphy of the Misener and Maquoketa is still the subject of debate. Figure 1.2 provides a diagrammatic column of the interval of interest.

Hallwood Petroleum Company (Denver, Colorado), the Kansas Geological Survey (KGS), and the Tertiary Oil Recovery Project of the University of Kansas (TORP) agreed to join efforts to study the possibility for improved recovery in the Zenith field. A final feasibility report was released recently by the Kansas Geological Survey and Tertiary Oil Recovery Project (1991). K. David Newell served as Zenith Field Project Coordinator for the Kansas Geological Survey. The report and in particular its recommendations are currently under evaluation by Hallwood Petroleum Company, operator of the field.

The Kansas Geological Survey, Mathematical Geology Section, and the Central Institute for Physics of the Earth (ZIPE), Potsdam, Germany, have been actively working on the formulation of a methodology for the regional partition of a geologic body into volumes as homogeneous as possible

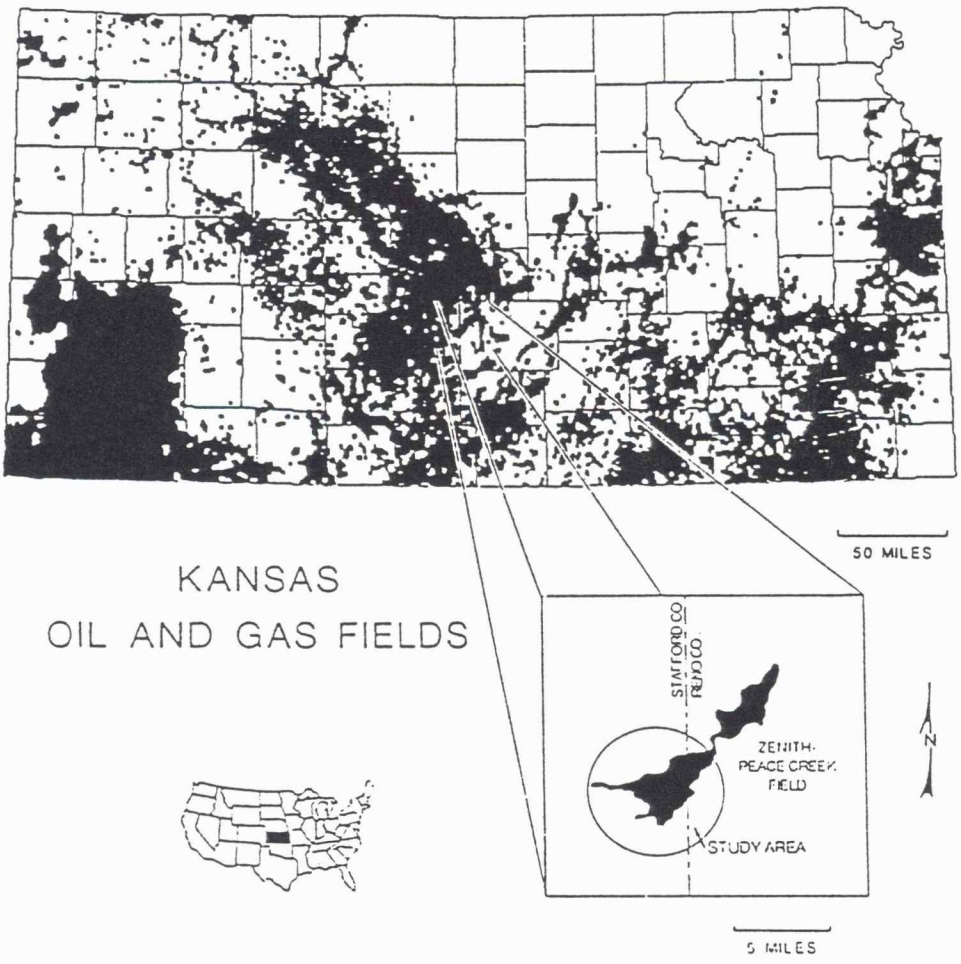


**Figure 1.1.** Location of the Zenith field (from KGS and TORP, 1991).

in terms of mineral resources (Harff and Davis, 1990). The accumulation of information generated by the Zenith field project has made its central Kansas area attractive for a pilot test to further test and refine this classification method and apply the results to the fluid flow modelling. The work was organized in three stages:

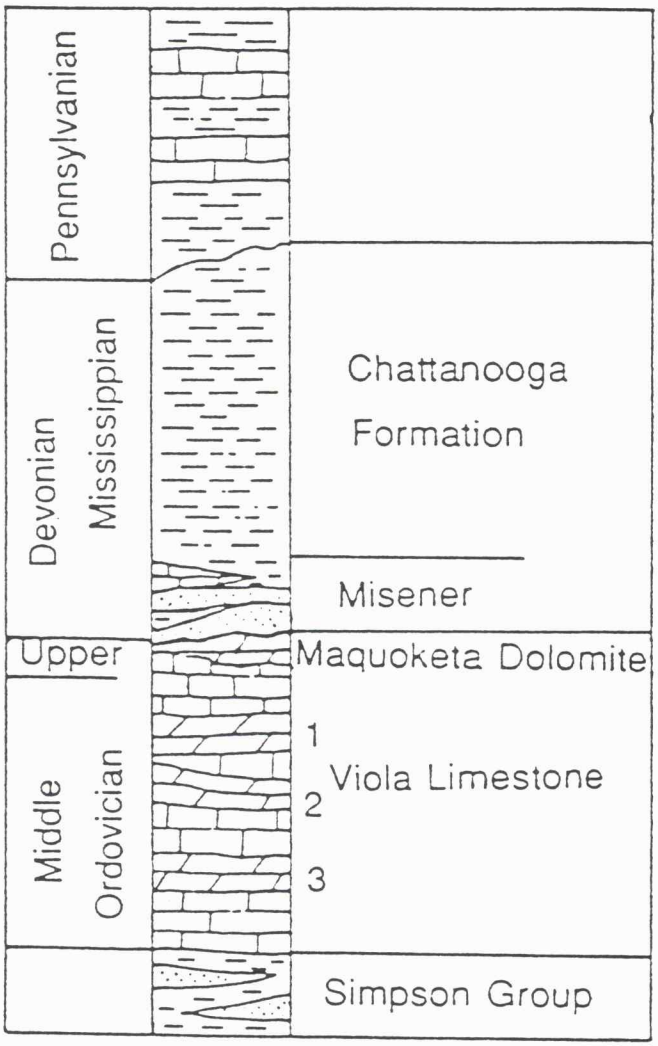


**Figure 1.2.** Generalized stratigraphic column of the interval of interest. (Modified from KGS and TORP, 1991.)

1. The stratigraphy of the reservoir was defined using CORRELATOR to trace all the markers of interest. The result is the breakdown of the

reservoir into quasi-horizontal layers. This report contains the findings obtained with the aid of the CORRELATOR computer software.
2. Regionalization was then used to further subdivide each layer into homogeneous regions.
3. Findings from the correlation and the regionalization will be used as input for a fluid-flow model.

### 1.3.1 Data

The Viola consists on average of 115 ft. of lime mudstone, crinoidal wackestone, and grainstone. The upper 15 to 20 ft. of the Viola generally is a bed of dense, coarsely crystalline wackestone or grainstone locally referred to as the Fernvale. Porosity in the Viola is entirely secondary and includes vuggy, intercrystalline, and minor moldic porosity where fossils are present. Production comes from three different zones: from top to bottom, the Viola 1, Viola 2, and Viola 3. The top two zones have been particularly prolific.

The Maquoketa is present in the north-central part of the field. Limited cuttings and core descriptions indicate that the Maquoketa may be a zone of diagenetic alteration of mudstone or wackestone at the top of the Viola. It has a maximum thickness of 17 ft. in the study area.

The Misener is a widely but erratically distributed unit present on both sides of the Kansas–Oklahoma state line. The Misener is a transgressive basal sandstone of the Chattanooga (Woodford) Shale and was deposited on a shallow shelf (KGS and TORP, 1991). Minor limestone facies are present in the unit. The Misener is less than 30 ft. thick in wells analyzed for this study.

### 1.3.2 Hardware/Software

Steps in the regionalization of the Zenith Field were carried out using the statistical package SPSS$^{TM}$ and the mapping package SURFACE III, both running on a Data General MV20000. The geological visualization package SGM (from Stratamodel, Inc.) running on a Silicon Graphics workstation was used to display the resulting model of the Zenith Field.

"Typification," or definition of classes, was based on a hierarchical cluster analysis of the measurements of the classifying variables (gamma-ray intensity, density, and neutron density) at the wells. Each variable was first standardized to zero mean and unit variance and the cluster analysis was then carried out using the SPSS "cluster" procedure. The Ward method with squared Euclidean distances between observations (in variable space) was used as the distance measure.

The probability of membership of each observation in each identified group or cluster was calculated using the SPSS "discriminant" procedure.

The grouping variable for discriminant analysis was the group membership predicted by cluster analysis. The original (rather than standardized) variables were used for discrimination.

Probabilities of membership in a specific group were interpolated from the well locations to a regular grid covering the study area, producing a map of probability of membership in the specified group. The interpolation was performed using SURFACE III. A scaled inverse distance squared weighting of probabilities at nearby wells was used to estimate the probability at each grid point. The grid points were separated by approximately 0.16 mile in each direction, producing a $28 \times 28$ grid over the study area. Grids were calculated for the probability of membership in each successive group, and the grid points were assigned to the group with the highest probability, producing a map of class membership. This procedure was repeated for each of the 11 stratigraphic intervals in the Zenith field. In addition, SURFACE III was used to produce maps of the structural elevations of the horizons.

The structural horizon maps together with the regions within each stratigraphic interval and the estimated mean porosity and permeability associated with these regions can be considered to form a three-dimensional model of the Zenith field. The SURFACE III grids describing the structural elevations and classification results were transferred to a Silicon Graphics Personal Iris and loaded into the geological visualization package, SGM. In SGM terminology, the grids of structural elevations define "events" and the stratigraphic intervals (each bounded above and below by an event) define "sequences." Each sequence can be divided into a number of layers consisting of grids of three-dimensional cells. Each cell can be assigned a set of attributes, either by interpolation from values at wells or, as in this study, by reading in a grid of attribute values for each layer. (One layer per sequence is used, so each layer in the SGM model corresponds directly to one of the stratigraphic intervals.) SGM can then be used to create a three-dimensional display of the classification results for the entire Zenith field. In addition, SGM "model operations" are used to assign an estimated mean permeability and mean porosity for each class to those cells assigned to that class. The resulting three-dimensional model of reservoir parameters (porosity and permeability) can be used as input to a reservoir simulator. In cooperation with the Chemical and Petroleum Engineering Department of The University of Kansas, experiments will be conducted using this three-dimensional model as input to a dual-porosity fluid-flow simulator.

Many of the steps involved in regionalization are implemented in the program BASIN (Springer, Lewerenz and Harff, 1990), developed at the Central Institute for the Physics of the Earth in Potsdam. BASIN runs on an IBM PC or compatible computer equipped with a VGA color monitor,

hard disk and mouse. BASIN incorporates all functions needed for the regionalization procedure, including cluster analysis (Henrion, Henrion and Henrion, 1988), three methods of regionalization (Harff and Davis, 1990), and two methods of gridding. Grid interpolations by splines are limited to 100 points and to 500 points using the refined inverse distance-weighting method. BASIN also contains routines to perform backstripping for reconstructing paleo-thicknesses or other paleo-values.

Preliminary analyses of subsidence and thermal maturation were performed using the program NL.TTI developed at the Kansas Geological Survey (Woods, Bohling, McElwee, and Newell, 1988) . NL.TTI is a one-dimensional, finite-difference program which solves the set of partial differential equations that describes fluid flow, heat flow, and compaction in a developing sedimentary basin. NL.TTI was developed and runs on the Data General MV20000 computer.

## REFERENCES


Davis, J.C., Harff, J., and Watney, W.L., 1990, Determination of homogeneous components of a sedimentary basin, *in* Pflug, R. and K. Bitzer (eds.), *Three-dimensional Computer Graphics in Modeling Geologic Structures and Simulat ing Geologic Processes:* Freiburger geowiss. Beitr, Band 2, Freiburg, p. 22–24.

Fisher, R.A., 1936, The use of multiple measurements in taxonomic problems: *Annals of Eugenics,* no. 67, p. 179–188.

Harff, J. and Davis, J.C., 1990, Regionalization in geology by multivariate classification: *Mathematical Geology,* vol. 22, no. 5, p. 573–588.

Henrion, G., Henrion, A. and Henrion, R., 1988, *Beispiele zur Datenanalyse mit BASIC-Programmen:* Dt. Verl. d. Wissenschaften, Berlin, 363 pp.

Journel, A.G. and Huijbregts, C.J, 1978, *Mining Geostatistics:* Academic Press, London, 600 pp.

Kansas Geological Survey and Tertiary Oil Recovery Project, 1991, Zenith field—A field demonstration project for improved efficiency for oil and gas recovery in Kansas: *Final Report submitted to the Kansas Corporation Commission,* Topeka, Kansas, 263 pp.

Matheron, G., 1962, *Traité de Géostatistique Appliquée:* Mémoires du Bureau de Recherches Géologiques et Minières, v. 14, Editions Technip, Paris, 333 pp.

Olea, R.A., 1988, CORRELATOR: An interactive computer system for lithostratigraphic correlation of wireline logs: *Petrophysical Series 4*, Kansas Geol. Survey, Lawrence, KS, 85 pp.

Rodionov, D.A., 1981, *Statisticĕskie resĕnija v geologii.:* —Izd. "Nedra", Moskva, 231 pp.

Sampson, R.J., 1988, *A user's guide to SURFACE III:* Interactive Concepts Inc., Lawrence, Kansas, 277 pp.

Springer, J., Lewerenz, B. and Harff, J., 1990, *BASIN—Modeling of Sedimentary Basins: User's Guide:* ZIPE, Potsdam, FRG, 17 pp.

Tatsuoka, M.M., 1971, *Multivariate Analysis: Techniques for Educational and Psychological Research:* John Wiley & Sons Inc., New York, 310 pp.

Van Wagoner, J.C., Mitchem, R.M., Campion, K.M. and Rahmanian, V.D., 1990, *Siliciclastic Sequence Stratigraphy in Well Logs, Cores, and Outcrops: Concepts for High-Resolution Correlation of Time and Facies:* Am. Assoc. Petrolem Geologists, Methods in Exploration Series No. 7, 55 pp.

Voronin, Ju. A., 1967, *Geologija i matematika:* —Izd. "Nauka", Novosibirsk, 253 pp.

Woods, J.J., Bohling, G.C., McElwee, C.D., and Newell, K.D., 1988, Thermal basin modeling and analysis using the time–temperature index—An improved general basin model incorporating compaction, fluid flow and heat flow: *Kansas Geological Survey Open-file Report 88–28*, 153 pp.

## 2. GEOLOGY OF THE ZENITH FIELD

K.D. Newell and W.L. Watney

The Zenith oil field occurs in a stratigraphic trap developed on a broad anticline plunging to the south–southwest off the Central Kansas uplift. This field was discovered in 1937 and now covers approximately 10,500 acres. Five main pay zones are present in the field. Two zones of cherty porous dolomite in the Middle Ordovician Viola Limestone (upper and lower Viola reservoirs, also referred to as the Viola 1 and Viola 2, respectively) are the most laterally extensive reservoirs in the pool. A minor pay zone, the upper Ordovician Maquoketa dolomite, locally overlies the Viola Limestone. The Devonian/Mississippian Misener sandstone and a superjacent carbonate–chert reservoir rock, the Misener limestone, overlie the Ordovician carbonate reservoirs and are in direct contact with the Maquoketa dolomite in some places.

Zenith field produced over 23 million barrels of 40°API gravity oil by primary production through 1966. A waterflood implemented in 1966 added another one-half million barrels of oil. In 1983, another waterflood was implemented, but again only one-half million barrels of oil were produced. The field was initially developed on 10- to 20-acre spacings and approximately 350 wells have had some production history.

Zenith field is a truncation-type stratigraphic trap in which Lower Paleozoic sandstone and carbonate reservoirs dip southward and pinch out unconformably in the north beneath impermeable shales and conglomerates at the base of the Pennsylvanian System (Imbt, 1941; Paddleford, 1941). To the east, the reservoirs terminate against the downthrown side of a near-vertical fault along the north-northeast trending Peace Creek fault system. The oil accumulation is limited on the west either by stratigraphic pinchout or decreasing porosity in the reservoir units.

The northern part of the field is dominated by a narrow, east–southeast plunging anticline approximately 1/2 mile wide. Local culminations at Viola and other levels are present on this anticline. The southern part of the field is dominated by a homocline with minor anticlinal noses. The general rate of dip of the homocline is about 65 ft. per mile, or less than 1 degree.

Most of the present-day structure of the field was formed prior to Early Pennsylvanian time but subsequent to Late Devonian to Early Mississippian time, when the Chattanooga Shale and its associated Misener members were deposited. Its formation probably relates to an episode of structural deformation that affected the entire southern Midcontinent region in Late Mississippian to Early Pennsylvanian time (Merriam, 1963). The basal Pennsylvanian unconformity that truncates the Chattanooga Shale is also

folded, so some structural deformation also occurred during or shortly after deposition of Middle Pennsylvanian strata.

Published reports on the Zenith field (Imbt, 1941; Paddleford, 1941) note that all reservoirs in the field have a common oil/water contact (−2019 ft. subsea), indicating they are in hydraulic continuity. Stratigraphic correlations (Kansas Geological Survey and Tertiary Oil Recovery Project, 1991) suggest that fluids can be transferred circuitously between reservoirs because of their stratigraphic juxtaposition. Fractures may also facilitate more direct transfer of fluids vertically through several reservoirs. Some vertical fractures are reported in core descriptions, but the severity of fracturing is difficult to determine. Similarly, the possible volume of fluid movement through old well bores is difficult to determine from available data.

## 2.1 Stratigraphic Intervals

**Viola Limestone**—The Viola Limestone averages 115 ft. in thickness in areas where the unit is complete and not eroded. It is a very coarsely crystalline, white, pink or light gray limestone and finely crystalline, gray, cherty to non-cherty dolomite. Chert, commonly fractured, is present as lenticular bodies or thin beds approximately 2 to 3 in. thick (Imbt, 1941).

The upper 15–20 ft. of the Viola generally consists of a bed of dense, coarsely crystalline, white, pink or gray lime wackestone or grainstone. This bed is referred to locally as the "Fernvale member." Conformably below this bed is the upper Viola (Viola 1) reservoir. Most completions in the Zenith field are in this interval and most production comes from the Viola 1 reservoir. Both the Viola 1 and Viola 2 reservoirs consist of intervals of cherty dolomitized mudstone. The porosity in these reservoirs is secondary and includes vuggy, intercrystalline, and minor moldic porosity where fossils are present.

The thicknesses of the Viola 1 and Viola 2 pay zones are very consistent throughout the field, ranging from 11 to 26 ft. in the Viola 1 and 13 to 23 ft. in the Viola 2. Forty-two determinations of porosities from logs in the Viola 1 average 10.8%; 28 determinations in the Viola 2 average 10.6%.

The nonporous interval between the two Viola reservoirs averages 15 ft. in thickness and is composed of tightly cemented interbedded crinoidal packstones and grainstones. The grainstones and packstones contained abundant intergranular porosity at the time of their deposition. However, these pores were later cemented with calcite spar. The nonporous limestone between the two Viola reservoirs thins to the west and pinches out in the western part of the field. Farther west of the pinchout, the porous Viola 1 and Viola 2 are in contact and fluid is presumed to flow between them.

The Viola was deposited on a broad, low-relief marine shelf. The alternating succession of porous dolomitic mudstone and non-porous crinoidal grainstones is believed to result from oscillations in sea level. The pinchout of the grainstone between the Viola 1 and 2 probably represents the western lapout of the grainstone along a shoreline and reflects the interplay of a still-stand in sea level and the gently, easterly dipping shelf that extended across the area of the Zenith field. This evidence for a higher elevation along the western side of the field during Viola deposition is consistent with continued positive relief that affected deposition of the overlying Misener interval.

A 20-foot-thick nonporous lime grainstone occurs at the base of the Viola. Above this interval is a porous zone that extends to the base of the more porous Viola 2 reservoir. This zone, which averages about 50 ft. in thickness, is referred to as the Viola 3. Little is known about this unit except that cuttings from the interval appear chalky. It does not seem to be a reservoir rock and most of the interval lies below the oil–water contact.

**Maquoketa dolomite**—The Ordovician Maquoketa dolomite is a thin interval of dolomitic limestone and dolomite that overlies the "Fernvale." This unit changes erratically in thickness because of erosion at the base of the overlying Lower Mississippian–Upper Devonian Misener members. The lack of conformity with either the Viola below or the Misener above suggests the Maquoketa may also be a zone of diagenetic alteration at the top of the Viola.

The Maquoketa dolomite occupies two separate, irregular areas. The larger occurs in the west-central part of the Zenith field and has a thickness of up to 17 ft. A smaller area of Maquoketa is located in the southeastern corner of the Zenith field. Limited cuttings and core descriptions indicate that the Maquoketa dolomite is similar to dolomites of the Viola reservoirs and is a porous zone developed in dolomitized mudstone or wackestone. It is also described as being extremely vuggy (Imbt, 1941).

The Maquoketa is in contact with the Viola 1 reservoir in the northwestern part of the field. Average porosity in the Maquoketa dolomite, based on 16 determinations from well logs, is 8.3%.

**Chattanooga (Kinderhook) formation**—Light gray shale of the Mississippian/Devonian Chattanooga formation was distributed over much of the North American Midcontinent, including Kansas. The Chattanooga decreases in thickness northwestward in the Zenith field because of erosion at the basal Pennsylvanian unconformity. This unit forms an excellent seal for the underlying reservoir rocks.

**The Misener interval**—The Misener interval lies at the base of the Chattanooga formation and consists of three members—a lower sandstone, a limestone, and an upper sandstone. The upper sandstone member is thin, relatively nonporous, very limited in areal extent, and is not considered a significant reservoir. Overall distribution of the Misener sandstone in central Kansas suggests that it was deposited at several strandline or parallic positions on a shallow marine shelf along the McPherson embayment (Lee, 1956) to the east as sea level rose (Newell, 1989). Sand was probably derived from the ancestral Central Kansas uplift to the north where older Middle Ordovician Simpson sandstones were being eroded. Continued inundation led to deposition of the deeper water Chattanooga shales. The limestone and upper sandstone members of the Misener probably represent still-stands or minor reversals in sea level.

*Lower Misener sandstone*—The lower Misener sandstone is a major reservoir unit over the eastern half of the field. The sandstone is elongate and trends north–northeast. It is thicker in the southern half of the field where it reaches a maximum thickness of 32 ft. Areas of local thickening of the sandstone also occur on the western side of the field. These are connected to the main body of the sandstone and form semi-parallel lobes that have a dominant northeastern trend. The orientation and geometry of these lobes suggest transportation of sand to the south–southeast by currents or waves.

The lower Misener sandstone is characteristically a medium- to coarse-grained quartz arenite with a development of local conglomerate at or near its base. Near the base the sandstone is usually better sorted and grains are more rounded. The conglomerate consists of subrounded quartz, chert pebbles, and lithic fragments. These pebbles are also scattered throughout the lower 10 ft. of the sandstone. Marine depositional conditions are indicated by thin planar cross-laminations, abundant burrowing, and presence of fossils such as crinoid stems both within the sandstone and in very thin limestone beds that are interstratified with the sandstone. Irregular discontinuous clay laminations are common. The intergranular porosity that dominates this unit is partially occluded by quartz overgrowths on individual sand grains and by minor amounts of interstitial clay. The average porosity for the entire lower Misener sandstone is 10.9%, based on 36 determinations.

The lower Misener sandstone can be divided into three distinct beds—a lower sandstone bed, a shaly middle interval, and an upper sandstone bed. The basal bed of the lower Misener sandstone ranges in thickness from 2–5 ft. on the eastern side of Zenith field. This sandstone locally contains weathered chert that is similar to the chert found in the Viola formation.

The lower bed of the lower Misener sandstone has been a prolific producing interval (Imbt, 1941), and has an average porosity ranging from 12 to 15%.

Scattered phosphatized (apatite) bioclasts and pebbles occur in the basal sandstone (P. Hoth, personal comm., 1991). The phosphate may cause the high levels of gamma radiation detected by gamma ray logs because of the presence of uranium in this mineral. This may lead to erroneous estimates of porosity if gamma ray logs are used to estimate the shale content of the sandstone because the presence of uranium would decrease the apparent porosity of the sandstone.

The lower sandstone bed of the lower Misener sandstone is better sorted and coarser grained than the upper sandstone bed, suggesting higher wave and current energy levels in the shallow, transgressing sea as it covered the shelf. Conglomeratic cherts found in the eastern part of the field may represent a locally derived residual deposit formed of pebbles that were too coarse to be transported. The chert probably is a residuum from the dissolution of the Viola Limestone during emergence at the time of erosion at the base of the Chattanooga.

The upper sandstone bed of the lower Misener sandstone is a lower quality reservoir than the basal sandstone because of its greater shale content and lower permeability. Nevertheless, wells perforated in this interval have reported long-lived production. The upper sandstone bed of the lower Misener sandstone may represents a still-stand deposit formed after the sea deepened and transgressed farther to the west. The Misener limestone in the western half of the field may correlate in part with the upper bed of the lower Misener sandstone, and was deposited with further inundation of the platform.

*Misener limestone*—The Misener limestone overlies the lower Misener sandstone in the central portion of the field. In the western part of the field it generally overlies Chattanooga Shale but locally rests on Maquoketa dolomite or the Viola, making the distinction between the Misener limestone and Viola difficult (Imbt, 1941). The pattern of thickness variation in the Misener limestone is similar to that of the lower Misener sandstone with dominant north–northeast trends. However, the main development of the Misener limestone is offset to the west from the thickest part of the lower Misener sandstone. Maximum thickness is over 40 ft. in the southwestern part of the field with general thinning north–northeastward. Porosity in the Misener limestone, based on 25 determinations, averages 11.3%.

The lithology of the Misener limestone is variable, containing carbonates, cherts, and rarely shale. Calling the unit a "limestone" is somewhat misleading. It is an important producing interval in the western portion of the Zenith field. The chert varies from dense to weathered porcelainic or

tripolitic material with good but very fine porosity. The tripolitic chert, accompanied by porous limestone, forms an excellent reservoir rock (Imbt, 1941). On the western side of the field, cherts are most abundant and may even constitute 100% of this producing unit. Because these cherts are generally very porous, good porosity is evident in the western flank of the Misener limestone reservoir. The porosity is lower in the Misener limestone member in the eastern portion of the reservoir where limestone is the dominant lithology.

*Misener chert*—Two types of chert occur within the Misener limestone, a porous chert and a non-porous porcelaneous chert. Porous chert generally replaces bioclastic-, pelletal- and sponge spicule-bearing lime grainstones and less commonly replaces bioclastic mudstones, wackestones and packstones. Porosity is interparticle, moldic, and intercrystalline. Porous chert commonly occurs as thin rinds around porcelaneous chert nodules and laminations, suggesting that some porous chert is a product of alteration of porcelaneous chert.

Chert replacement of limestone allochems may not be complete because in some areas bioclastic debris such as echinoids escaped replacement. In areas of partial replacement, siliceous rims of chert commonly surround allochems and may be a replacement of isopachous cement or micritic envelopes. The degree of silicification ranges from complete to partial replacement of all original carbonate.

The depositional environment of the limestone that most of the cherts replace is interpreted as restricted intertidal to supratidal. This interpretation is based on the abundance of fine-grained pelleted sediment, restricted fauna, light color of the sediment (which indicates oxidizing conditions during deposition), fenestral fabric, mudcracks, burrows indicating occasional submergence, and autobrecciation. It is possible that the autobreccia is related to dissolution of preexisting evaporites or karstification associated with subaerial exposure. In some cores a few thin lime grainstones and lime packstones containing echinoids and fossil fragments are present in the lower part of the Misener limestone. These suggest a shallowing-upward depositional sequence from normal marine to restricted intertidal and supratidal environments.

Limestones present in the Misener limestone on the eastern side of the reservoir are mostly nonporous and commonly are mixed with porous and porcelaneous chert. They are gray lime grainstones and packstones, and occasional wackestones. Small-scale cross-laminations are common. Echinoids are the dominant allochem but bryozoans, bivalves, ostracods, pellets, and intraclasts also are present. The diversity of marine fauna and the presence of small-scale cross-laminations indicate deposition in subtidal

open-marine conditions. Porosity is very low and there is less replacement by chert in localities farther west.

## REFERENCES


Imbt, W.C., 1941, Zenith pool, Stafford County, Kansas—An example of stratigraphic trap accumulation, *in* Levorsen, A.I. (ed.), *Stratigraphic Type Oil Fields:* Am. Assoc. Petroleum Geologists, Tulsa, Oklahoma, p. 139–165.

Kansas Geological Survey and Tertiary Oil Recovery Project, 1991, Zenith field—A field demonstration project for improved efficiency for oil and gas recovery in Kansas: *Final Report submitted to the Kansas Corporation Commission*, Topeka, Kansas, 263 pp.

Lee, W., 1956, Stratigraphy and structural development of the Salina basin area: *Kansas Geological Survey Bulletin 121*, 167 pp.

Merriam, D.F., 1963, The geologic history of Kansas: *Kansas Geological Survey Bulletin 162*, 317 pp.

Newell, K.D., 1989, Distribution of Upper Devonian–Lower Mississippian Misener sandstone in Salina basin: *Kansas Geological Survey, Open-File Report 89–18*, (1:1,000,000 scale map, with discussion).

Paddleford, J.T., 1941, The Zenith pool of Stafford and Reno counties, Kansas: *Mines Magazine*, v. 31, p. 445–448, 454, 470, 472.

# 3. LITHOSTRATIGRAPHIC AND MINERALOGICAL DETERMINATIONS

**J. Harff, R.A. Olea, K.D. Newell, P. Hoth and K.J. Cunningham**

Data for the Zenith field study were derived from different sources. Well-log measurements, including gamma-ray ($I_{GR}$), porosity ($PORW$), corrected neutron-porosity ($\Phi_{Ncorr}$), density-porosity ($\Phi_{Dcorr}$) and $V_{Shale}$ for the Misener and Viola reservoirs in 40 wells were provided by K. D. Newell. Data were recorded every 2 ft. in each well profile. These data were used for typification of lithologies and for discrimination.

Zonation was performed on wireline logs of 38 wells digitized by R.A. Olea and J. Harff. The $I_{GR}$-curve and the $\Phi_{Ncorr}$-log were recorded every 0.5 foot. Relationships between permeability, porosity, and wireline log properties were based on core-sample analyses provided by K.D. Newell from three wells: Braden–Zenith ZU 1, Braden–Zenith 2W2, and Braden–Zenith ZU 3. Thickness data for the stratigraphic sequence from the overburden of the Zenith field were interpreted from wireline correlation by P. Hoth, under the supervision of W.L. Watney. Petrographic and mineralogical data for the assessment of diagenetic processes were provided by K.D. Newell and K.J. Cunningham. Hoth and Cunningham conducted additional petrographic investigation on the high gamma-ray intensity portion of the Misener sandstone and limestone.

## 3.1 Diagenetic Processes

### 3.1.1 Petrographic Investigation of Misener Interval

Petrographic investigations of the Misener interval within the Zenith oil field focused on two questions:

1) What kinds of clay minerals exist within the Misener interval?
2) What mineralogical characteristics cause the relatively high gamma-ray measurements detected by wireline logs in some sandstones?

Both questions are important for a complete reservoir description of the Misener interval. Because of the relatively brief time available for the investigation, the initial step of the petrographic investigation used X-ray diffraction and SEM techniques.

Cores from four wells in the Zenith field were used—the Braden–Zenith No. 1 (BZ1), Braden–Zenith ZU 3 (ZU3), Glenn McComb No. 5 (McC5) and the Stewart No. 6 (St6). Table 3.1 gives the locations and general descriptions of the samples.

**Table 3.1.** Sample Locations and Core Descriptions, Misener Interval

| Sample | Box (Depth) | Location | Sample Description | Analysis |
|---|---|---|---|---|
| BZ 1/1 | 820 (3774–3783) | 23 in. from top | green "clays" in vugs of Misener Ls. | whole rock XRD, SEM |
| BZ 1/2a | 820 | 57 in. from top | green "clays" with brown cover (oil) | SEM |
| BZ 1/2b | 820 | 55 in. from top | green "clays" from large cavity | whole rock XRD, SEM |
| BZ 1/2c | 820 | 58 in. from top | brown minerals filling cavity | whole rock XRD |
| ZU 3/1a | 353 (3706–3711) | 47 in. from top | succession of cemented and extremely porous sandstones | SEM |
| ZU 3/1 | 354 (3711–3713) | top | sandstone, extremely porous, oil staining | whole rock XRD, SEM |
| ZU 3/2 | 354 | 5 in. from top | sandstone, cemented | whole rock XRD,SEM |
| ZU 3/3 | 816 (3713–3719) | 20 in. from top | shaly limestone thin bedded | |
| ST 6/1 | (3720–3729) | 10 in. from top | siltstone | whole rock XRD, SEM |
| ST 6/2 | (3720–3729) | 35 in. from top | green "clay"-rich layer within sandstone | whole rock XRD, SEM |

(*Cont.*)

**Table 3.1** (*Cont.*). Sample Locations and Core Descriptions of Misener

| Sample | Box (Depth) | Location | Sample Description | Analysis |
|---|---|---|---|---|
| McC 5/1 | 719 (3797–3802) | 5 in. from top | siltstone | whole rock XRD |
| McC 5/2a<br>McC 5/2b | 719<br>719 | 1 in. below 3797 ft. | minerali-zations | XRD, SEM |
| McC 5/3 | 719 | 23 in. from top | concentra-tion of green "clays" within bedding plane of sandstone | XRD |
| McC 5/4 | 719 | 22 in. from top | green "clay" infiltration in sandstone | SEM |
| McC 5/5 | 719 | | dark pebbles and grains very common in sandstones | XRD of concentrate of black pebbles |

Preliminary results indicate that the green material that fills vugs and cavities of Misener carbonates and cherts in well BZ 1 consists mainly of clay minerals and fine quartz (see Figs. 3.1 and 3.5). Sedimented slides, obtained by a settling technique in cylinders, were used for clay mineral analysis. Figures 3.2 and 3.6 show the results of normal preparation by air drying; illite and chlorite are clearly detectable. The illite has a small shoulder on the low-angle side, but there is no significant difference between XRD curves for air-dried or glycolated samples (Figs. 3.3 and 3.7). The width of the 001 illite peak at half-height shows little variation after glycolization. In addition to sharpening the 001 peak, a small shift of the 001 peak is detectable after heating (Fig. 3.4). These signs indicate that the illite is slightly weathered. Since no hint of authigenesis could be detected by SEM investigation, slightly weathered detrital illite is suggested.

Detected chlorite peaks disappear after heating (Fig. 3.4), suggesting that the chlorite is either very poorly crystallized or iron-rich (see Thorez, 1976). Initial results suggest iron-rich chlorite, but further investigations should be conducted to assess kaolinite content. The swelling capability of

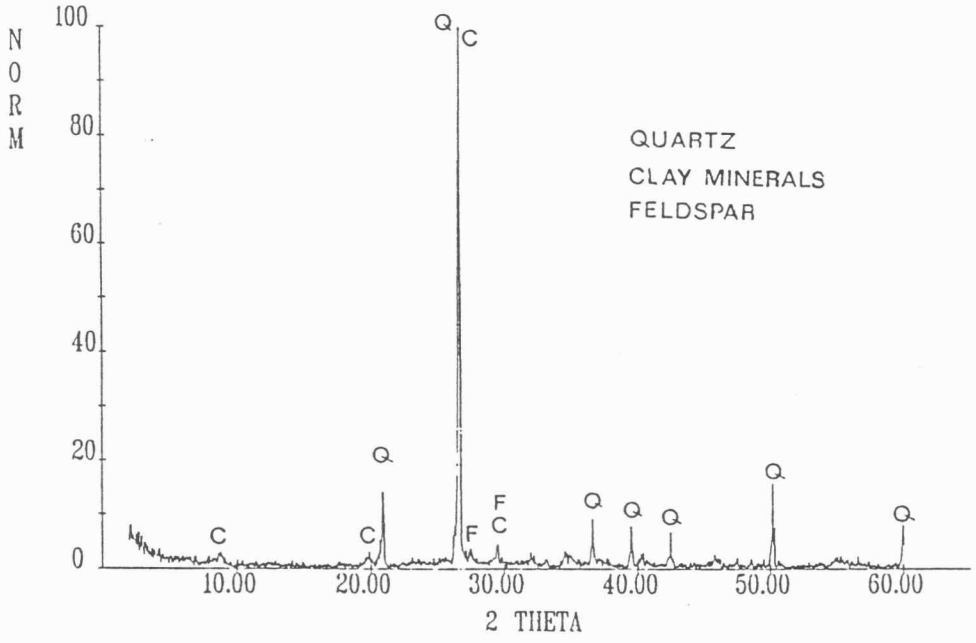


**Figure 3.1.** X-ray diffractometer record of clay minerals (C) and quartz (Q) filling vugs and cavities of Misener carbonates and cherts in the Braden–Zenith No. 1 well. Whole rock analysis of sample number BZ1/1 (3776 ft.).

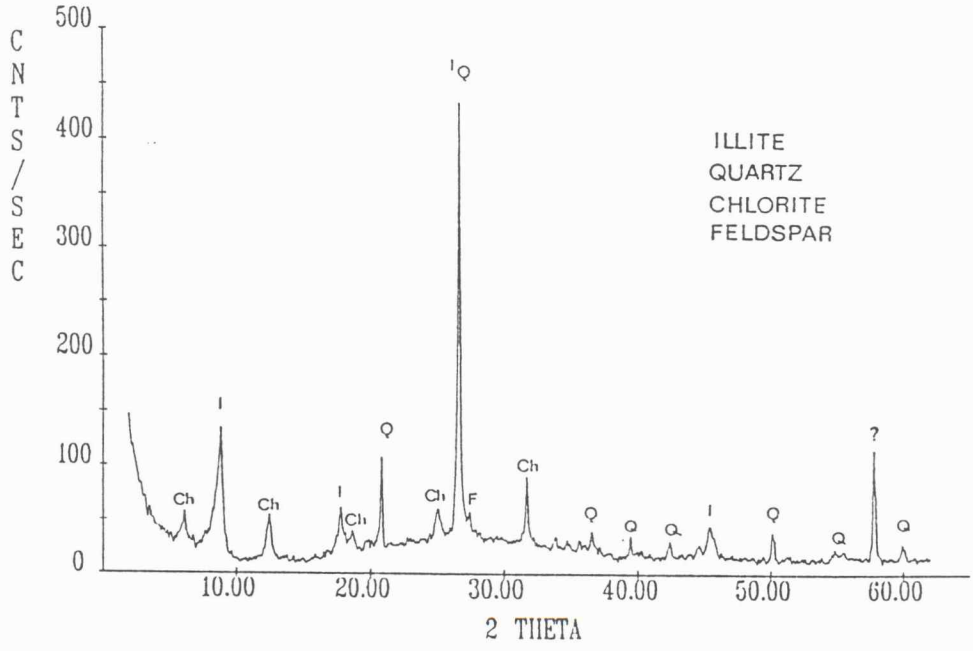


**Figure 3.2.** X-ray diffractometer record of illite (I), quartz (Q), chlorite (C), and feldspar (F) filling vugs and cavities of Misener carbonates and cherts in the Braden–Zenith No. 1 well. Sedimented slide prepared by air drying of sample number BZ1/1 (3776 ft.).

all detected clay minerals seems to be low. Experiments with drilling fluids would be necessary to verify this observation.

Typically there are two types of sandstone within the cored interval from well ZU 3. The first (Fig. 3.8) is extremely porous and shows some oil staining. Quartz is dominant and, in addition, apatite and a very small amount of calcite are detectable. Further investigation is necessary to determine if apatite occurs within the dark grains and pebbles, or exists also as cement. The second sandstone type contains a large amount of calcite cement (Fig. 3.9). SEM pictures of calcite show dissolution forms in both sandstone types .

Siltstones from the Stewart 6 well are a mixture of quartz, dolomite, clay minerals, and feldspar (Fig. 3.10). The quartz content is higher than in a normal siltstone, but quantitative XRD analysis requires further investigation.

A green material is typical of sandstones in the Stewart well. It is concentrated at bedding planes and to some extent in infiltration zones and shows only a slight clay content. In addition to dominant quartz, an Na-rich feldspar is an important component of these samples.

The components of the gray-green siltstones in the McComb 5 well include quartz, clay minerals, and feldspar (Fig. 3.11). The clay minerals are clearly dominated by illite. Detailed clay analyses will be given in a subsequent report. The boundary between siltstones and sandstones at about 3797 ft. shows an interesting mineral composition (Figs. 3.12 and 3.13). The main components, in addition to quartz, are pyrite, jarosite, clay minerals, and feldspar. Jarosite presumably is the weathering product of pyrite and is a typical mineral of oxidation zones. Further sedimentological investigations should prove whether or not the boundary plane is connected with erosion processes. Results of analyses of green material from the sandstone were the same as for other wells (Fig. 3.14).

Figure 3.15 shows the XRD curve of a concentrate of black pebbles and grains which commonly occur, and sometimes are strongly concentrated, in some sandstone intervals. These grains, which range in size from a millimeter up to a maximum of 1.5 cm. in diameter, consist mainly of apatite with a small amount of quartz. The grains and pebbles could be interpreted as reworked apatite nodules which were silicified during sandstone diagenesis. Because apatite contains radioactive elements such as uranium, these pebbles may cause Misener sandstones to display unusually high gamma radiation readings on wireline logs.

The preliminary results for the Zenith field reported here must be augmented by additional studies such as geochemical analyses and direct measurements of the gamma radiation of pebble concentrates. This will be undertaken during the next period of cooperative investigations.

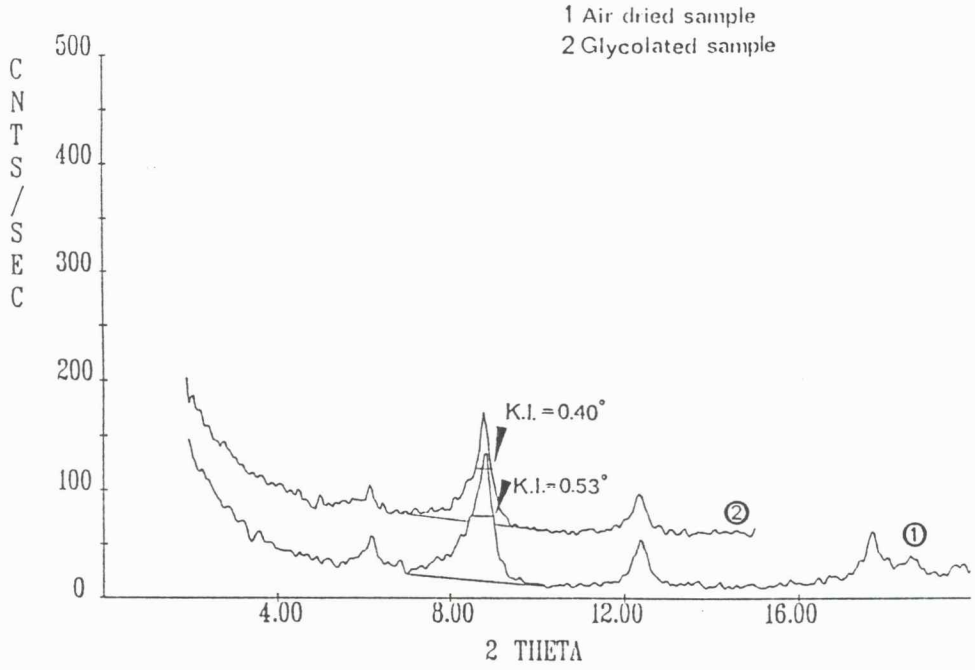


**Figure 3.3.** X-ray diffractometer record showing illite peak with small shoulder on low-angle side (arrows), but there is no significant difference between XRD curves for air-dried (1) or glycolated (2) samples. Sample number BZ1/1 (3776 ft.) from Braden–Zenith No. 1 well.

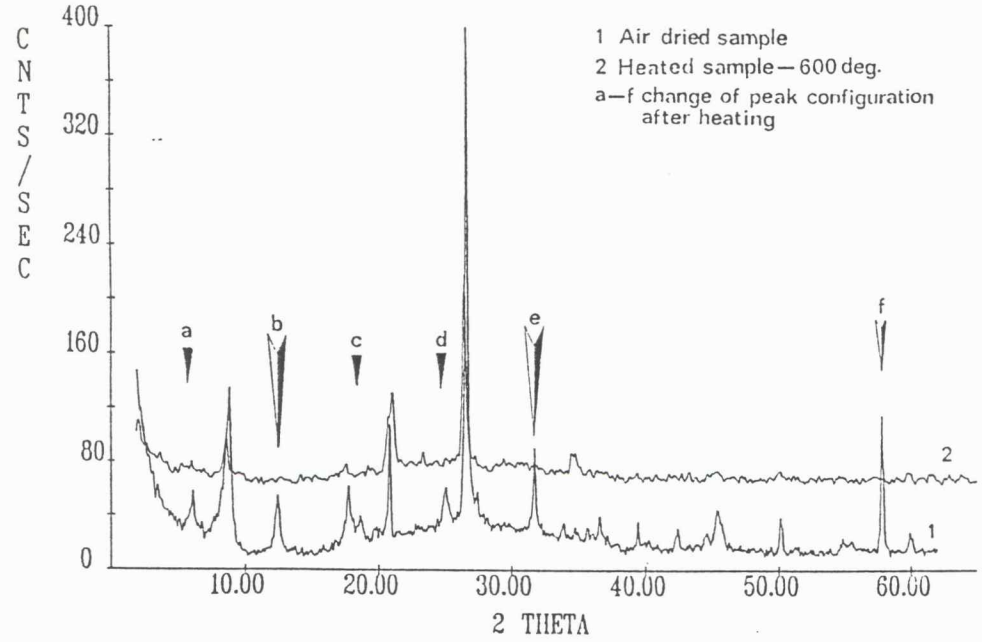


**Figure 3.4.** X-ray diffractometer record showing quartz and clay mineral peaks of air-dried (1) and heated (2) samples. A small shift of the 001 illite peak is detectable after heating (a–f). Chlorite peaks disappear after heating. Sample numbered BZ1/1 (3776 ft.) from Braden–Zenith No. 1 well.

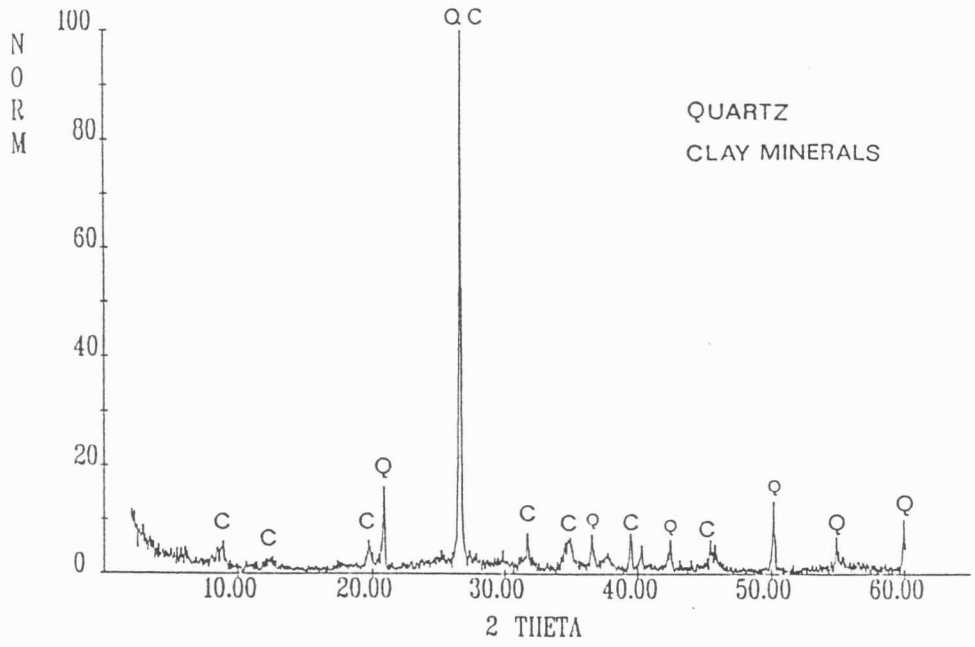


**Figure 3.5.** X-ray diffractometer record of clay minerals (C) and quartz (Q) filling vugs and cavities of Misener carbonates and cherts in the Braden–Zenith No. 1 well. Whole rock analysis of sample number BZ1/2b (3779 ft.).

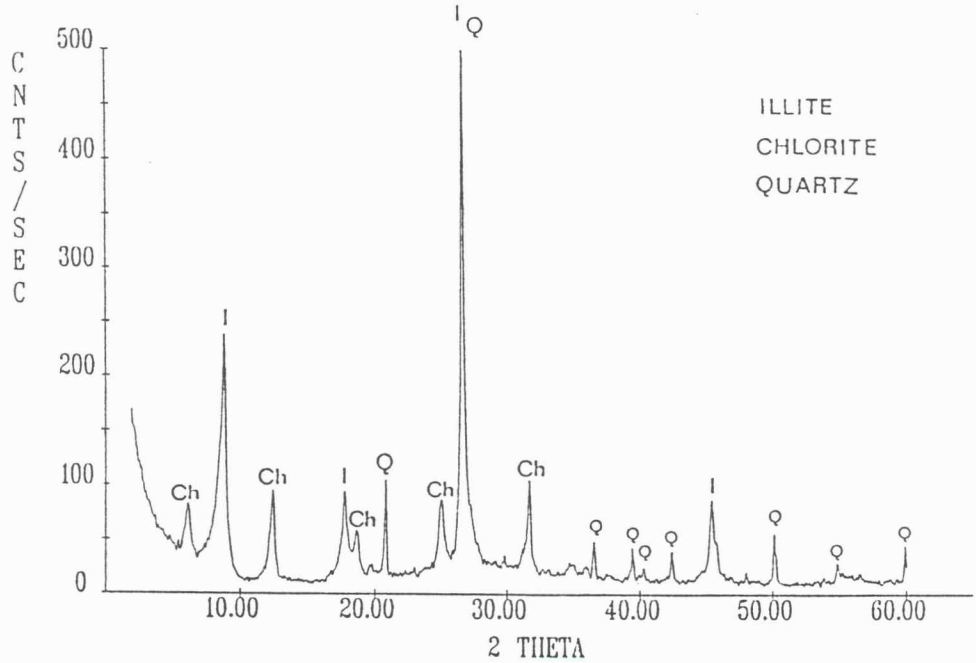


**Figure 3.6.** X-ray diffractometer record of illite (I), chlorite (C), and quartz (Q) filling vugs and cavities of Misener carbonates and cherts in the Braden–Zenith No. 1 well. Sedimented slide prepared by air drying of sample number BZ1/2b (3779 ft.).

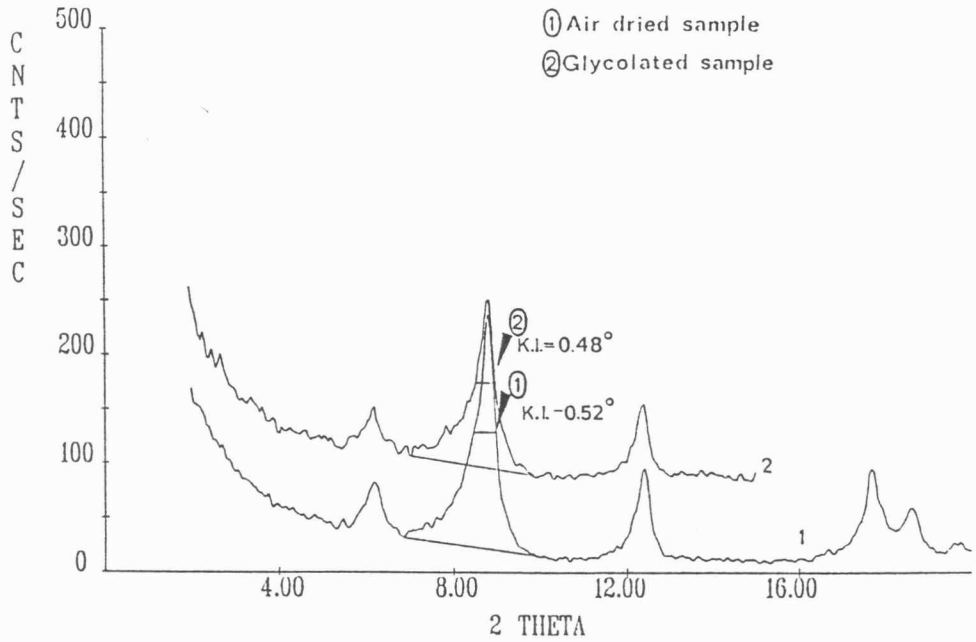


**Figure 3.7.** X-ray diffractometer record showing illite peak with small shoulder on low-angle side (arrows), but there is no significant difference between XRD curves for air-dried (1) or glycolated (2) samples. Sample number BZ1/2b (3779 ft.) from Braden–Zenith No. 1 well.

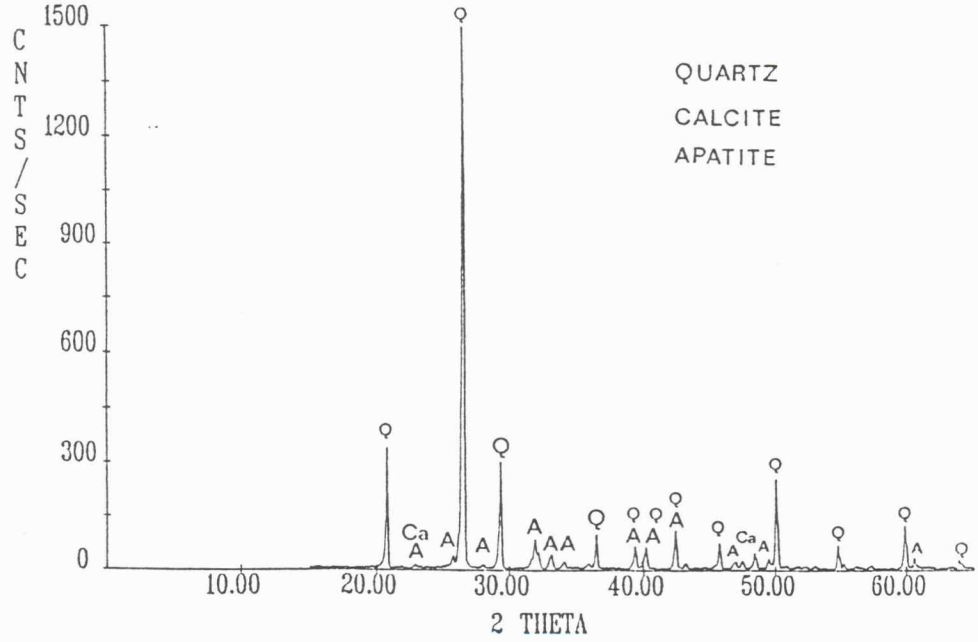


**Figure 3.8.** X-ray diffraction record of Misener sandstone (3711 ft. ) from Braden–Zenith ZU 3 well. Quartz (Q), apatite (A), and calcite (Ca) peaks are detectable. Sample number ZU3/1.

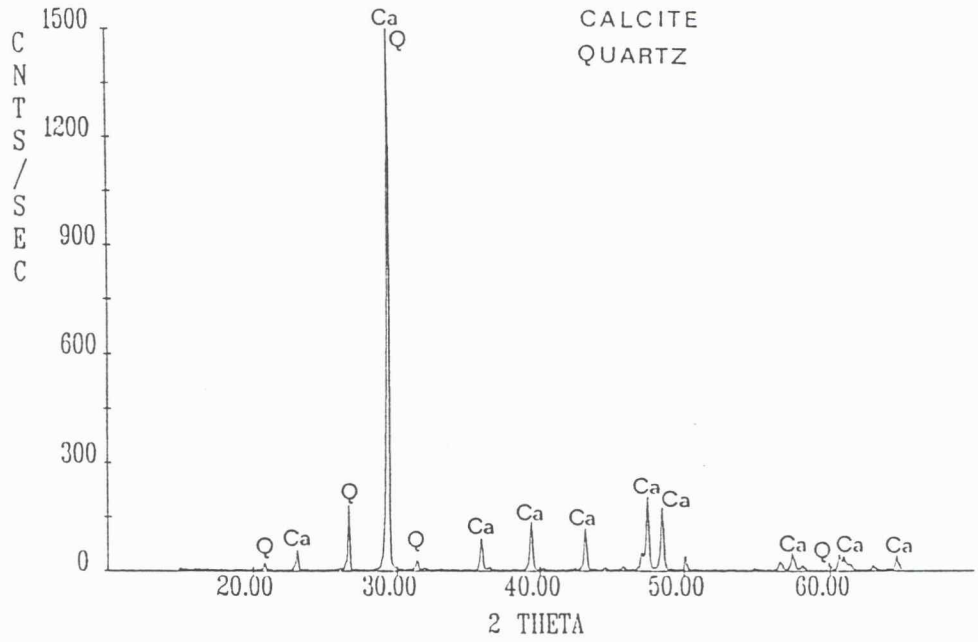


**Figure 3.9.** X-ray diffraction record of Misener sandstone (3711.5 ft.) from Braden–Zenith ZU 3 well. Quartz (Q) and calcite (Ca) are detectable. Sample number ZU3/2.

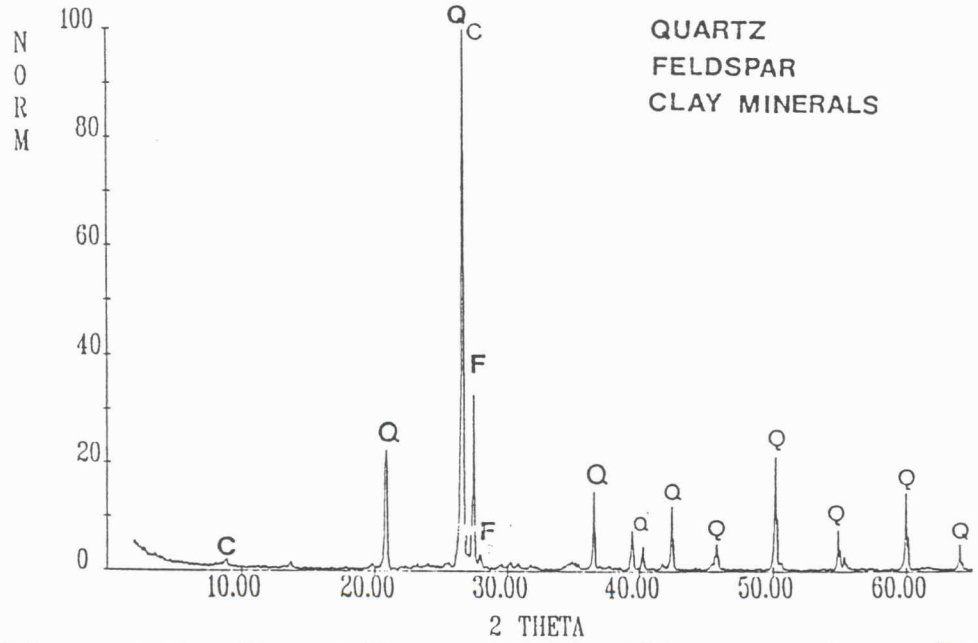


**Figure 3.10.** X-ray diffraction record of Misener sandstone (3723 ft.) from Stewart No. 6 well. Quartz (Q), feldspar (F), and clay minerals (c) are detectable. Sample number St6/2.

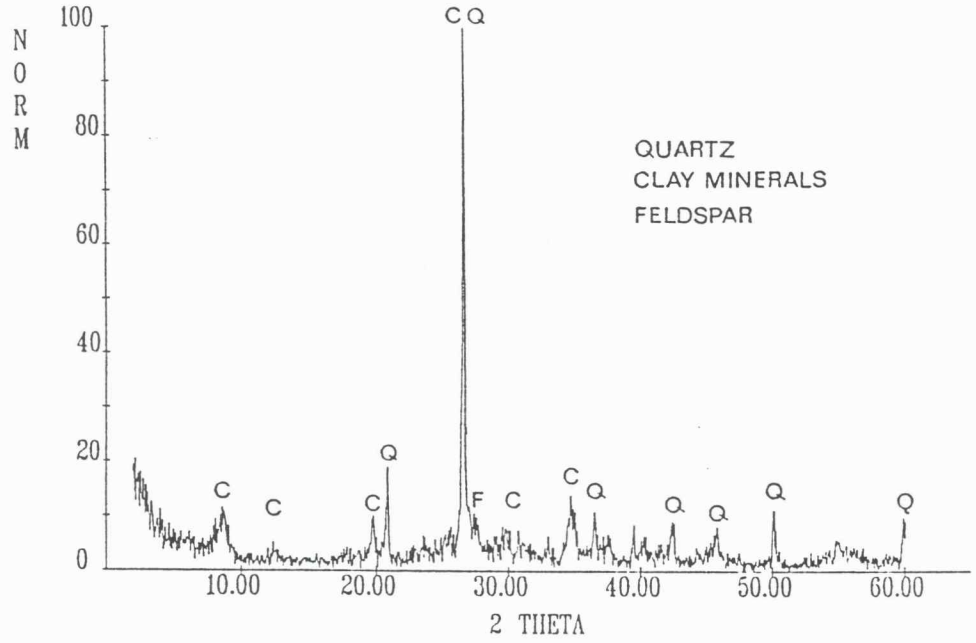


**Figure 3.11.** X-ray diffraction record of gray-green siltstones (3797.5 ft.) from the Misener sandstone in the McComb No. 5 well. Quartz (Q), clay minerals (c), and feldspar (F) are detectable. Sample number McC5/1.

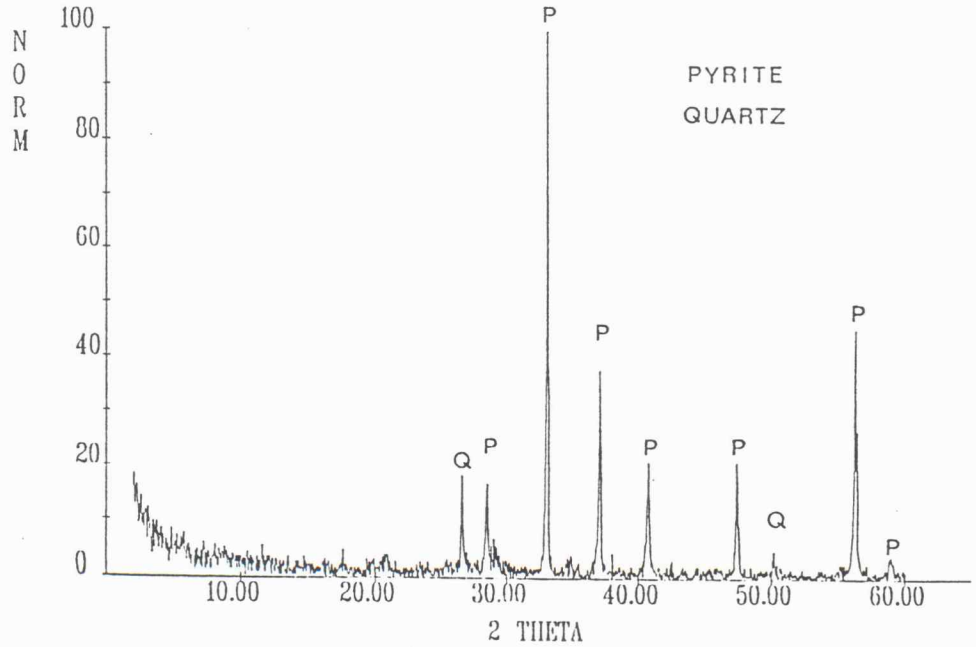


**Figure 3.12.** X-ray diffraction record of sample number McC5/2b at top of Misener sandstone in McComb No. 5 well (3797.1 ft.). Quartz (Q) and pyrite (P) are detectable.

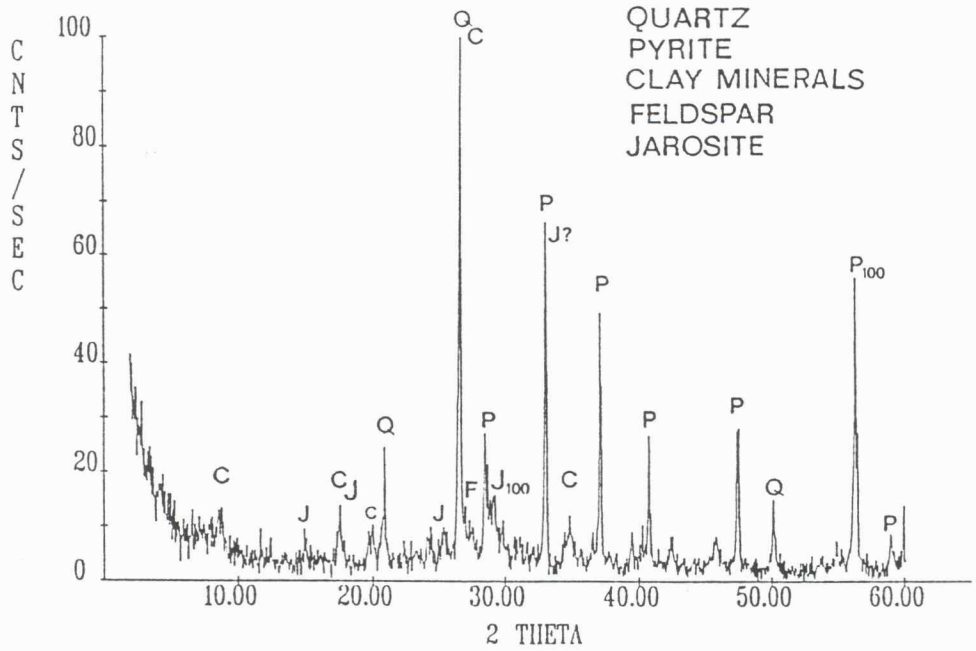


**Figure 3.13.** X-ray diffraction record of sample number McC5/2a at top of Misener sandstone in McComb No. 5 well (3797.1 ft.). Quartz (Q), pyrite (P), clay minerals (c), feldspar (F), and jarosite (J) are detectable. Jarosite may be indicative of an exposure surface.

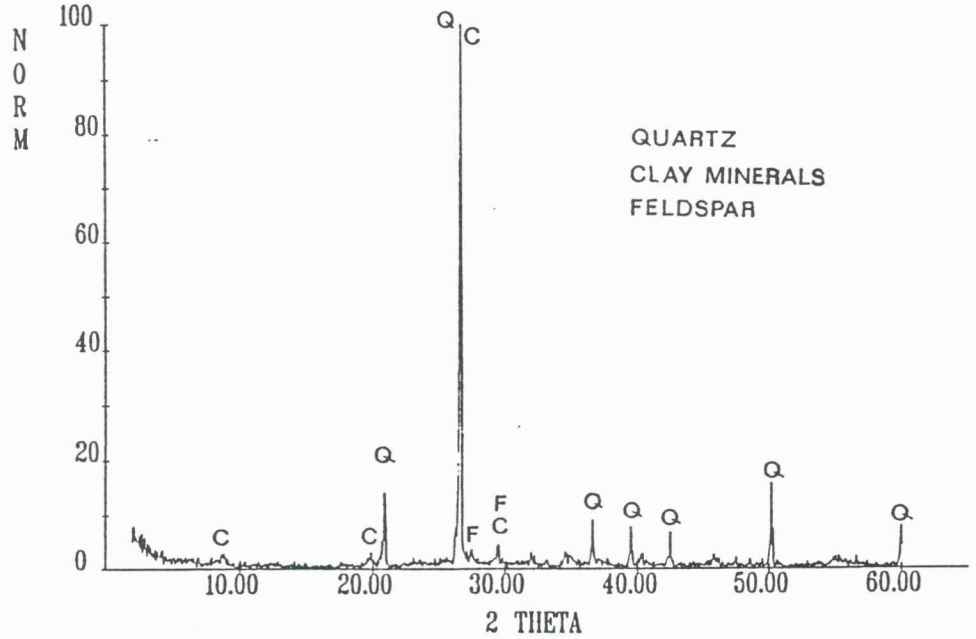


**Figure 3.14.** X-ray diffraction record of green clays from Misener sandstone (3799 ft.) in McComb No. 5 well. Quartz (Q), clay minerals (c), and feldspar (F) are detectable. Sample number McC5/3.

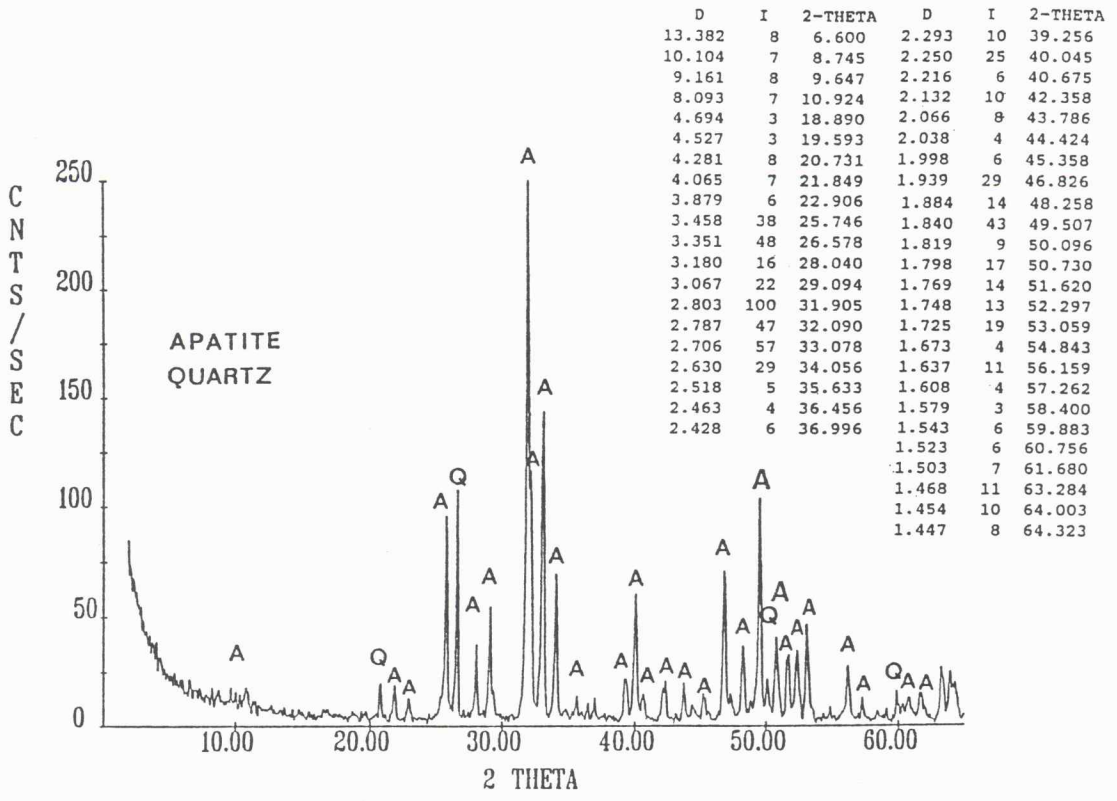


| D | I | 2-THETA | D | I | 2-THETA |
|---|---|---|---|---|---|
| 13.382 | 8 | 6.600 | 2.293 | 10 | 39.256 |
| 10.104 | 7 | 8.745 | 2.250 | 25 | 40.045 |
| 9.161 | 8 | 9.647 | 2.216 | 6 | 40.675 |
| 8.093 | 7 | 10.924 | 2.132 | 10 | 42.358 |
| 4.694 | 3 | 18.890 | 2.066 | 8 | 43.786 |
| 4.527 | 3 | 19.593 | 2.038 | 4 | 44.424 |
| 4.281 | 8 | 20.731 | 1.998 | 6 | 45.358 |
| 4.065 | 7 | 21.849 | 1.939 | 29 | 46.826 |
| 3.879 | 6 | 22.906 | 1.884 | 14 | 48.258 |
| 3.458 | 38 | 25.746 | 1.840 | 43 | 49.507 |
| 3.351 | 48 | 26.578 | 1.819 | 9 | 50.096 |
| 3.180 | 16 | 28.040 | 1.798 | 17 | 50.730 |
| 3.067 | 22 | 29.094 | 1.769 | 14 | 51.620 |
| 2.803 | 100 | 31.905 | 1.748 | 13 | 52.297 |
| 2.787 | 47 | 32.090 | 1.725 | 19 | 53.059 |
| 2.706 | 57 | 33.078 | 1.673 | 4 | 54.843 |
| 2.630 | 29 | 34.056 | 1.637 | 11 | 56.159 |
| 2.518 | 5 | 35.633 | 1.608 | 4 | 57.262 |
| 2.463 | 4 | 36.456 | 1.579 | 3 | 58.400 |
| 2.428 | 6 | 36.996 | 1.543 | 6 | 59.883 |
| | | | 1.523 | 6 | 60.756 |
| | | | 1.503 | 7 | 61.680 |
| | | | 1.468 | 11 | 63.284 |
| | | | 1.454 | 10 | 64.003 |
| | | | 1.447 | 8 | 64.323 |

**Figure 3.15.** X-ray diffraction record of a concentrate of black pebbles from Misener sandstone in McComb No. 5 well. Apatite (A) and quartz ((Q) are detectable. Sample number McC5/5.

## REFERENCES

Thorez, Jacques, 1976, *Practical identification of clay minerals:* Ed. G. Lelotte, Dison, Belgium, 90 pp.

# 4. STRUCTURAL MODELING

J. Harff, J.C. Davis, R.A. Olea, B. Lewerenz and W.L. Watney

## 4.1 Stratigraphic Correlation

Ordovician carbonates and Devonian–Mississippian siliciclastics were zoned and correlated separately. For carbonates, wells were zoned by K.D. Newell based on porosity logs if the tops of the zones coincided with a change of the vertical succession of classes derived from cluster analysis (see Chap. 4.2). If a change in class succession did not match the zonation, the zonation was corrected.

For the Misener and Chattanooga sequence, CORRELATOR, an interactive system for lithostratigraphic correlation of geophysical well logs, was applied (Olea, 1988). Table 4.1 lists the sequence of stratigraphic layers distinguished in this report.

**Table 4.1.** Stratigraphic Zones within the Zenith Field, Kansas

| Layer | Petrographic Description | Stratigraphic Code |
|---|---|---|
| Chattanooga | Shale | 1 |
| Misener I (upper Misener) | Sandstone/Limestone/ Chert | 2 |
| Misener II | Shale/Limestone/ "Hard Streak" | 3 |
| Misener III (Lower Misener) | Sandstone | 4 |
| Misener IV | Shale | 5 |
| Maquoketa | Dolomite | 6 |
| Fernvale | Limestone | 7 |
| Viola 1 | Limestone/Dolomite | 8 |
| "Hard Streak" | Limestone | 9 |
| Viola 2 | Limestone | 10 |
| Viola 3 | Limestone | 11 |

### 4.1.1 CORRELATOR Methodology

Experienced subsurface geologists tend to follow a common set of procedures when correlating wireline logs and developing subsurface cross sections. Even when seeking the correlations along a traverse composed of many wells, manual correlation is never based on the trace of a single logging tool. In spite of the number of different types of logs available, geologists tend to concentrate on two of the most common logs: a spontaneous-potential log to discriminate between shales and clean formations and a shallow-resistivity log on which the correlations themselves are based.

The computer program CORRELATOR also uses only two log traces, but these may be any pair of logs that function in a way similar to the classical SP-resistivity pair. That is, one log must be sensitive to the amount of shale in the stratigraphic sequence, and the other must be able to measure, with high resolution, some petrophysical property that is persistent for extensive distances. Generically, these wireline logs are referred to as *shale* and *correlation* logs, respectively.

CORRELATOR uses the shale log to break the stratigraphic sequence into rock units according to a binary lithological classification. Prior to analysis, any two intervals in the pair of wells being correlated are likely to be geologically equivalent. Once the information contained in the shale logs has been utilized, the number of likely solutions is reduced significantly because the possible matches are now restricted to intervals having comparable lithologies. The correlation of clearly different lithotypes, such as a clean limestone and a black shale, is not encouraged. A *normalized shale similarity coefficient*, $\alpha_{1,2}(i,k,n)$, is computed in order to measure the degree of similarity in the amount of shale in the two sequences $\xi_1(\cdot)$ and $\xi_2(\cdot)$ being compared. Given that the two sequences vary between $\xi_{\min 1} < \xi_{\max 1}$ and $\xi_{\min 2} < \xi_{\max 2}$, respectively, and that they have been sampled at regular intervals

$$\alpha_{1,2}(i,k,n) = 1 - \frac{1}{2n+1} \sum_{j=i-n}^{i+n} \left| \frac{\xi_1(j) - \xi_{\min 1}}{\xi_{\max 1} - \xi_{\min 1}} - \frac{\xi_2(j+k) - \xi_{\min 2}}{\xi_{\max 2} - \xi_{\min 2}} \right| \quad (1)$$

where $(2n+1)$ is the length of the sub-sequences being compared whose centers are at $i$ and $(i+k)$, respectively. The coefficient reaches a minimum value of 0 when all the values in one sequence are equal to the maximum value and all the values in the other are equal to the minimum value; the coefficient is equal to the maximum value of 1 when, for every possible value of $j$, the relative proportion $\big(\xi_1(j) - \xi_{\min 1}\big)/\big(\xi_{\max 1} - \xi_{\min 1}\big)$ is equal to the relative proportion $\big(\xi_2(j+k) - \xi_{\min 2}\big)/\big(\xi_{\max 2} - \xi_{\min 2}\big)$.

On the display of wireline logs, for logs that are sensitive to shale content, the convention is that the farther the reading is to the right, the greater the amount of shale in the unit. In Figure 4.1, a shale arbitrarily labeled A shows the greatest similarity with units P, R, T, and V, which also are shales. Conversely, unit A has minimal similarity to the clean units Q, S, and U. Because CORRELATOR seeks an equivalent interval in the right-hand well for a given interval in the left-hand well, in the graphical presentations and calculations, the well on the left is referred to as the *reference well*, and the well on the right as the *matching well*.

$$r_{1,2}(i,k,n) = \frac{\mathrm{cov}_{1,2}(i,k,n)}{s_1(i,n)s_2(k,n)} \tag{2}$$

Statistical correlation (Eq. 2) is used to measure the similarity between pairs of correlation logs because of its simplicity and relative success in related applications. The method measures the similarity in log shapes, or the signatures of the traces, and is not adversely affected by the presence of gaps in the stratigraphic record, nor by lateral changes in thickness of equivalent intervals. Weighting the cross-correlation coefficient $r_{1,2}(i,k,n)$ in Eq. 2 by the coefficient of similarity in shale content $\alpha_{1,2}(i,k,n)$ in Eq. 1 produces a compound coefficient, or *weighted correlation coefficient*

$$\omega_{1,2}(i,k,n) = \alpha_{1,2}(i,k,n)r_{1,2}(i,k,n) \tag{3}$$

Since $r_{1,2}(i,k,n)$ varies between $-1$ and 1, and $\alpha_{1,2}(i,k,n)$ can fluctuate between 0 and 1, the weighted coefficient will vary between $-1$ and 1 and will measure the joint similarity in shale as well as in signature matching as provided by two independent sets of measurements. The weighted coefficient provides a joint discrimination both in terms of shale content and log trace signature. Continuing with the example in Figure 4.1, of all possible correlative intervals shown, shale S best matches shale A (Figure 4.2).

Provided that there is one and only one matching interval, selecting the matching depth providing the highest weighted correlation coefficient as the lithologically equivalent depth seems natural. A *threshold* or *cutoff in the weighted correlation coefficient* is introduced to take care of the case when there is actually no equivalence. Although there will always be a highest weighted correlation coefficient, in the absence of any real matching, the coefficient will only be the least worst value out of an unacceptable set. By conveniently setting a threshold, these low haphazard matchings will be weeded out. The only disadvantage of this fairly straightforward procedure is that not only false correlations will be deleted, but also weak but true correlations.

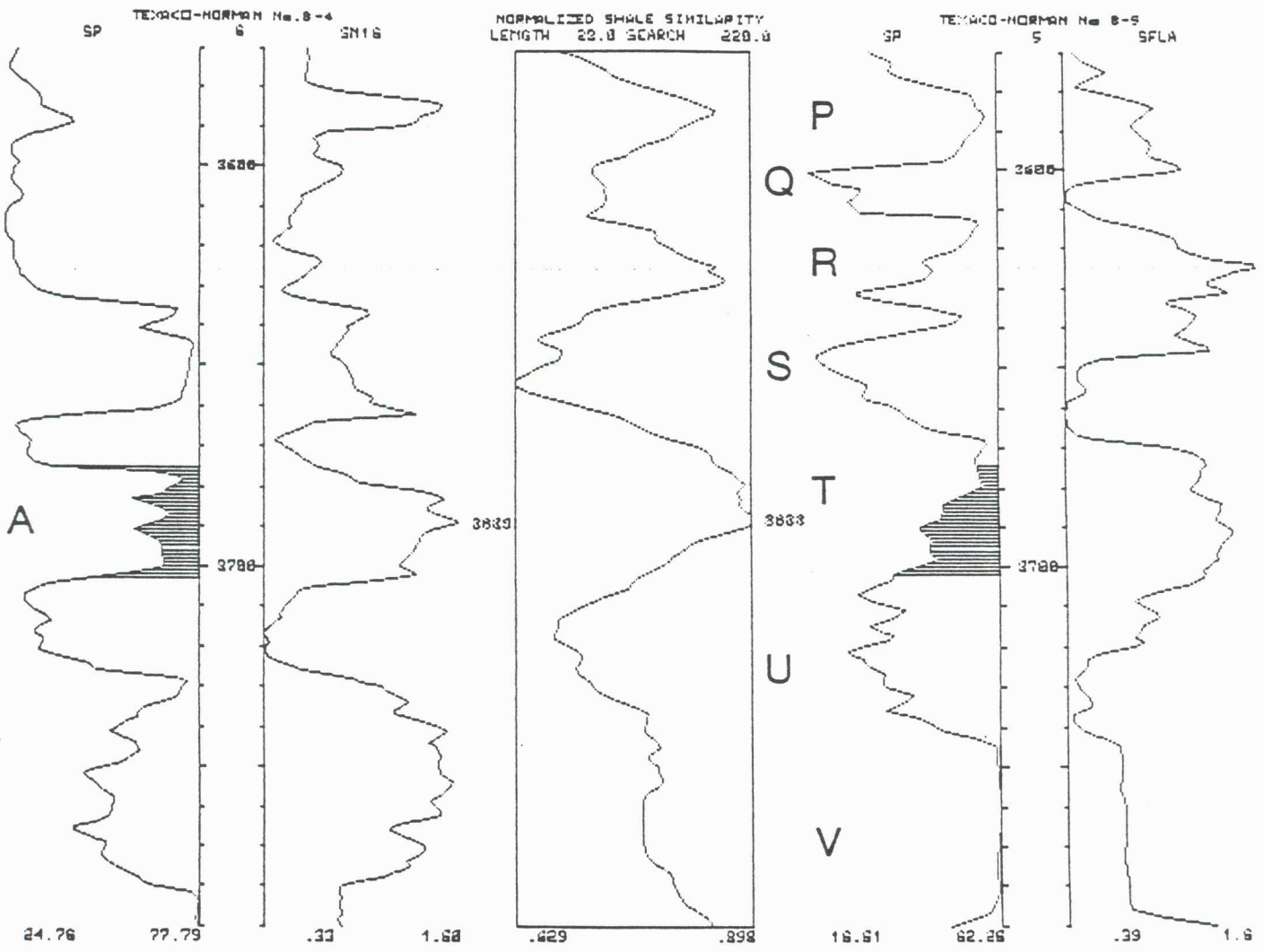


**Figure 4.1.** Normalized shale similarity between gamma-ray logs of two wells. Central track shows similarity in amount of shale between unit A centered at 8,689 ft. in left-hand well, and all possible intervals between 8,570 and 8,790 ft. in right-hand. All intervals compared are 28 ft. in length. Best matches to unit A are with shale units P, R, T, and V.

This procedure yields the best correlation between two wells, calculated a single reference interval at a time. A complete set of correlations can be obtained by repeating the operation for all possible reference intervals in a

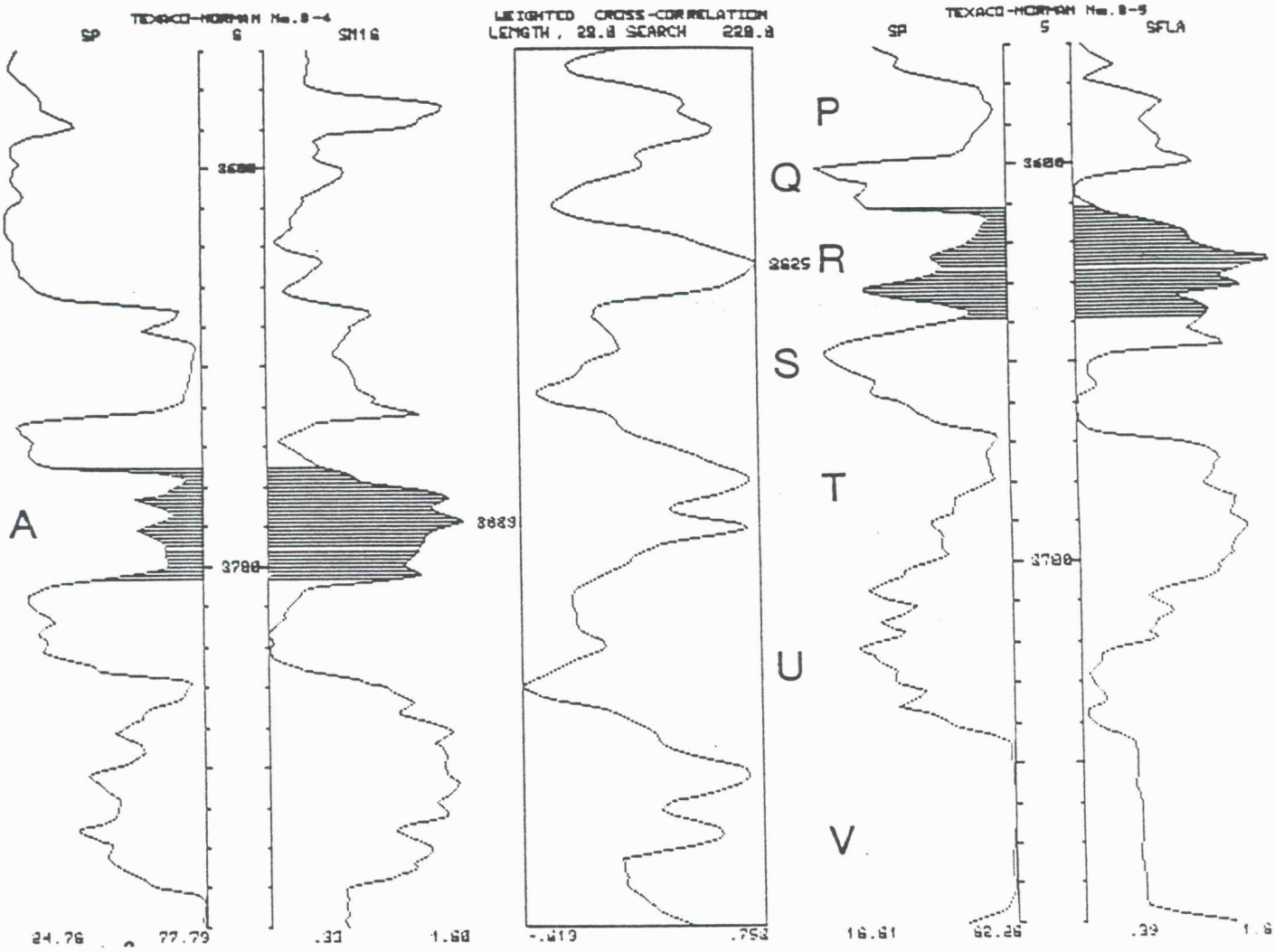


**Figure 4.2.** Weighted correlation coefficient between logs of two wells. Central track shows product of normalized shale similarity and the cross-correlation coefficient between rock unit A in left-hand well and all possible intervals of same size in right-hand well. Best match is between units A and R, which is correct geological correlation.

pair of wells.

Since successive correlations are established independently, crossing correlations may occur. Detecting and eliminating incorrect correlations

is done with the help of an expert system (Olea and Davis, 1989). The process can be extended to produce a geologic cross section that includes many wells by working successively with all pairs of wells along the traverse. Resulting correlations are stored on correlation files. Preparation of interpreted traverses is done by interpolating evaluations in the correlation files. The user indicates markers of interest in any given well along the cross-section. CORRELATOR automatically traces such markers to all other wells and displays the results in tabular as well as graphical form.

### 4.1.2 Results of Stratigraphic Correlation of Zenith Field Using CORRELATOR

Uncertainties in correlation can be more easily resolved by expanding the interval studied to include other stratigraphic units that have better lateral continuity. In the Zenith field, the Pennsylvanian cyclothems of the Kansas City Group, which lies unconformably above the monotonous Chattanooga Shale, have high continuity. Since the Viola is the deepest target in the area, no log information for deeper intervals is available. In fact, most wells do not even penetrate through the entire Viola. Because of erratic drilling below the Viola 1, this study is limited to the top of the Viola 1. Regionalization of the Viola 2 and Viola 3 is based on manual correlations, as the units were not considered in the present study.

Figure 4.3 shows the locations of 38 wells and 12 profiles used to model the stratigraphy of the Zenith field. Ten of the profiles are closed traverses, which have the advantage of allowing the checking of closure errors. The north–south profile roughly follows the regional dip. The total number of wells in the Zenith field is 502, but only the 38 wells shown in Figure 4.3 have both a gamma-ray and a neutron log, the most common pair of shale/nonshale logs from the area. All logs were digitized from paper records and stored on file M.DIG, listed in Appendix A. A listing of all wells is given in Appendix B. Numbers in parentheses are identification numbers used during the preparation of the KGS–TORP (1991) report.

**Results**—Correlation files were used to produce lithostratigraphic cross-sections which display the lateral continuity of selected markers defined at certain wells. The maximum closure error along the closed traverses is 1 ft., a remarkably low value. Maximum discrepancy between markers at wells on crossing traverses was 1.5 ft. Tables 4.2 and 4.3 contain all markers from the top of the Chattanooga to the top of the Viola 1 for all wells in the study. Complete results can be found in Olea, Newell and Harff (1991). Thirty-six cross-sections that provide a detailed view of the geology of the field are included in that report.

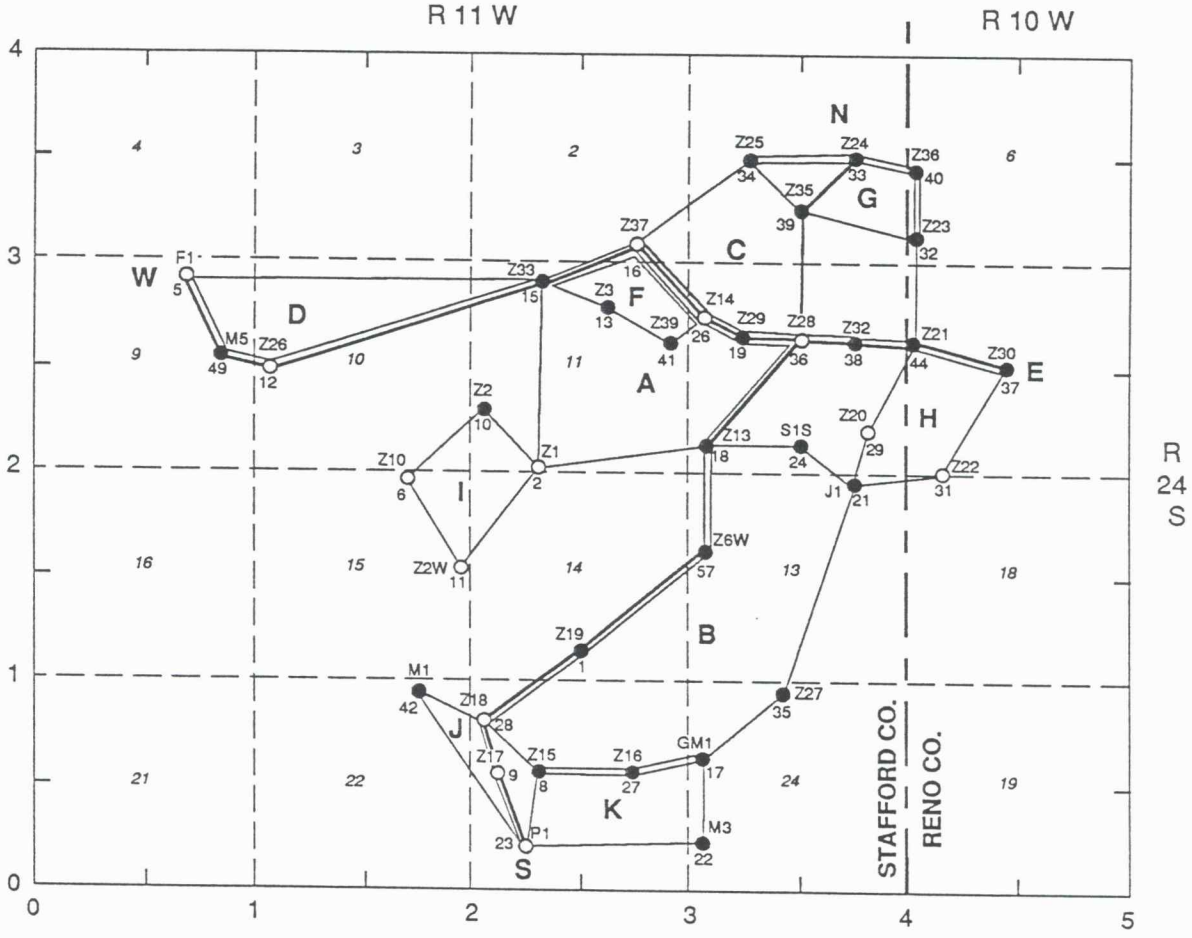


**Figure 4.3.** Location of traverses used in the study. The label above the well symbol is the abbreviated well name; the label underneath is the sequential number in the CORRELATOR well file listed in Appendix B.

## 4.2 Regionalization

### 4.2.1 Typification

The regionalization process requires the prior development of a typification model. Because the reservoir consists of a lower carbonate and an upper clastic unit which are not directly comparable, typification was conducted separately for the carbonates and the clastics. Hierarchical cluster analyses were used to define lithotypes (Harff and Davis, 1990) using three wireline log variables for classification:

**Table 4.2.** Correlations for the Chattanooga and the Misener, Zenith Field, Kansas. Datum: Sea Level [ft]

| No. | Well Name | KB | Chatt. | (Upper Misener) | | (Lower Misener) | |
|---|---|---|---|---|---|---|---|
| | | | Top | Top | Base | Top | Base |
| 1 | Zenith 37(16) | 1805.0 | 1841.0 | 1873.0 | 1879.5 | 1880.5 | 1888.0 |
| 2 | Zenith 14(26) | 1813.0 | 1866.0 | 1894.0 | 1903.5 | 1904.5 | 1915.0 |
| 3 | Zenith 29(19) | 1820.0 | 1864.0 | 1899.0 | 1908.0 | 1909.0 | 1923.0 |
| 4 | Zenith 28(36) | 1816.0 | 1870.5 | 1900.5 | 1910.5 | 1912.0 | 1921.5 |
| 5 | Zenith 32(38) | 1805.0 | 1874.0 | 1913.5 | 1921.0 | 1922.0 | 1929.5 |
| 6 | Zenith 39(41) | 1808.0 | 1875.0 | 1909.5 | 1911.5 | 1912.5 | 1928.5 |
| 7 | Zenith 3(13) | 1813.0 | 1866.5 | 1894.0 | 1903.5 | 1904.5 | 1910.5 |
| 8 | Zenith 25(34) | 1804.0 | 1871.0 | 1906.5 | 1918.5 | 1919.5 | 1927.0 |
| 9 | Zenith 21(44) | 1812.0 | 1849.0 | 1890.0 | 1894.5 | 1895.0 | 1899.5 |
| 10 | Zenith 30(37) | 1785.0 | 1871.0 | 1909.0 | 1914.5 | 1915.0 | 1919.5 |
| 11 | Zenith 17(9) | 1814.0 | 1905.0 | 1983.5 | 1996.5 | 1996.5 | 2011.0 |
| 12 | Zenith 18(28) | 1817.0 | 1895.0 | 1980.5 | 1991.5 | 1991.5 | 2006.5 |
| 13 | Zenith 19(1) | 1811.0 | 1908.0 | 1982.0 | 1991.5 | 1991.5 | 2006.5 |
| 14 | Zenith 6W(57) | 1805.0 | 1898.5 | 1959.5 | 1968.5 | 1970.0 | 1979.5 |
| 15 | Zenith 13(18) | 1809.0 | 1879.0 | 1927.0 | 1938.0 | 1940.0 | 1949.5 |
| 16 | Zenith 35(39) | 1803.0 | 1861.0 | 1999.0 | 1908.0 | 1908.5 | 1914.0 |
| 17 | Zenith 24(33) | 1812.0 | 1865.0 | 1897.0 | 1907.5 | 1908.0 | 1913.0 |
| 18 | Paulsen L 1(23) | 1804.0 | 1919.0 | 2006.5 | 2016.0 | 2016.0 | 2031.0 |
| 19 | Johnson 1-5(21) | 1794.0 | 1886.0 | 1946.0 | 1954.0 | 1954.5 | 1966.0 |
| 20 | Stewart 1S(24) | 1794.0 | 1882.0 | 1935.5 | 1948.5 | 1948.5 | 1956.0 |
| 21 | Zenith 1(2) | 1816.0 | 1884.5 | 1945.0 | 1953.5 | 1954.5 | 1966.5 |
| 22 | Zenith 10(6) | 1820.0 | 1883.5 | 1939.5 | 1947.0 | 1947.5 | 1965.0 |
| 23 | McComb 1(42) | 1819.0 | 1901.0 | 1990.5 | 2001.0 | 2001.0 | 2014.0 |
| 24 | Zenith 15(8) | 1807.0 | 1903.5 | 1986.5 | 2000.0 | 2000.0 | 2013.0 |
| 25 | Zenith 16(27) | 1809.0 | 1909.0 | 1983.0 | 1990.5 | 1990.5 | 2004.0 |
| 26 | G. McComb 1(17) | 1801.0 | 1914.0 | 1992.0 | 1997.5 | 1997.5 | 2009.5 |
| 27 | Zenith 27(35) | 1791.0 | 1940.5 | 2022.0 | 2032.0 | 2032.0 | 2040.0 |
| 28 | Zenith 33(15) | 1808.0 | 1859.0 | 1882.0 | 1890.0 | 1891.0 | 1901.5 |
| 29 | Zenith 23(32) | 1807.0 | 1865.0 | 1904.5 | 1913.5 | 1914.0 | 1917.5 |
| 30 | Zenith 36(40) | 1807.0 | 1860.5 | 1896.0 | 1904.0 | 1904.5 | 1908.5 |
| 31 | Zenith 22(31) | 1811.0 | 1893.0 | 1950.0 | 1958.5 | 1959.0 | 1964.0 |
| 32 | Zenith 20(29) | 1796.0 | 1876.0 | 1933.0 | 1943.0 | 1943.0 | 1952.0 |
| 33 | Maxie 3(22) | 1813.0 | 1945.5 | 2022.0 | 2031.5 | 2031.5 | 2037.0 |
| 34 | Zenith 2(10) | 1813.0 | 1867.5 | 1920.5 | 1928.5 | 1929.0 | 1933.0 |

(*Cont.*)

**Table 4.2.** (*Cont.*) Correlations for Chattanooga and Misener, Zenith Field

| No. | Well Name | KB | Chatt. Top | (Upper Misener) Top | Base | (Lower Misener) Top | Base |
|---|---|---|---|---|---|---|---|
| 35 | Zenith 2W(11) | 1816.0 | 1903.5 | 1967.5 | 1975.5 | 1976.0 | 1989.0 |
| 36 | Maxie 5(49) | 1826.0 | 1897.0 | 1930.0 | 1936.5 | 1937.5 | 1950.5 |
| 37 | Zenith 26(12) | 1822.0 | 1895.0 | 1935.5 | 1942.5 | 1943.5 | 1964.5 |
| 38 | Figger 1(5) | 1822.0 | 1883.0 | 1910.0 | 1922.0 | 1923.0 | 1935.0 |

gamma-ray intensity ($I_{GR}$)
corrected neutron porosity ($\Phi_{Ncorr}$)
corrected density porosity ($\Phi_{Dcorr}$).

The classification of 1385 observations of carbonates from the Viola 3 to the Maquoketa dolomite are shown in Figure 4.4, which also provides a cross-plot of porosity versus lithology based on ($\Phi_{Ncorr}$) and ($\Phi_{Dcorr}$) (Schlumberger, 1989).

In the cross-plot, the classes are represented by the ($\Phi_{Ncorr}$) and ($\Phi_{Dcorr}$) centroids or expected values. Also given are the means for $I_{GR}$ and porosity calculated from wireline log data, although porosity was not used in the numerical classification. A dendrogram (Fig. 4.4) shows the relation between classes resulting from clustering using Ward's algorithm as implemented in the SPSS$^{TM}$ package. Classes 1 and 6 were combined into a single class, as class 6 contains only 36 observations. This combined class represents limestones having the largest average porosity and the best reservoir characteristics. Class 2 includes dolomites that have lower average porosities. Classes 3 and 4 represent slightly porous carbonates which seal the reservoirs.

For typification of the clastics, 321 observations from the stratigraphic units Misener IV through Misener I were clustered. Results are displayed in Figure 4.5. The clastics can be partitioned into four classes numbered 7 through 10. Class 7 includes shales, classes 9 and 10 include the Misener sandstones, with class 10 distinguished by greater average values of $PORW$ and $I_{GR}$ values.

High gamma-ray values in the sandstones may result from the presence of apatite, as discussed in Section 3. Class 8 is the "Misener limestone." For interpretation it must be taken into account that the porous representatives of the "Misener limestone" in the southwest of the Zenith field have not been considered in the analysis because of lack of data. The rocks represented by class 8 are located in the south-central part of the field and are characterized by low average porosity.

**Table 4.3.** Correlations for the Maquoketa and the Viola, Zenith Field, Kansas. Datum: Sea Level [ft]

| No. | Well Name | KB | Maquoketa Top | Viola Top | Viola 1 Top |
|---|---|---|---|---|---|
| 1 | Zenith 37(16) | 1805.0 | 1891.0 | 1897.5 | 1921.0 |
| 2 | Zenith 14(26) | 1813.0 | 1917.5 | 1921.5 | 1942.0 |
| 3 | Zenith 29(19) | 1820.0 | 1925.5 | 1929.0 | 1944.5 |
| 4 | Zenith 28(36) | 1816.0 | 1924.5 | 1930.0 | 1951.5 |
| 5 | Zenith 32(38) | 1805.0 | 1933.0 | 1937.5 | 1958.0 |
| 6 | Zenith 39(41) | 1808.0 | 1933.5 | 1939.0 | 1960.0 |
| 7 | Zenith 3(13) | 1813.0 | 1918.5 | 1923.5 | 1942.0 |
| 8 | Zenith 25(34) | 1804.0 | 1932.5 | 1938.5 | 1961.0 |
| 9 | Zenith 21(44) | 1812.0 | 1902.0 | 1905.5 | 1926.5 |
| 10 | Zenith 30(37) | 1785.0 | 1922.0 | 1929.0 | 1946.0 |
| 11 | Zenith 17(9) | 1814.0 | | 2011.0 | 2029.5 |
| 12 | Zenith 18(28) | 1817.0 | | 2006.5 | 2026.0 |
| 13 | Zenith 19(1) | 1811.0 | | 2006.5 | 2029.5 |
| 14 | Zenith 6W(57) | 1805.0 | 1980.5 | 1986.0 | 2006.5 |
| 15 | Zenith 13(18) | 1809.0 | 1950.5 | 1956.0 | 1978.0 |
| 16 | Zenith 35(39) | 1803.0 | 1919.0 | 1926.5 | 1949.0 |
| 17 | Zenith 24(33) | 1812.0 | 1916.5 | 1921.0 | 1940.0 |
| 18 | Paulsen L 1(23) | 1804.0 | | 2031.5 | 2047.0 |
| 19 | Johnson 1-5(21) | 1794.0 | | 1968.5 | 1987.0 |
| 20 | Stewart 1S(24) | 1794.0 | | 1961.5 | 1978.5 |
| 21 | Zenith 1(2) | 1816.0 | 1969.5 | 1975.5 | 1996.0 |
| 22 | Zenith 10(6) | 1820.0 | 1969.0 | 1976.0 | 1996.0 |
| 23 | McComb 1(42) | 1819.0 | | 2014.0 | 2035.0 |
| 24 | Zenith 15(8) | 1807.0 | | 2013.0 | 2033.5 |
| 25 | Zenith 16(27) | 1809.0 | | 2004.0 | 2024.0 |
| 26 | G. McComb 1(17) | 1801.0 | | 2009.5 | 2034.0 |
| 27 | Zenith 27(35) | 1791.0 | | 2040.0 | 2063.0 |
| 28 | Zenith 33(15) | 1808.0 | 1905.0 | 1910.5 | 1930.5 |
| 29 | Zenith 23(32) | 1807.0 | 1920.5 | 1926.0 | 1947.0 |
| 30 | Zenith 36(40) | 1807.0 | 1912.0 | 1918.5 | 1936.0 |
| 31 | Zenith 22(31) | 1811.0 | | 1969.5 | 1987.5 |
| 32 | Zenith 20(29) | 1796.0 | 1954.5 | 1956.5 | 1976.5 |
| 33 | Maxie 3(22) | 1813.0 | | 2037.0 | 2058.5 |
| 34 | Zenith 2(10) | 1813.0 | 1941.0 | 1951.5 | 1971.5 |
| 35 | Zenith 2W(11) | 1816.0 | 1991.5 | 1997.0 | 2017.0 |
| 36 | Maxie 5(49) | 1826.0 | | 1954.0 | 1989.0 |
| 37 | Zenith 26(12) | 1822.0 | | 1970.0 | 1995.5 |
| 38 | Figger 1(5) | 1822.0 | | 1938.5 | 1966.5 |

### 4.2.2 Regionalization of Single Layers

Discrimination was carried out by allocating the zones within each well, using the *reduced data model* of classes determined by cluster analysis. The discrimination required two separate steps.

Applying the discriminant analysis options in SPSS$^{TM}$ to each zone in the wells, the probability of class membership was allocated to form a *generalized data model.* Interpolation within each layer was done using an inverse distance weighting (IDW) method. For each of the stratigraphic layers from the Viola 3 up to the Chattanooga Shale, a regular array of $29 \times 29$ cell grids was obtained. The maximum probability and allocation to a class was estimated for each cell. The result is a *generalized layered model* of the Zenith field.

Figure 4.6 shows the regionalization scheme for Viola 3, the lowermost layer. It is characterized in the center and in the south by homogeneous units representing the low porous limestones of class 5. To the northwest and northeast, the layer consists of areas of class 2. These results confirm the poor reservoir characteristics of the Viola 3 layer.

The Viola 2 layer (Fig. 4.7) is dominated by a homogeneous east–west striking area belonging to class 4, which contains dolomites. Subareas in the south and north belong to class 1. The regionalization coincides with the favorable reservoir character of the Viola 2 reservoir.

The regionalization of the "Hard Streak" (Fig. 4.8) confirms its properties as a seal between Viola 2 and Viola 1; all of its subunits belong to classes 3 and 5.

The Viola 1 (Fig. 4.9) has the most favorable reservoir properties, with a homogeneous area belonging to class 1 in the south and adjacent subareas belonging to class 4 (dolomite). The northwest consists of class 2.

Figure 4.10 shows the Fernvale, which acts as a seal within the reservoir. It consists of class 3 and, to a lesser extent, of class 5 between the Viola 1 and the Maquoketa. The characterization of the Maquoketa as a dolomitic reservoir is confirmed by the regionalization given in Figure 4.11.

The Misener IV layer (Fig. 4.12) is represented mostly by shale of class 7. Note the coincidence of the regional occurrence of the Maquoketa dolomite and Misener IV shale.

The "lower Misener" (Fig. 4.13) shows a northwest–southeast area that sequentially consists of class 7, to class 8, to class 9, to class 10. Taking into account the paleogeographical uplift that occurred within the basin, this succession may be interpreted as a sequence of coastal mudstone, to nearshore carbonates and chert, to marine shallow-water sandstones.

The Misener II occurs as a shale only in some isolated areas (Fig. 4.14). This layer is not a reservoir unit. The Misener I ("upper Misener") layer

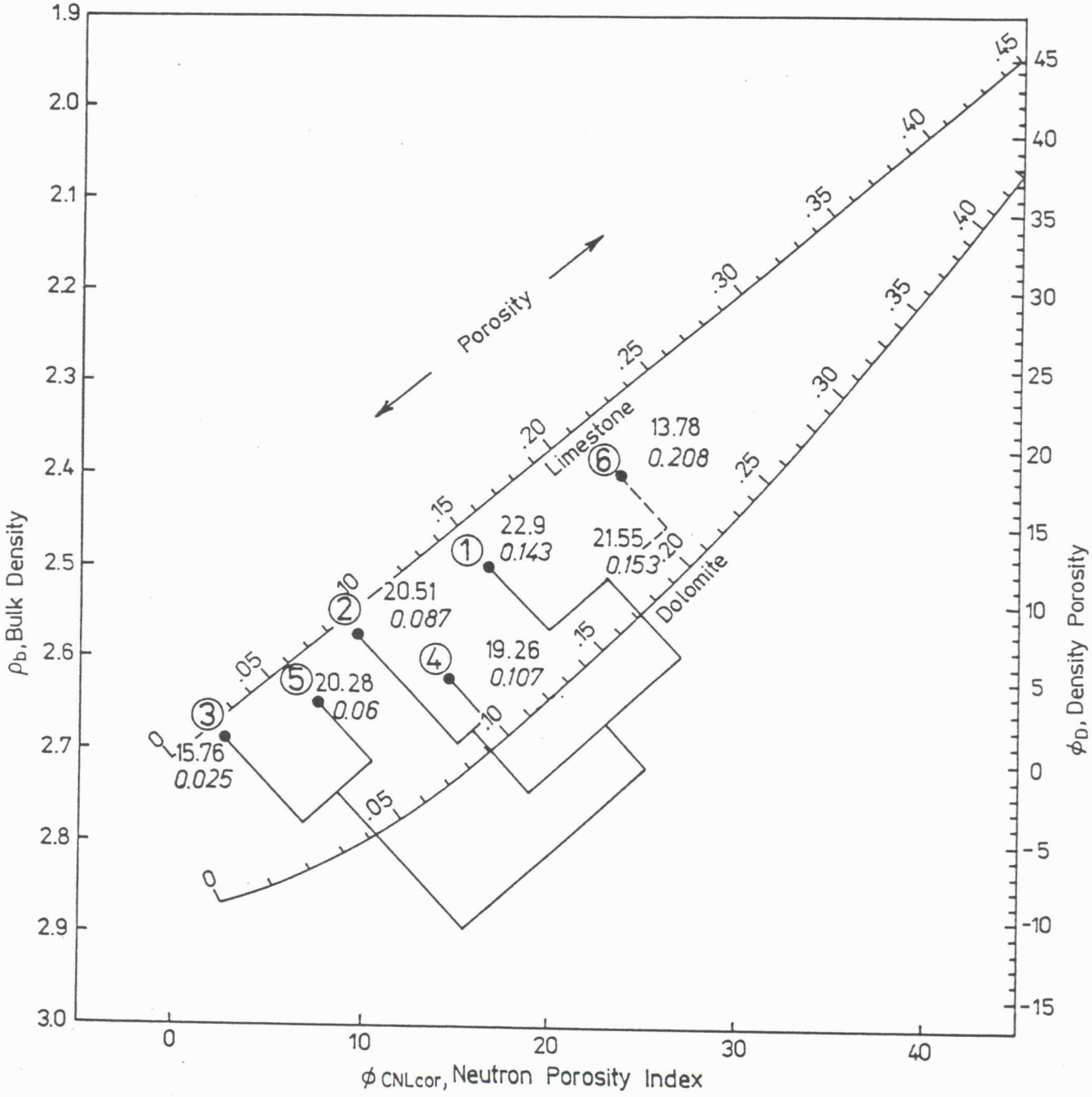


**Figure 4.4.** Typification of Ordovician carbonates within the Zenith field. Dots represent centroids of classes. Numbers in circles indicate class number. Average $GR = 22.9$. Average porosity $= 0.143$.

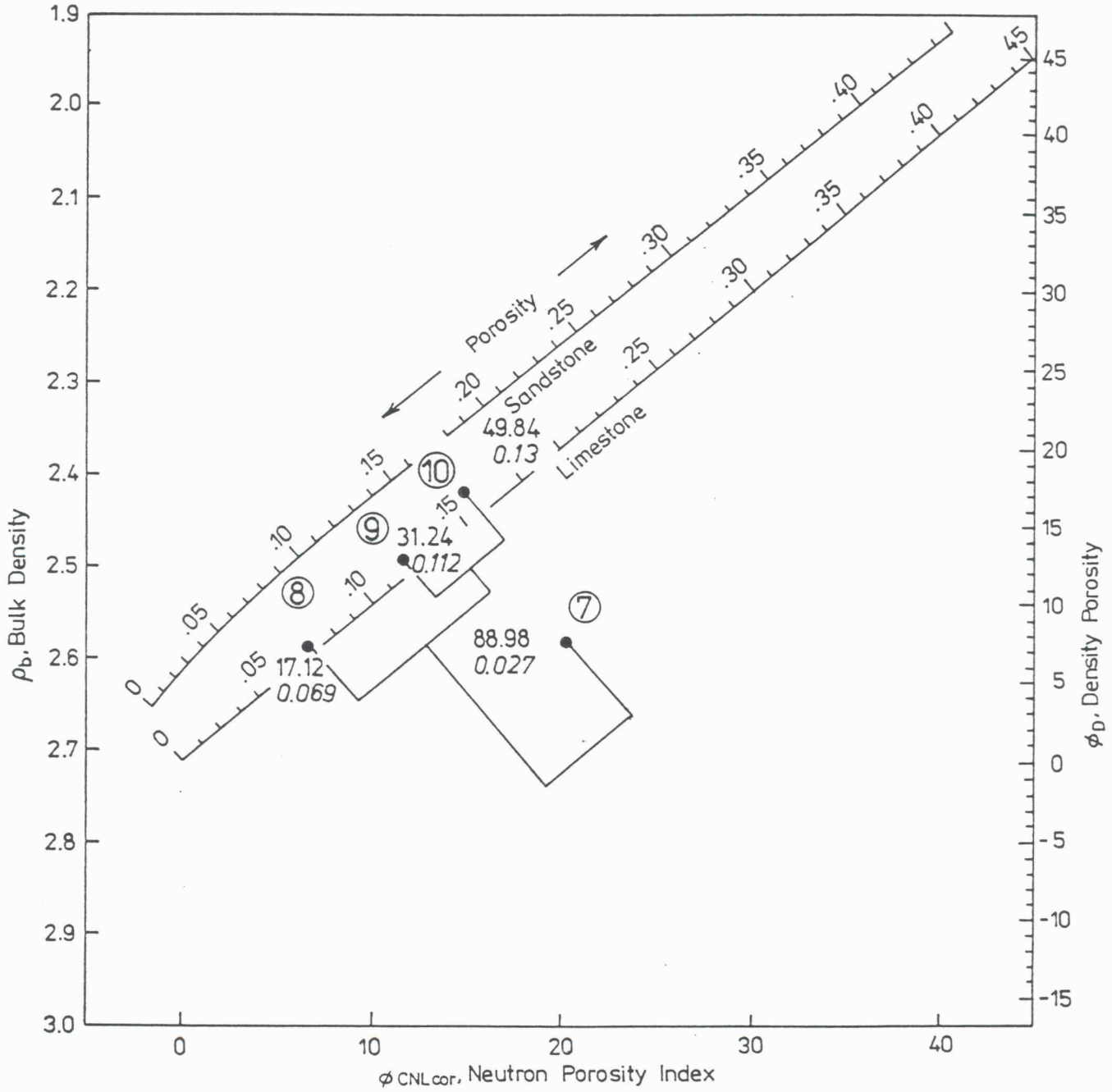


**Figure 4.5.** Typification of Devonian/Mississippian siliciclastics within the Zenith field. Dots represent centroids of classes. Numbers in circles indicate class number. Average $GR = 88.98$. Average porosity $= 0.027$.

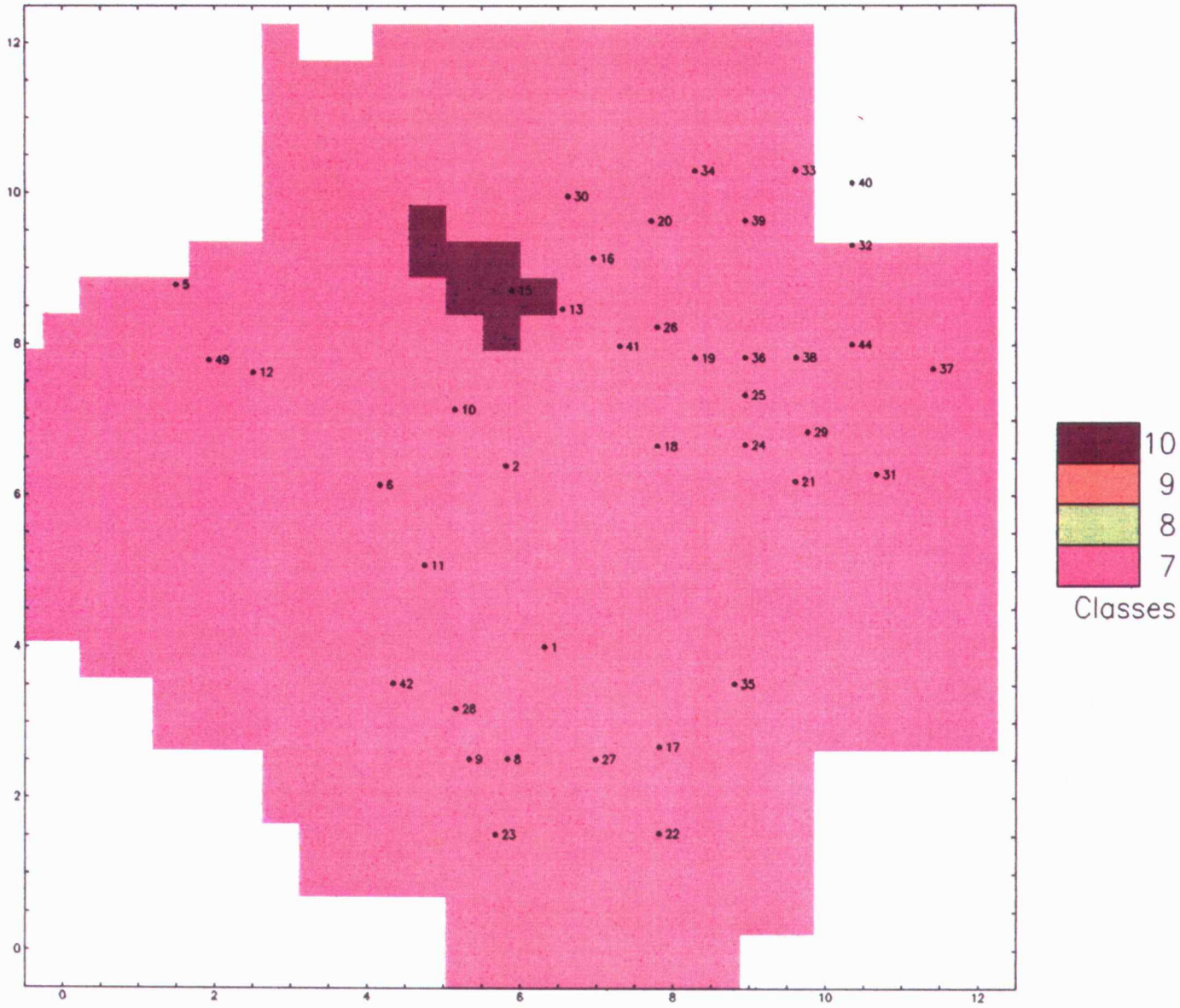


**Figure 4.6.** Regionalization of the Viola 3, Zenith field.

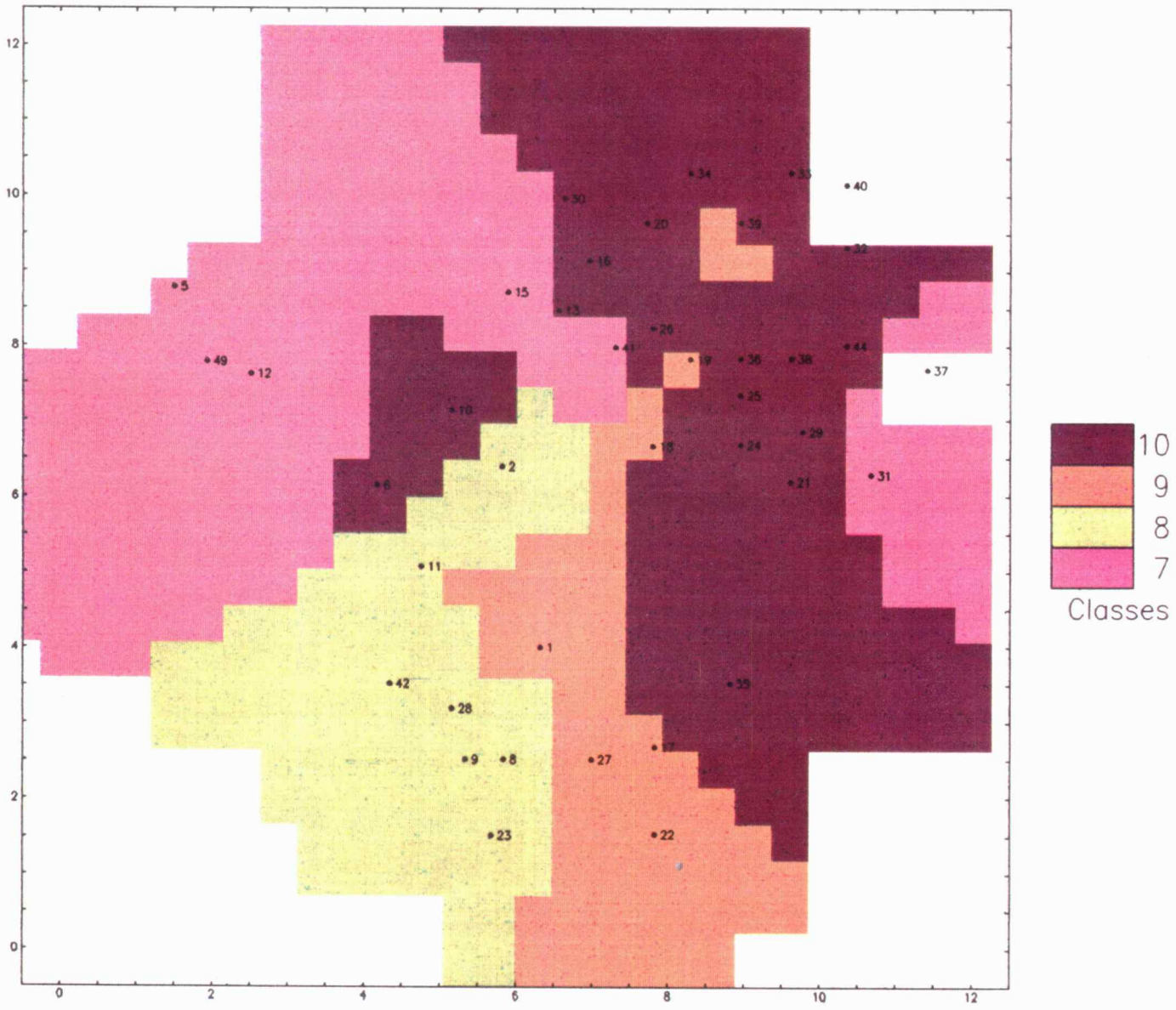


**Figure 4.7.** Regionalization of the Viola 2, Zenith field.

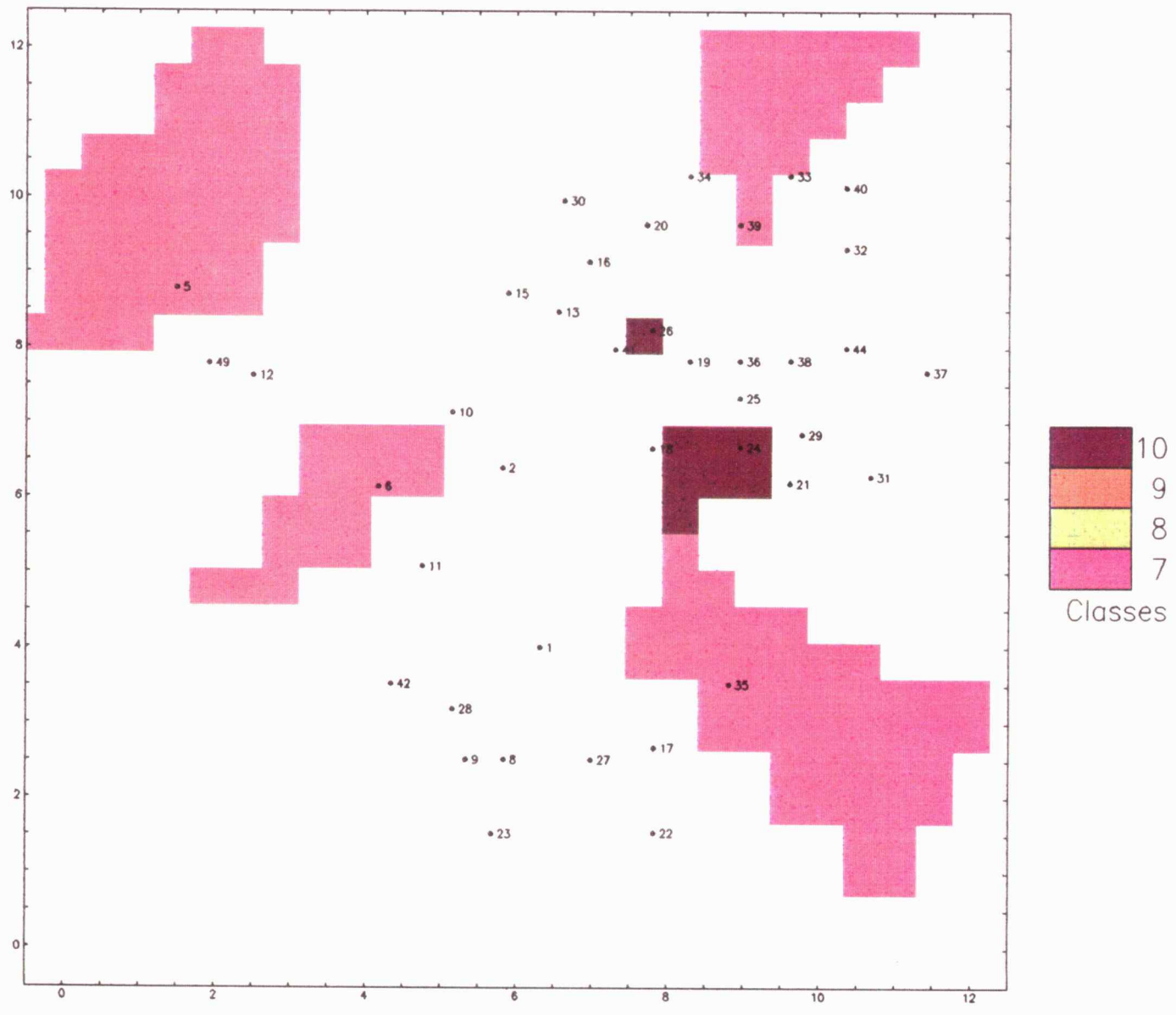


**Figure 4.8.** Regionalization of the "Hard Streak," Zenith field.

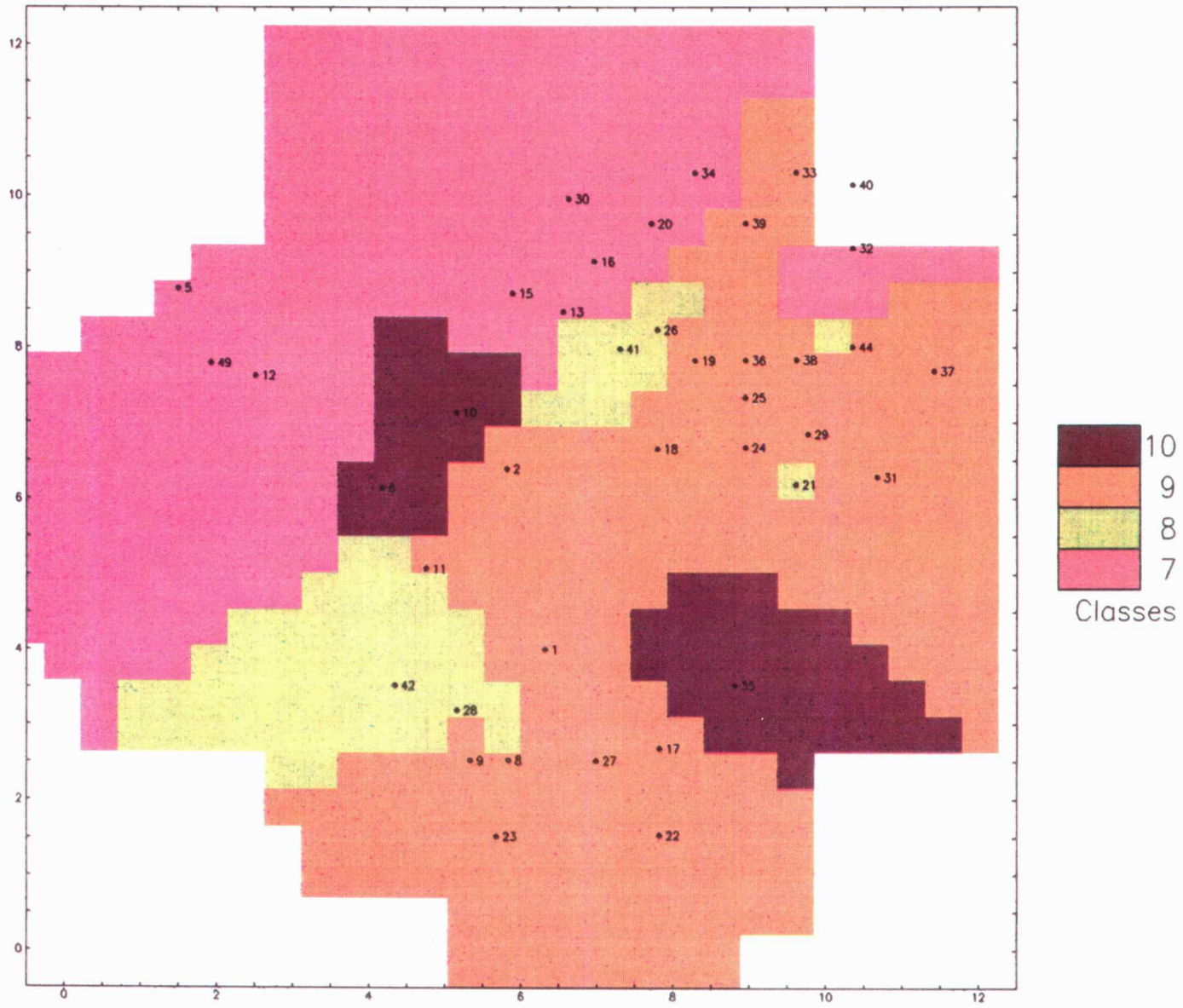


**Figure 4.9.** Regionalization of the Viola 1, Zenith field.

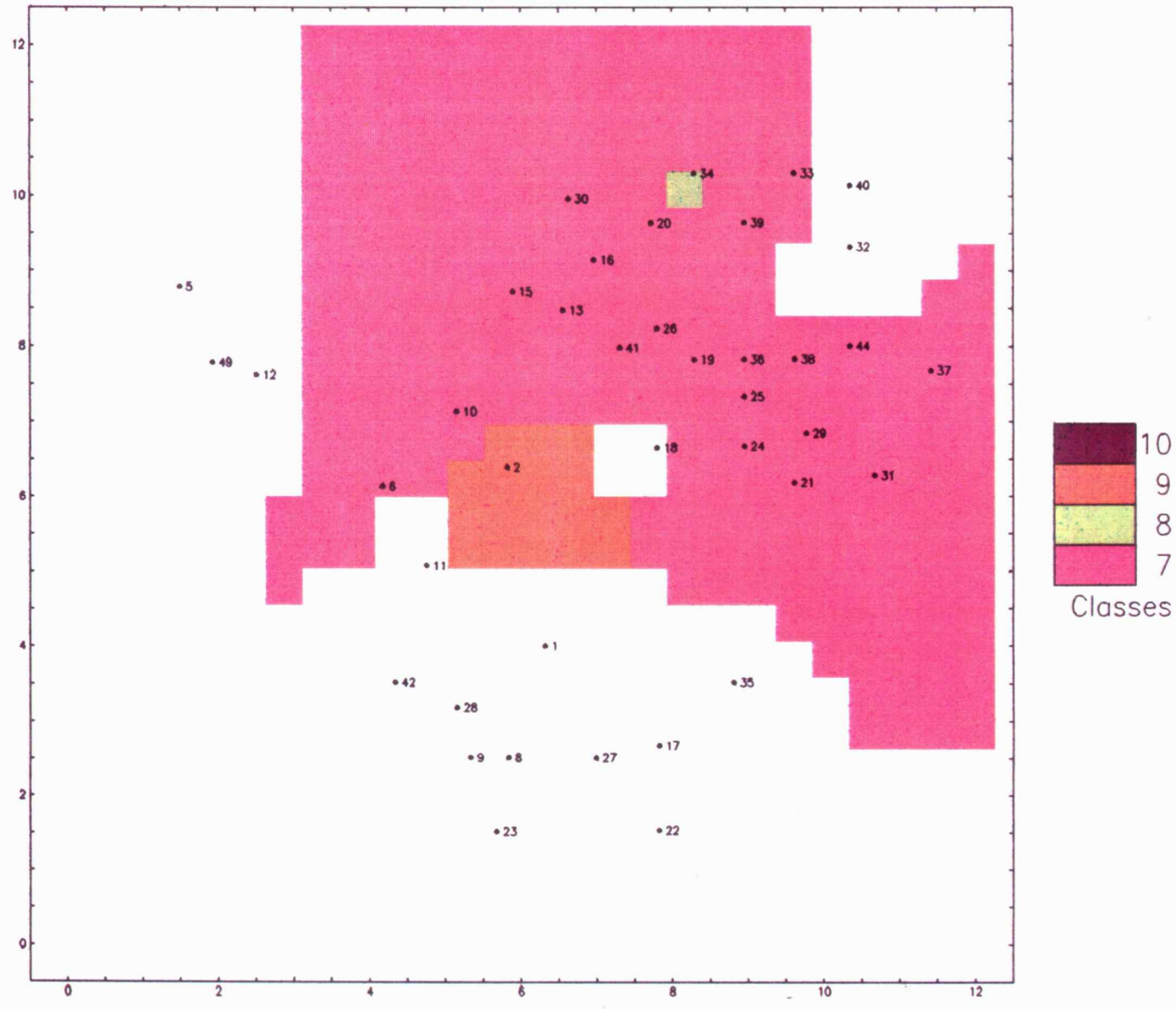


**Figure 4.10.** Regionalization of the Fernvale, Zenith field.

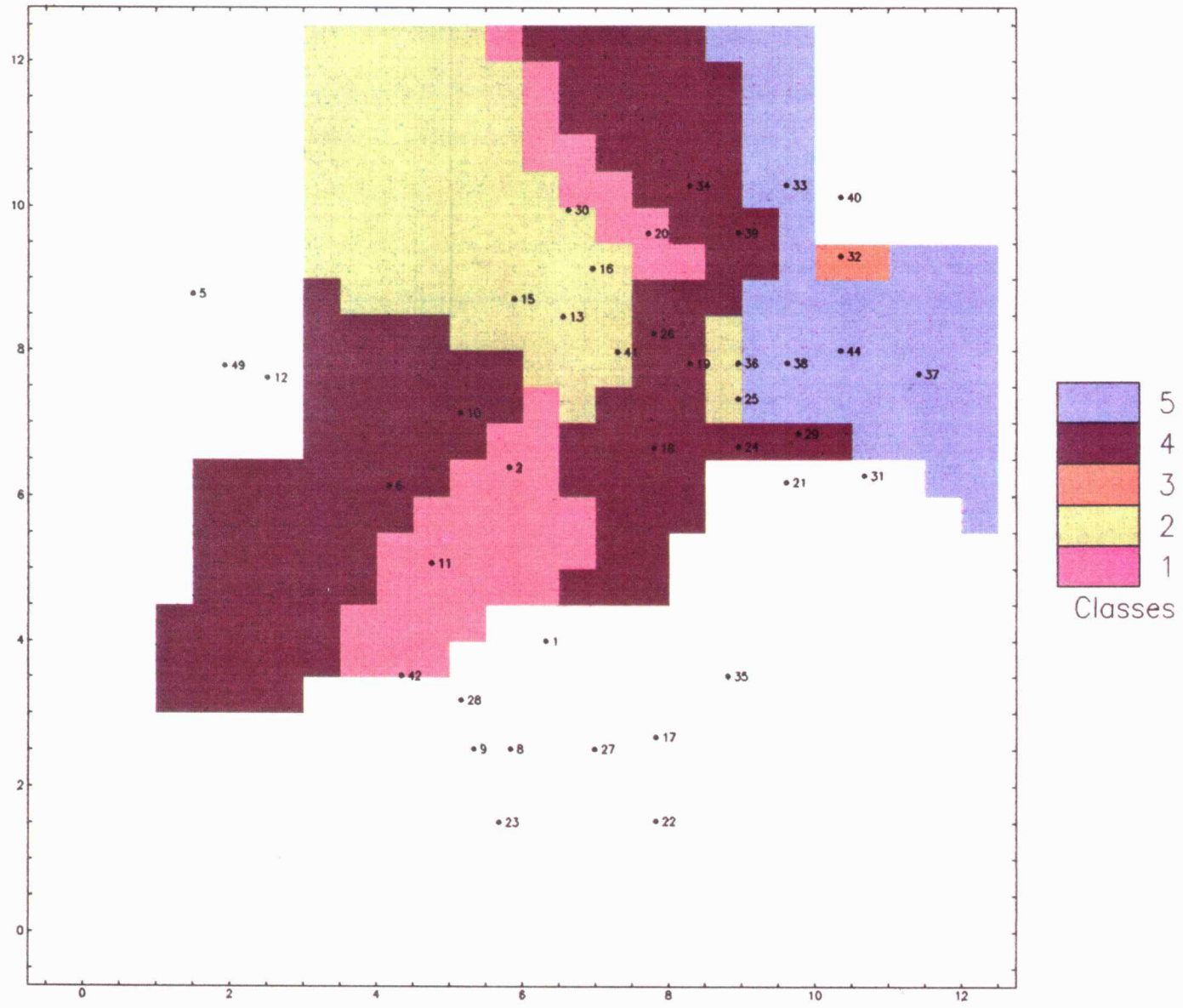


**Figure 4.11.** Regionalization of the Maquoketa layer, Zenith field.

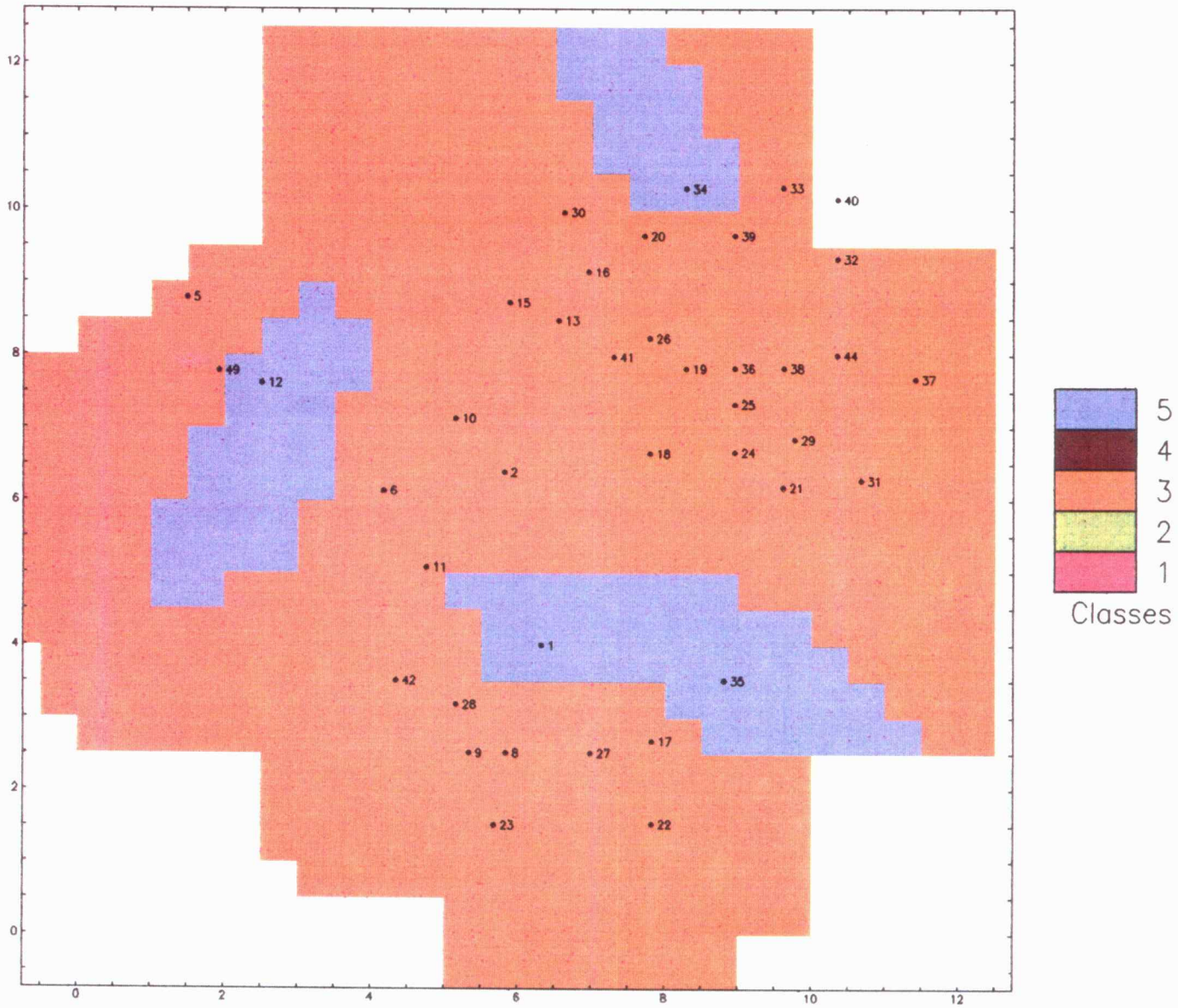


**Figure 4.12.** Regionalization of the Misener IV layer, Zenith field.

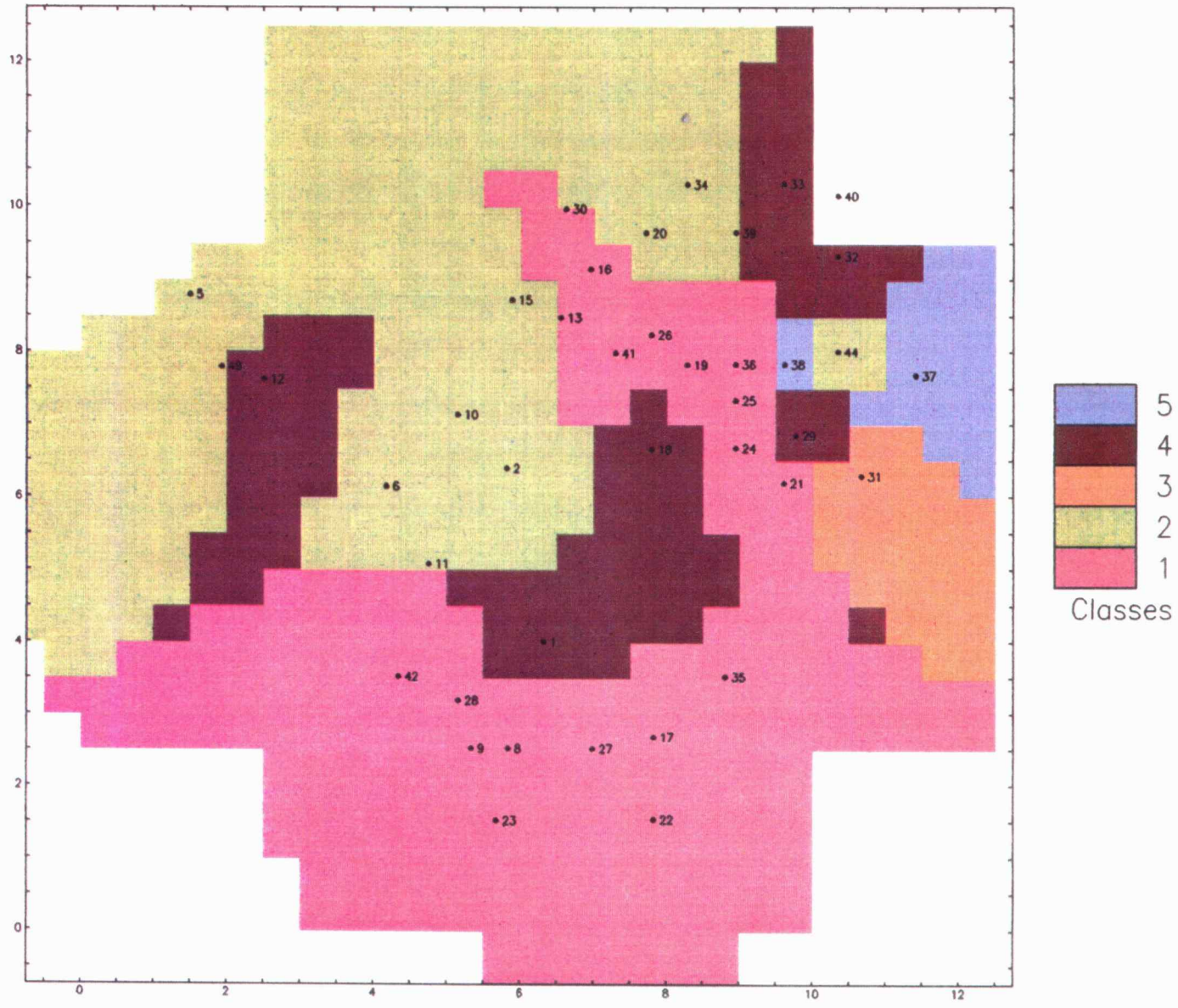


**Figure 4.13.** Regionalization of the Misener III ("lower Misener") layer, Zenith field.

has a regionalization (Fig. 4.15) similar to the "lower Misener." Note the regional increase in the "Misener limestone" (class 8) to the east. This coincides with onlapping in the geological model developed by Newell *et al.* (1991). The large area occupied by class 10 to the east also is notable.

The Chattanooga Shale (Fig. 4.16) is represented mostly by class 7, which represents shales. The small subregion belonging to class 10 is caused by sandy beds within the Chattanooga interval. These beds were assigned by Newell *et al.* (1991) to the Misener sandstone.

A three-dimensional display of the generalized data model of the Zenith field is given in Figure 4.17. Figures 4.18 and 4.19 show a graphics workstation display of a north–south and west–east cross-section.

## 4.3 Using the PC Program BASIN for Structural Modeling

In this study, regionalization of the Zenith field required using a combination of SPSS$^{TM}$, SURFACE III, and CORRELATOR programs. The software package BASIN (Springer, Lewerenz and Harff, 1990), developed at the Central Institute for Physics of the Earth, can also perform the regionalization and gridding processes.

Because BASIN uses its own format to store and interpolate grids, a program named GRIDCON converts the grids into column-oriented ASCII files. These ASCII files can be read by the SGM program running on the Silicon Graphics workstation.

The file containing results of zonation (ZENMEAN.DAT) provided the $x$ and $y$ coordinates and the thicknesses which are necessary to create a data base in the BASIN software. This file (ZENITH.SUB) also contained data from higher stratigraphic intervals which are not included in the ZENMEAN.DAT file. In addition, file ZENITH.REG, containing the stratigraphy, time scale, and lithotypes was provided. From these data surfaces representing the Chattanooga Shale, Misener I–Misener IV, Maquoketa dolomite, Fernvale, Viola I, "Hard Streak," Viola II, and Viola III were selected, interpolated to a $50 \times 50$ grid, and converted into ASCII files. With the aid of SGM, a structure model was built from these layers and two displays were created. Figures 4.20 and 4.21 show the entire structural model and a cross-section from northwest to southeast. Unfortunately, SGM does not support color output devices, so the figures are copies of photographs of the screen display of the Silicon Graphics workstation.

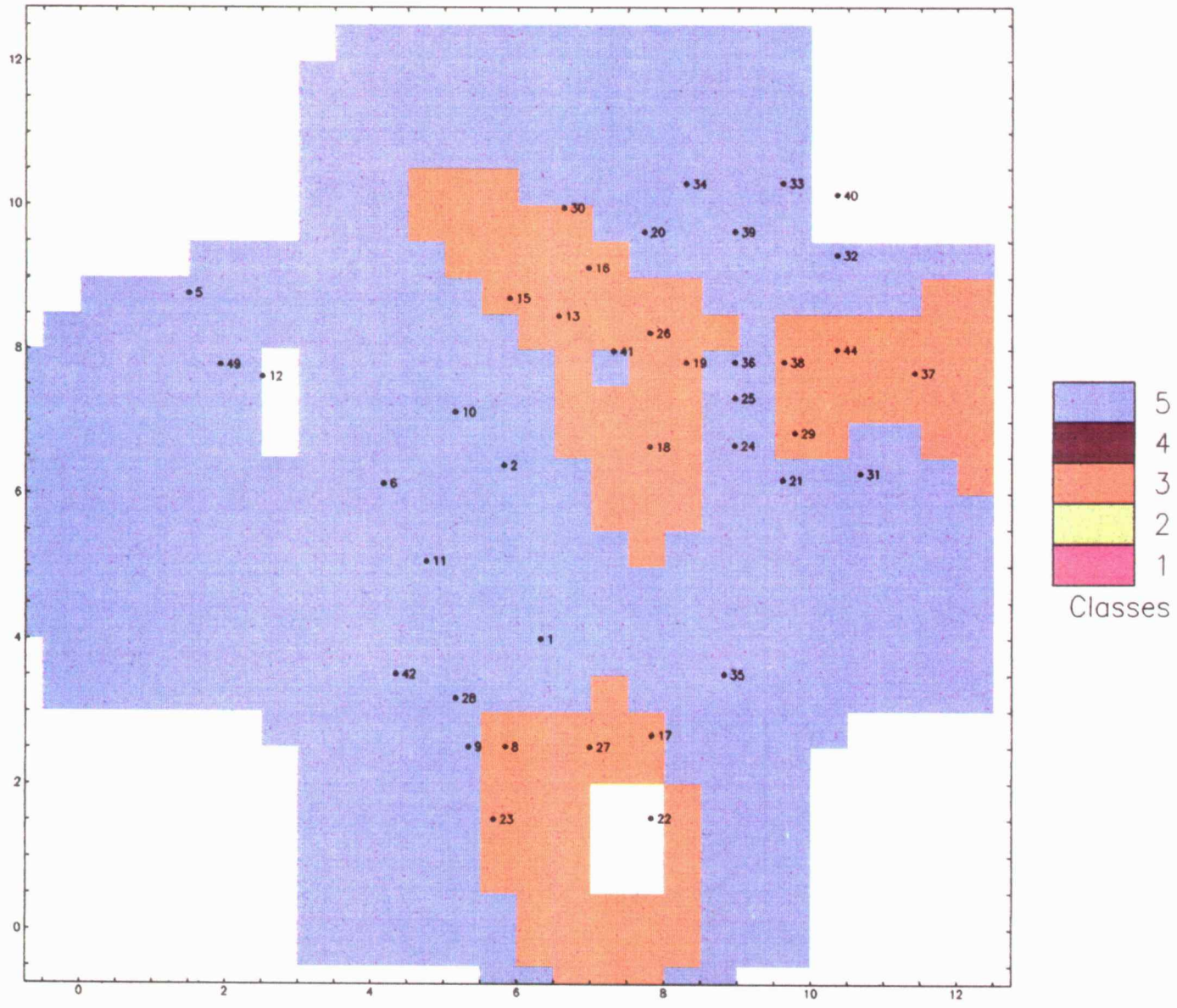


**Figure 4.14.** Regionalization of the Misener II layer, Zenith field.

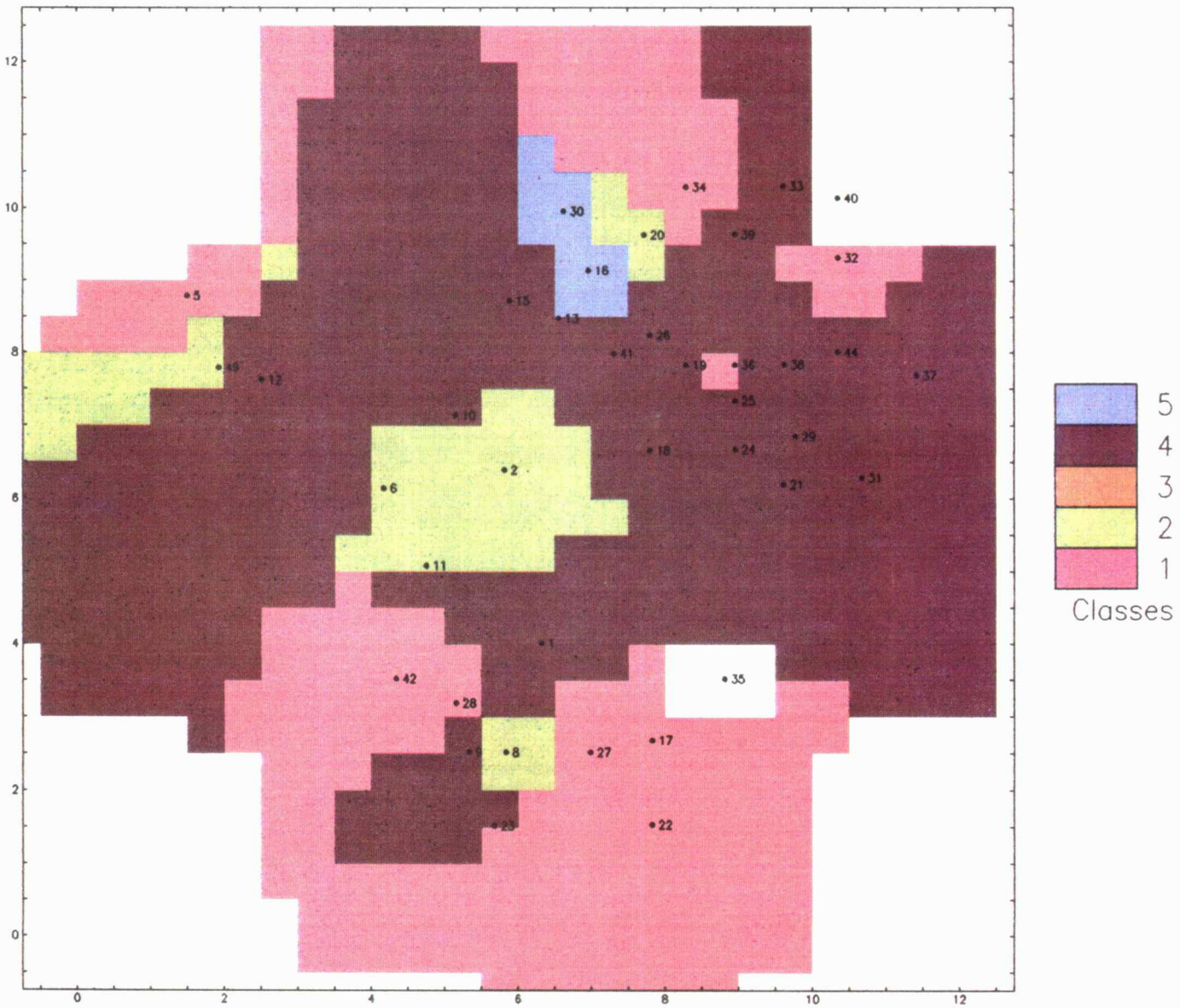


**Figure 4.15.** Regionalization of the Misener I ("upper Misener") layer, Zenith field.

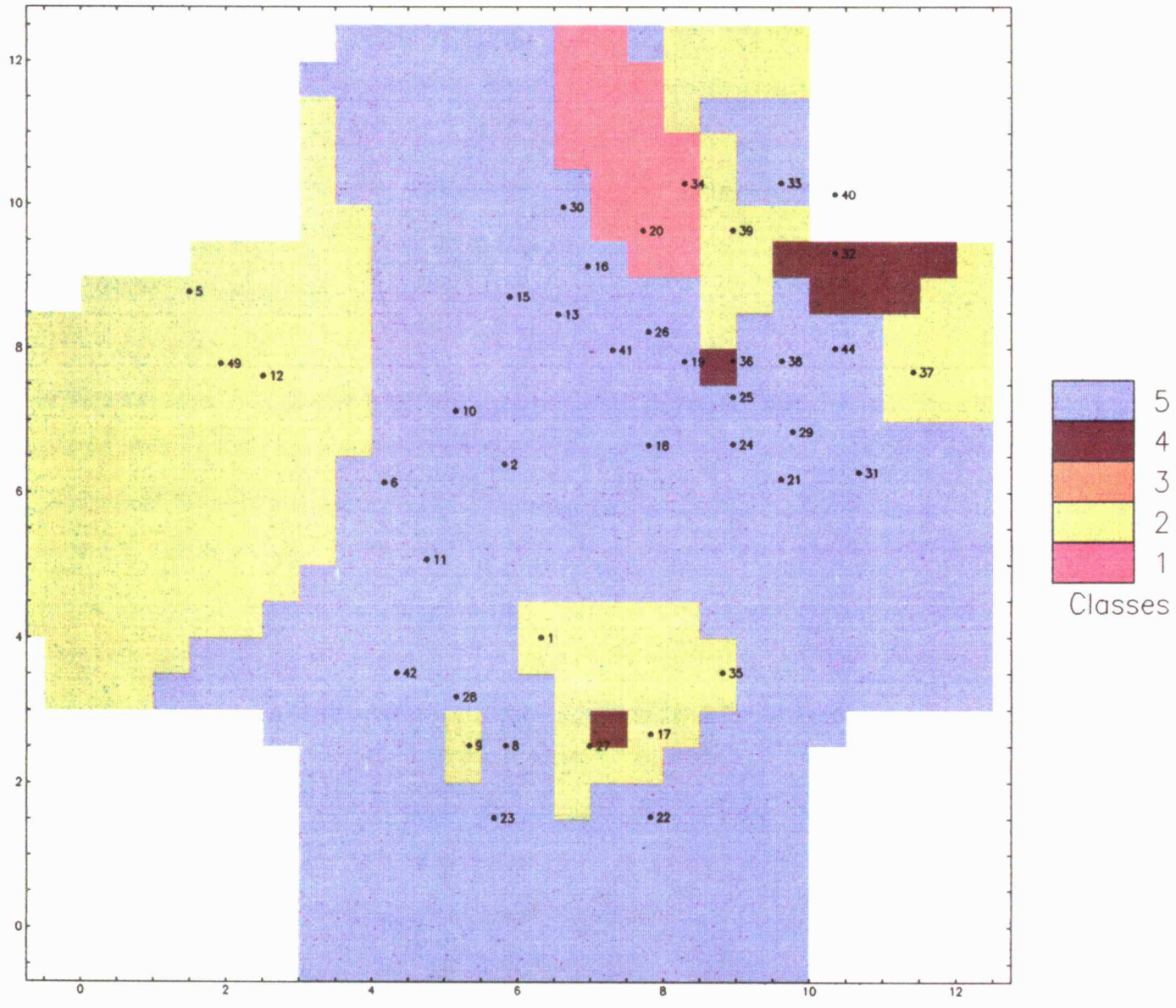


**Figure 4.16.** Regionalization of the Chattanooga Shale, Zenith field.

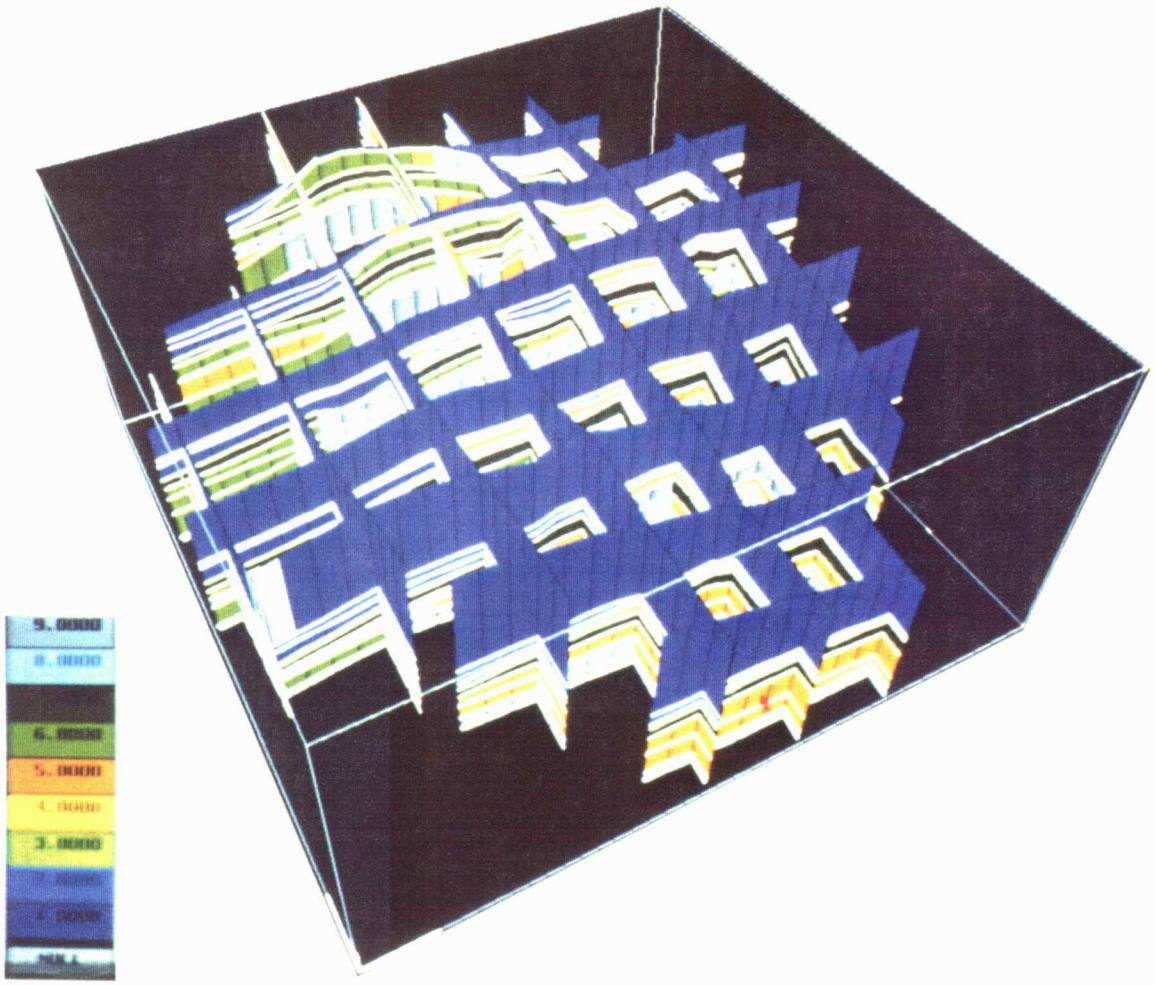


**Figure 4.17.** Results of regionalization, Zenith field.

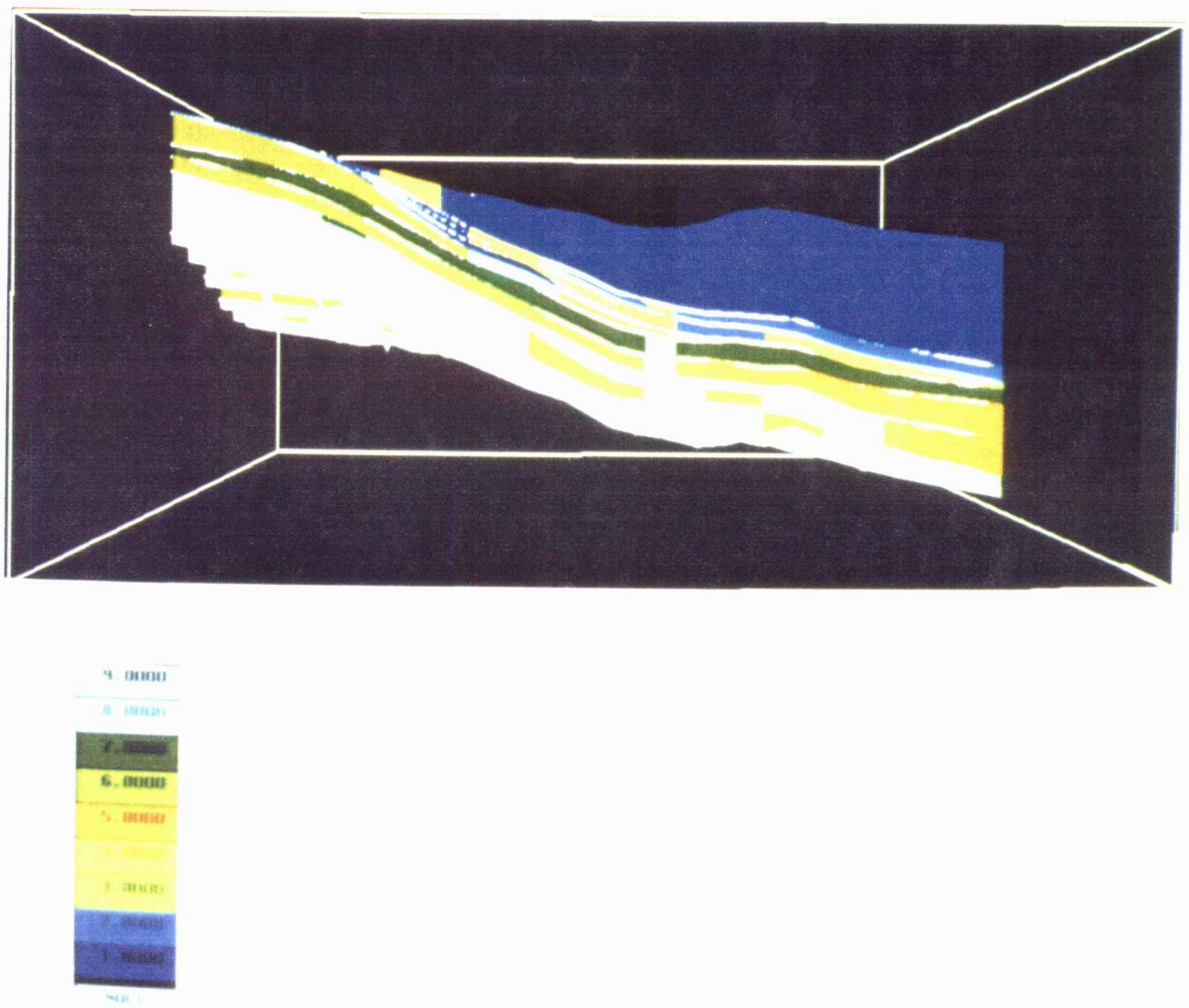

**Figure 4.18.** Result of regionalization–north/south cross-section.

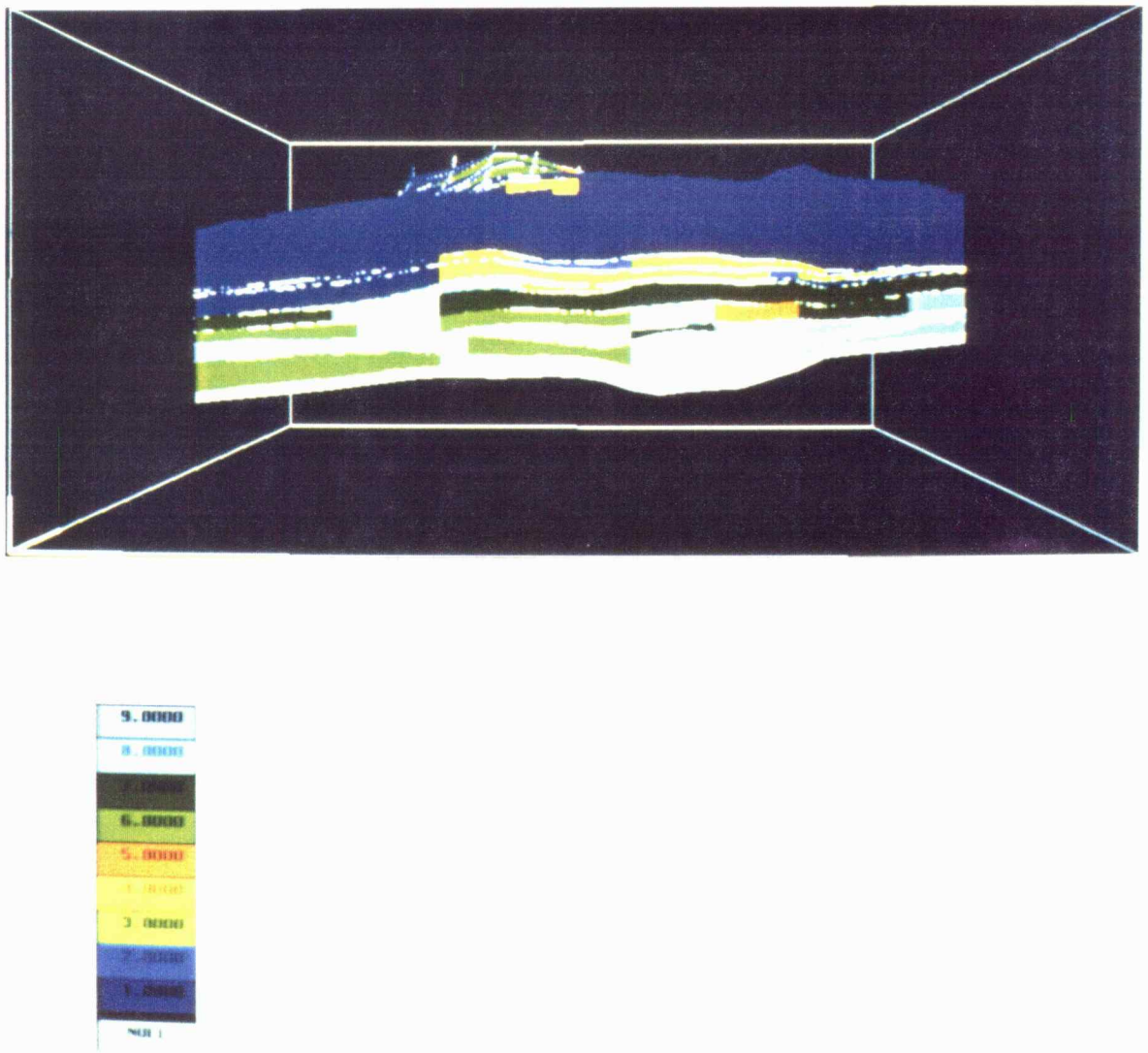


**Figure 4.19.** Result of regionalization-east/west cross-section.

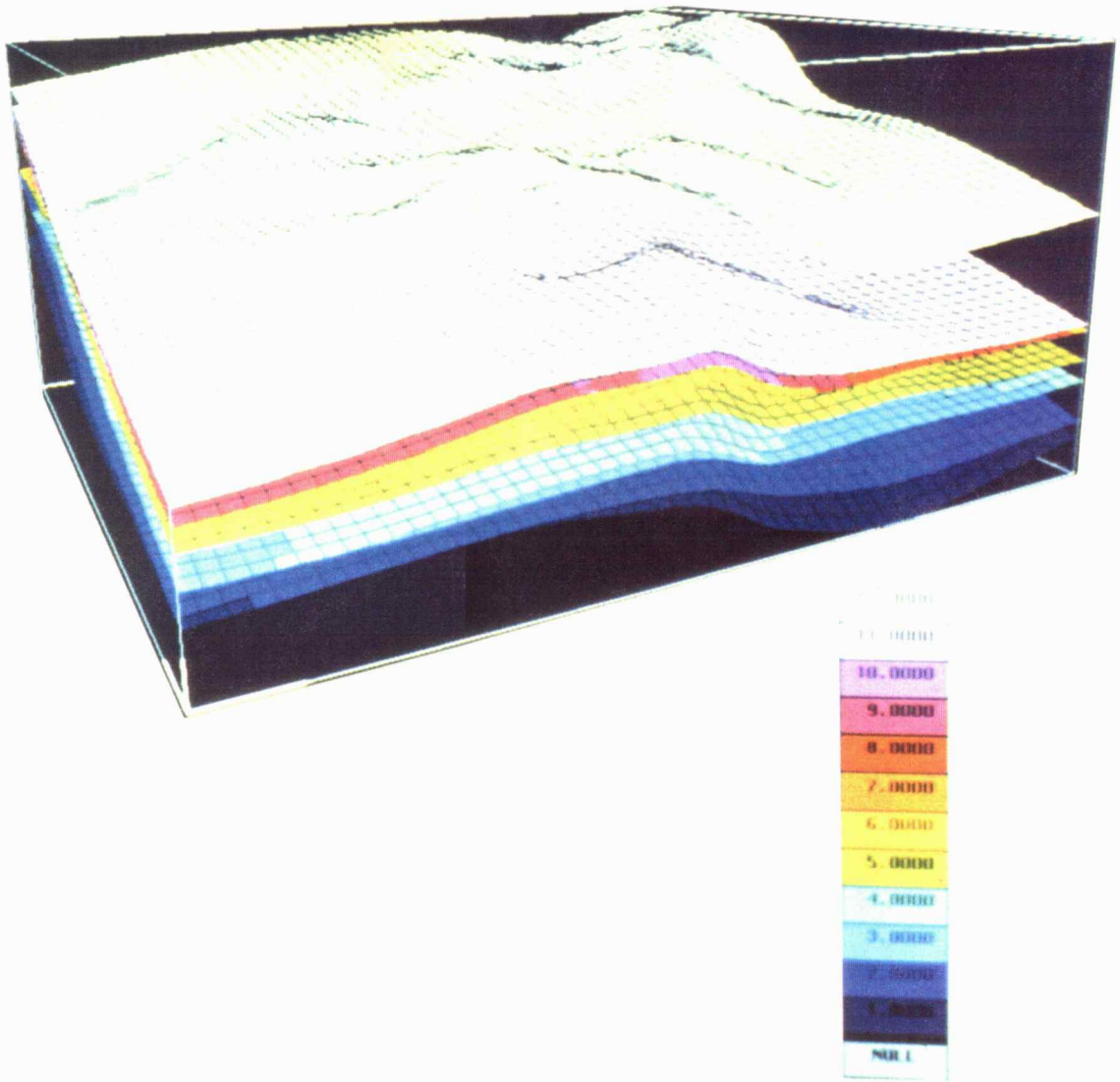


**Figure 4.20.** Structure of the Zenith oil field.

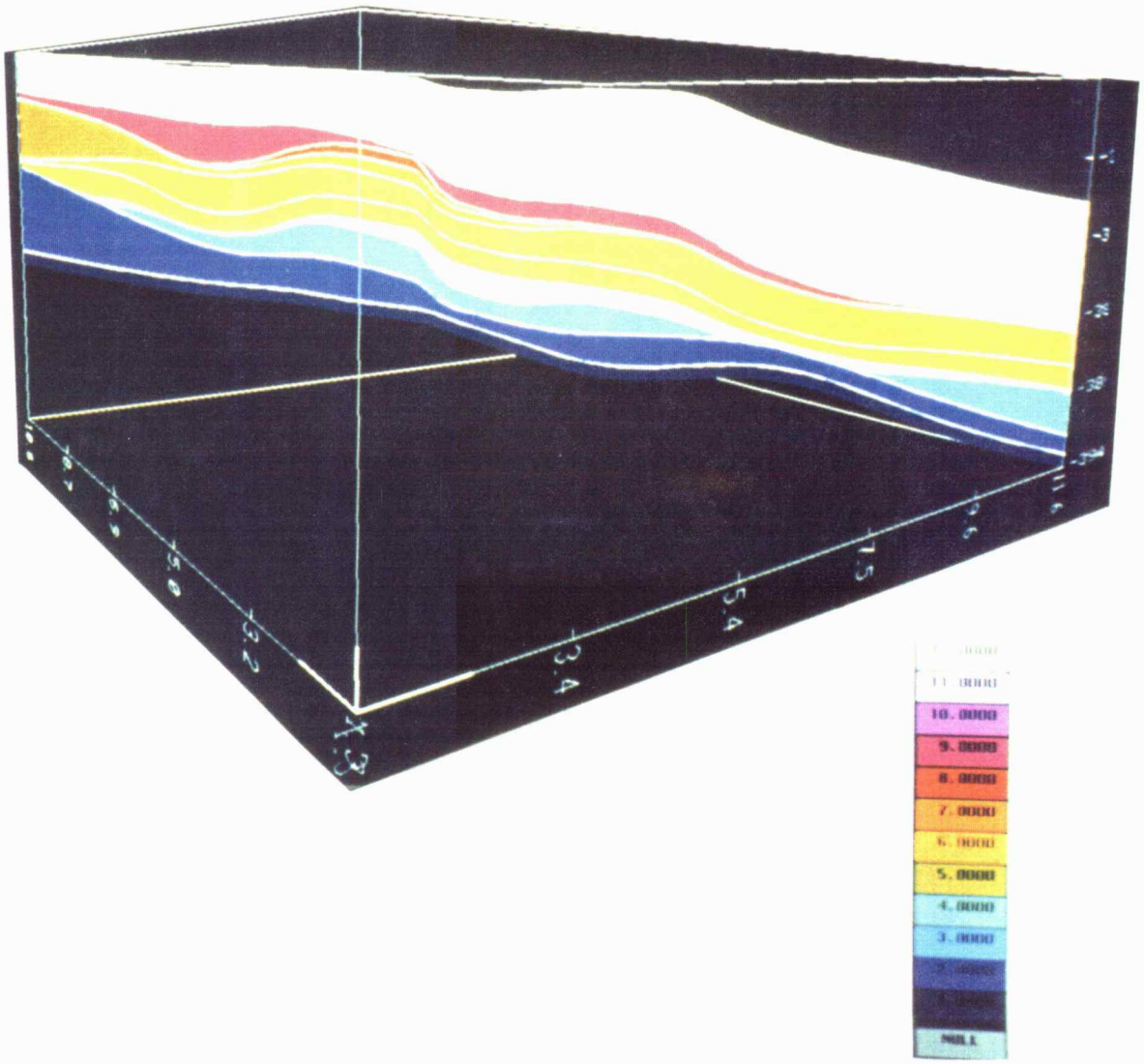


**Figure 4.21.** Cross-section through the layers of the Zenith oil field (NW–SE).

## REFERENCES


Harff, J. and Davis, J.C., 1990, Regionalization in geology by multivariate classification: *Mathematical Geology*, vol. 22, no. 5, p. 573–588.

Kansas Geological Survey and Tertiary Oil Recovery Project, 1991, Zenith field—A field demonstration project for improved efficiency for oil and gas recovery in Kansas: *Final Report submitted to the Kansas Corporation Commission*, Topeka, Kansas, 263 pp.

Krumbein, W.C. and Sloss, L.L., 1963, *Stratigraphy and Sedimentation:* W.H. Freeman & Co., San Francisco, California, 660 pp.

Olea, R.A., 1988, CORRELATOR—An Interactive Computer System for Lithostratigraphic Correlation of Wireline Logs: *Kansas Geological Survey, Petrophysical Series no. 4*, University of Kansas, Lawrence, Kansas, 85 pp.

Olea, R.A. and Davis, J.C., 1989, An expert system for the correlation of geophysical well logs, *in* Simaan, M. and F. Aminzadeh (eds.), *Advances in Geophysical Data Processing*, Vol. III: Jai Press, Inc., Greenwich, Connecticut, p. 279–307.

Olea, R.A., Newell, K.D., and Harff, J., 1991, Geologic modeling of the Zenith field, Kansas, using CORRELATOR: *Kansas Geological Survey, Open-File Report no. 91-39 (two vols.)*, University of Kansas, Lawrence, Kansas, 456 pp.

Springer, J., Lewerenz, B. and Harff, J., 1990, *BASIN—Modeling of Sedimentary Basins: User's Guide:* ZIPE, Potsdam, FRG, 17 pp.

Weaver, C.E., 1958, Geologic interpretation of argillaceous sediments, parts I and II: *Am. Assoc. Petroleum Geologists Bulletin*, vol. 42, no. 2, p. 254–309.

# 5. PARAMETER MODELS

J.H. Doveton, J. Harff, J.C. Davis, J. Springer, and P. Hoth

## 5.1 Permeability Prediction and Parameter Models

The aim of parameter modeling is to derive permeability $k$ from wireline logs. Traditional methods to predict permeability from logs use empirical equations of the type:

$$k = A\Phi^B$$

where $A$ and $B$ are constants determined from core measurements and then applied to log measurements of porosity ($\Phi$) to generate predictions of permeability ($k$). The results may be adequate for homogeneous sandstones, but prediction errors are often large in more typical sandstones, and the errors in predicted permeability commonly range across orders of magnitude when applied to carbonates. This is because permeability is not exclusively determined by pore volume, but is also controlled by internal surface area, pore network tortuosity, pore throat geometry, and other variables.

The widely used equation of Timur (1968) linked permeability with both porosity and irreducible water saturation ($S_{wi}$) in sandstones and, based on laboratory measurements of core, suggested a considerable improvement in permeability estimation. Unfortunately, the use of irreducible water saturation as an input variable restricts the method to virgin hydrocarbon reservoir zones. Further, the log calculations of irreducible water saturation are themselves estimates, whose error magnitude is controlled by choices of values for Archie's cementation factor and saturation exponent.

In spite of these limitations, the success of the Timur equation, whose generic form is:

$$k = \frac{A\Phi^B}{S_{wi}^C},$$

can be understood when it is compared with the classic Kozeny-Carman equation:

$$k = \frac{A\Phi^3}{(1-\Phi)^2 S^2},$$

which incorporates the specific surface area, $S$. The specific surface area is the ratio of surface area to volume of framework solid and is difficult to measure directly by conventional methods. However, the specific surface area is inextricably linked with pore size, which in turn controls irreducible water saturation. The irreducible water saturation term in the Timur equation therefore functions as a surrogate variable for specific surface area, and this accounts for the improvement in permeability estimates when incorporated with porosity.

The morphology of the rock framework is the exact complement of the internal geometry of the pore network. Therefore, measures which are sensitive to characteristics such as grain or crystal size will be useful indicators of specific surface, and estimators of permeability. The control of permeability by grain size and sorting in sandstones has been documented for many years (*e.g.*, Krumbein and Monk, 1942). Analogous relationships which link porosity and crystal or grain size in carbonates also have been widely reported (*e.g.*, Choquette and Traut, 1963).

Modern logging tools are sensitive to framework compositions rather than directly to grain size. Herron (1987) pointed out that rather than being a limitation, this characteristic has definite advantages. Within clastics, permeability is controlled by a complex association of disparate factors such as texture (grain size, shape, and sorting), and the quantity and types of cementing minerals and clay minerals. Textural maturity, cements, and clays are all reflected in mineral compositions and these can be deduced from several types of logs. Herron (1987) has applied this concept successfully in an adaptation of the Kozeny-Carman equation which substitutes mineral-assemblage estimates from logs for the specific surface term. In experiments with clastics, he was able to develop useful predictive relationships for permeability by multiple regression analysis of elemental log data.

These ideas can be extended to carbonates in models which incorporate factors of depositional fabric together with diagenesis. Several log measures should be useful, particularly since diagenesis is commonly linked with changes in mineral composition.

### 5.1.1 Regression Prediction of Permeability

In the Zenith field study, predictive models for permeability were based on the following variables:

Permeability $k$ [md]
Porosity determined from core analysis $PORC$ [%]
Neutron porosity (corrected)

$$\Phi_{Ncorr} = \Phi_N - \left[\frac{\Phi_{Nclay}}{0.45} * 0.3 * V_{sh}\right]$$

Density porosity (corrected)

$$\Phi_{Dcorr} = \Phi_D - \left[\frac{\Phi_{Nclay}}{0.45} * 0.3 * V_{sh}\right]$$

Porosity determined from wireline logs

$$PORW = \sqrt{\frac{\Phi^2_{Ncorr} + \Phi^2_{Dcorr}}{2.0}}$$

Intensity of natural gamma radiation $GAM$

$V_{sh}$ is not involved in the analysis, but is used for calculating $\Phi_{Dcorr}$ and $\Phi_{Ncorr}$. $V_{sh}$ is defined by

$$V_{sh} = 0.33\left[2^{(2*I_{GR})} - 1.0\right].$$

The equations were taken from Asquith and Gibson (1982).

Data from three wells (ZU 1, ZU 3, ZU2W2) were used in a separate analysis for the clastics (layers 2–4) and the carbonates (layers 6–10). Permeability was expressed in logarithmic units as $LOGk$, because raw permeability measurements tend to follow a positively skewed distribution which may be lognormal. An additional variable was defined,

$$L = \Phi_{Ncorr} - \Phi_{Dcorr},$$

which is a useful measure of either shaliness or reservoir framework mineralogy, as will be discussed in connection with the regression prediction models for permeability.

Crossplots of these variables for carbonates (46 samples) are shown in Figure 5.1 and for clastics ("Misener") in Figure 5.2 (16 samples). For both carbonate and clastic samples, the multivariate linear regression model

$$LOGk = a_0 + a_1 PORW + a_2 L + a_3 GAM$$

was applied to the samples separately. Because of petrographic and petrophysical differences between clastics and carbonates, the physical significance of these variables also differs. In both samples, the volumetric porosity $PORW$ is expected to be positively correlated with permeability. However, the association will be affected by the relative homogeneity of pore types and the dominant pore geometry, which will determine both the degree of correlation and the slope coefficient within the regression equation.

The quantity $L$ is the difference between the neutron and density porosity measurements as recorded on an apparent limestone porosity scale. Within clastics, $L$ is expected to be primarily a measure of clay-mineral content, expressed by higher positive values of $L$. If clay minerals play a significant role in permeability reduction in the "Misener" clastics, this variable may make a useful contribution to permeability prediction. In

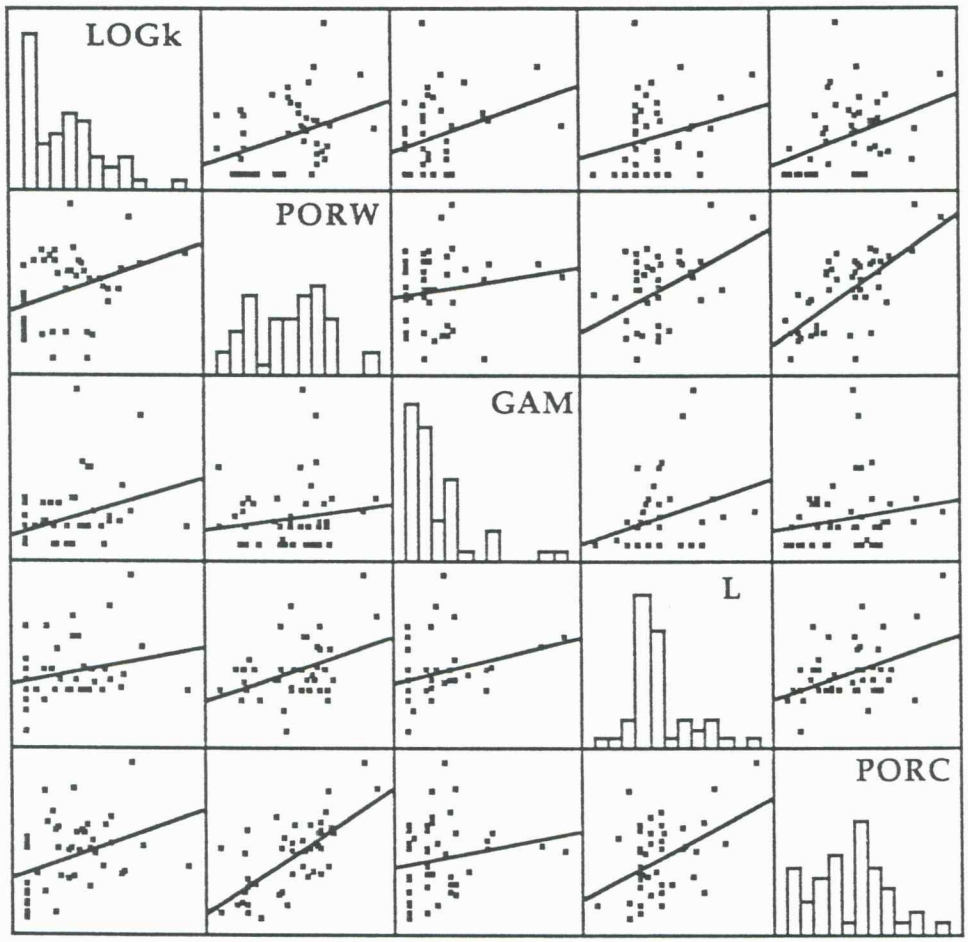


**Figure 5.1.** Cross-plots between variables *LOGk*, *PORW*, *GAM*, *L*, and *PORC* for the carbonate Ordovician sequence of the Zenith field.

shale-free carbonates, $L$ provides a crude measure of dominant matrix mineralogy. The expected value for $L$ is zero in pure limestone zones. Increasingly larger positive values of $L$ reflect higher levels of dolomitization. Negative values of $L$ are caused by "silica," either as quartz sand or chert nodules. If $L$ is a significant variable in predicting permeability, the most likely explanation is that the variable has picked up significant differences in pore geometry linked with petrographic facies types.

The variable *GAM* is a measure of natural gamma radiation from potassium and the thorium and uranium families of isotopes. Within clas-

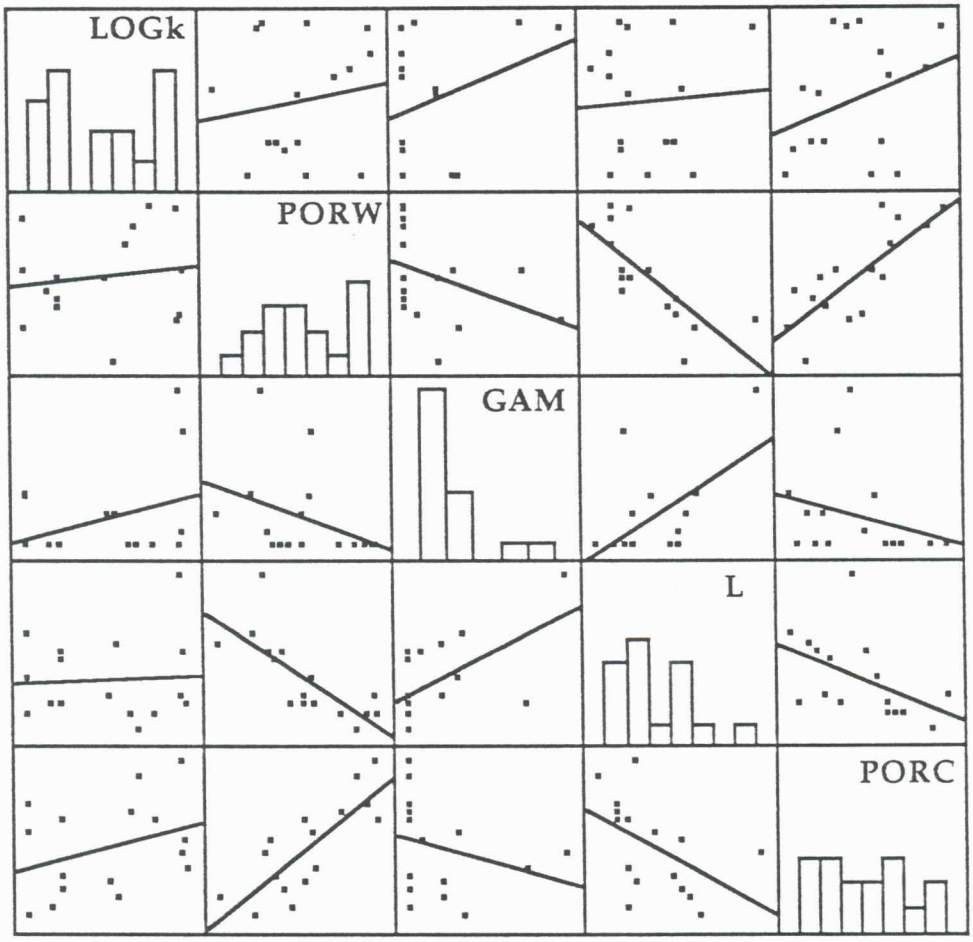


**Figure 5.2.** Cross-plots between the variables *LOGk*, *PORW*, *GAM*, *L*, and *PORC* for the clastic ("Misener") sequence of the Zenith field.

tics, the major source of radioactivity is clay minerals. However, other radioactive minerals such as feldspars, micas, and zircons may also contribute. It should be possible to distinguish between radioactivity attributable to clays and to other sources in this regression model, because the variable $L$ is also sensitive to clay minerals. Shale-free carbonates generally have low levels of radioactivity. Exceptions have been observed where uranium concentrations precipitated by fluids migrating through fractures have caused radioactive zones.

Exploratory multiple regression analysis of permeability, $LOGk$, as a function of these three log variables shows that $L$ makes no significant contribution to prediction in either clastics or carbonates. In the case of the "Misener" clastics, this suggests that clay-mineral content is not a major control on permeablity, although its deleterious effects cannot be discounted entirely. For the carbonates, the lack of significance for $L$ means that differences in reservoir matrix mineralogy cannot be construed as a major factor in textural controls of permeability. However, this does not imply that there are no differences in pore volume in different lithofacies; relationships between permeability and porosity should be reflected in the $PORW$ variable.

With elimination of the lithology variable, $L$, the models for both clastics and carbonates are reduced to regressions of permeability on porosity and gamma radiation intensity. Coefficients for the regression functions are given in Table 5.1. In both cases, there is a positive relationship between porosity and permeability, and the difference in loading reflects distinctions between clastic and carbonate pore morphology.

In addition, there is a positive correlation between $LOGk$ and $GAM$ in both clastics and carbonates (see also Figs. 4.6 and 4.7). Initially, this positive link of permeability with gamma-ray readings in the "Misener" clastics seemed at variance with the expectation that $GAM$ reflects clay mineral content, and should be negatively correlated with permeability. However, the elimination of the lithology variable, $L$, from the regression model indicates that shale is not a significant factor. Instead, the relationship can be explained by the occurrence of significant quantities of apatite within the "Misener sandstone." Uranium associated with apatite accounts for the increase in gamma-ray values within these zones and their positive relation with permeability.

Within the carbonates, there is also a positive contribution of the gamma-ray log reading to permeability prediction. As with the clastics, the lack of significance of the lithology variable $L$ tends to discount shale as a potential control of permeability. This association is probably caused by uranium mineralization introduced by the migration of fluids through fracture systems. These fracture zones may be marked by enhanced permeabilities.

The small sample size (16 observations) available for permeability prediction in "Misener" clastics precludes a statistically significant result. The multiple regression accounts for only 21% of the total variance and shows that predictions of permeability at 1-foot depth increments have high associated error. However, the adverse implications are significantly reduced because predictions are made only at the much coarser level of average permeabilities for the different lithotypes.

**Table 5.1.** Results of Regression Analysis and Analysis of Variance for (a) Ordovician Carbonates and (b) Devonian ("Misener") Clastics of the Zenith Field.

| | |
|---|---|
| Dep. Var.: *LOGk* | Squared Multiple R: 0.213 |
| N: 46 | Adjusted Squared Multiple R: 0.176 |
| Multiple R: 0.461 | Standard Error of Estimate: 0.972 |

| Variable | Coeff | Std Error | Std Coeff | Tolerance | t | P(2 Tail) |
|---|---|---|---|---|---|---|
| Constant | -1.403 | 0.503 | 0.000 | — | -2.791 | 0 .008 |
| *PORW* | 8.375 | 3.580 | 0.321 | 0.975 | 2.339 | 0.024 |
| *GAM* | 0.054 | 0.026 | 0.285 | 0.975 | 2 .078 | 0.044 |

ANALYSIS OF VARIANCE

| Source | Sum-of-Squares | DF | Mean-Square | F-Ratio | P |
|---|---|---|---|---|---|
| Regression | 10.967 | 2 | 5.484 | 5.807 | 0.006 |
| Residual | 40.604 | 43 | 0.944 | — | — |

(a)

| | |
|---|---|
| Dep. Var.: *LOGk* | Squared Multiple R: 0.208 |
| N: 16 | Adjusted Squared Multiple R: 0.086 |
| Multiple R: 0.456 | Standard Error of Estimate: 0.699 |

| Variable | Coeff | Std Error | Std Coeff | Tolerance | t | P(2 Tail) |
|---|---|---|---|---|---|---|
| Constant | -0.937 | 0.716 | 0.000 | — | -1.309 | 0.213 |
| *PORW* | 7.168 | 5.806 | 0.328 | 0.865 | 1.235 | 0.239 |
| *GAM* | 0.030 | 0.017 | 0.459 | 0.865 | 1.729 | 0.107 |

ANALYSIS OF VARIANCE

| Source | Sum-of-Squares | DF | Mean-Square | F-Ratio | P |
|---|---|---|---|---|---|
| Regression | 1.666 | 2 | 0.833 | 1.703 | 0.220 |
| Residual | 6.359 | 13 | 0.489 | — | — |

(b)

Within the carbonates, the multiple regression model accounts for only 21% of the total variability. However, because of the larger sample size (46 observations), the analysis of variance is highly significant. These results imply that a systematic link has been determined between permeability

and both porosity and gamma-ray response, but that there are large error bounds around estimates of permeabilities at small depth increments. Again, the use of average permeabilities for regionalization reduces these error ranges substantially.

Permeability variations with respect to porosity and gamma-ray response for carbonates (Fig. 5.3) and clastics (Fig. 5.4) are shown as bubble-trend plots. In each illustration, the linear contours map the trend expressed by the regression model of *LOGk* based on *PORW* and *GAM*. The sizes of "bubbles" are determined by measured core permeabilities and their centroids are located at log readings of porosity and gamma radiation.

The regression functions were used to determine "mean" permeabilities for the lithotypes represented by classes 1–16 shown on Figures 4.6 and 4.7. The mean values of *GAM* and *PORW* for the classes were used to estimate the corresponding permeabilities. Table 5.2 gives the results. The mean values were assigned to the cells in the three-dimensional generalized data model of the Zenith field (Figs. 5.5–5.6).

**Table 5.2.** Experimental Means and Porosity and Natural Gamma Radiation and Permeability Estimated by Regression Function for Lithotypes (Classes) in the Zenith Field

| | Class No. | PORW | GAM | K |
|---|---|---|---|---|
| | 10 | 0.130 | 49.84 | 30.89 |
| Misener/ | 9 | 0.112 | 31.24 | 6.35 |
| Chattanooga | 8 | 0.069 | 17.12 | 1.17 |
| | 7 | 0.027 | 88.98 | 0.0 |
| | 5 | 0.060 | 20.28 | 1.56 |
| Maquoketa/ | 4 | 0.107 | 19.26 | 3.41 |
| Viola | 3 | 0.025 | 15.76 | 0.45 |
| | 2 | 0.087 | 20.51 | 2.71 |
| | 1 | 0.153 | 21.55 | 11.02 |

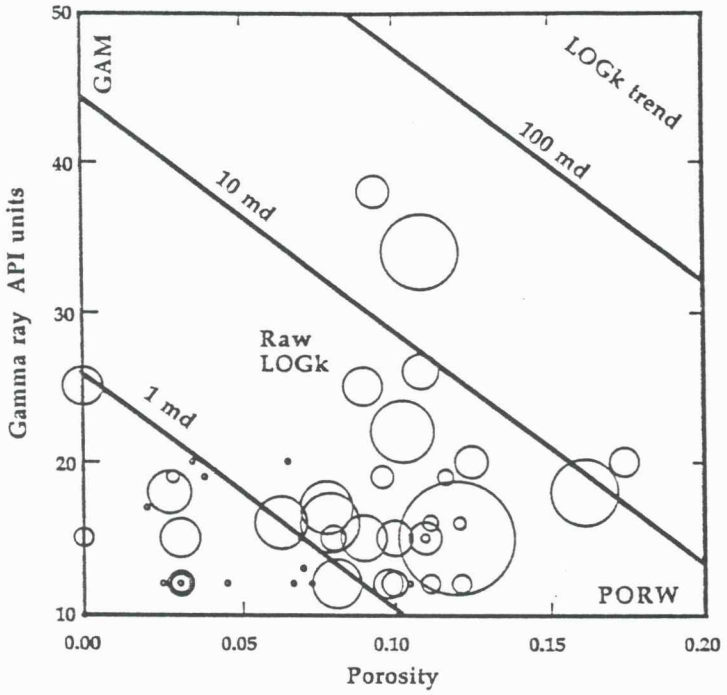


**Figure 5.3.** Map of regression function used to predict mean permeabilities, based on porosity and gamma-ray values for carbonate Ordovician sequence in Zenith field. "Bubbles" on plot are raw values of core permeabilities used to develop regression function.

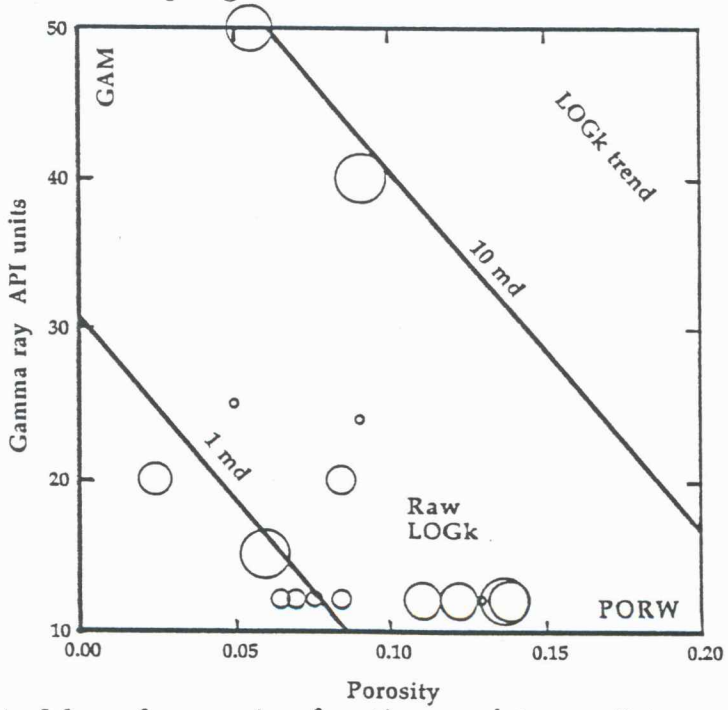


**Figure 5.4.** Map of regression function used to predict mean permeabilities, based on porosity and gamma-ray values for clastic ("Misener") sequence in Zenith field. "Bubbles" on plot are raw values of core permeabilities used to develop regression function.

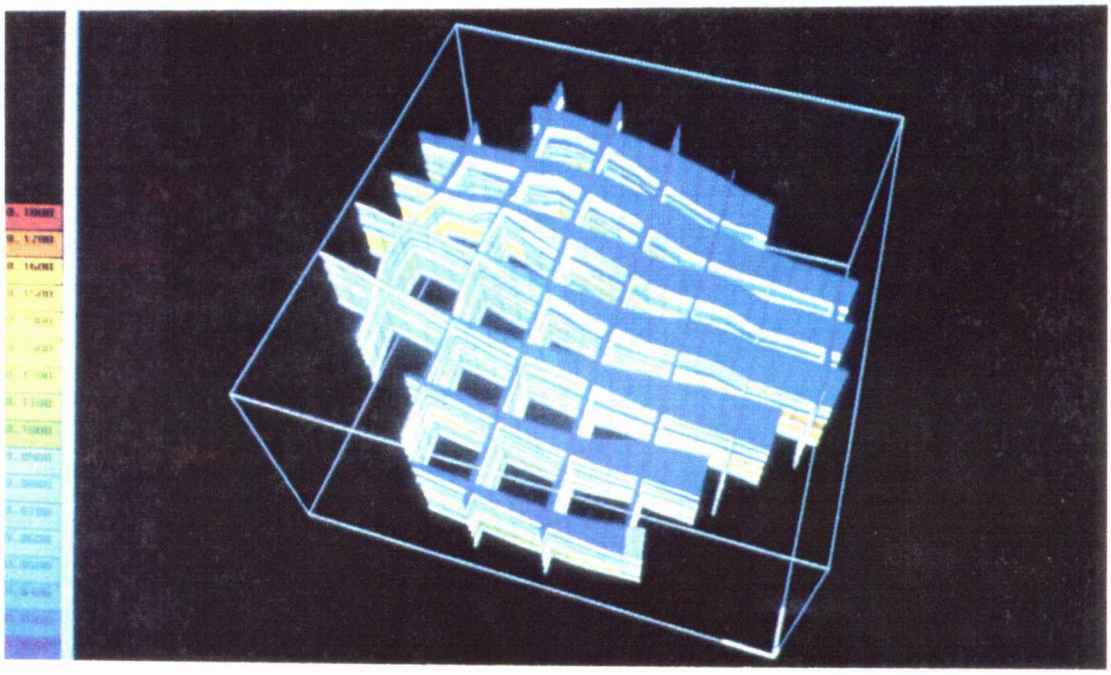

**Figure 5.5.** Porosities assigned to classes in three-dimensional model of the Zenith field, displayed using SGM software.

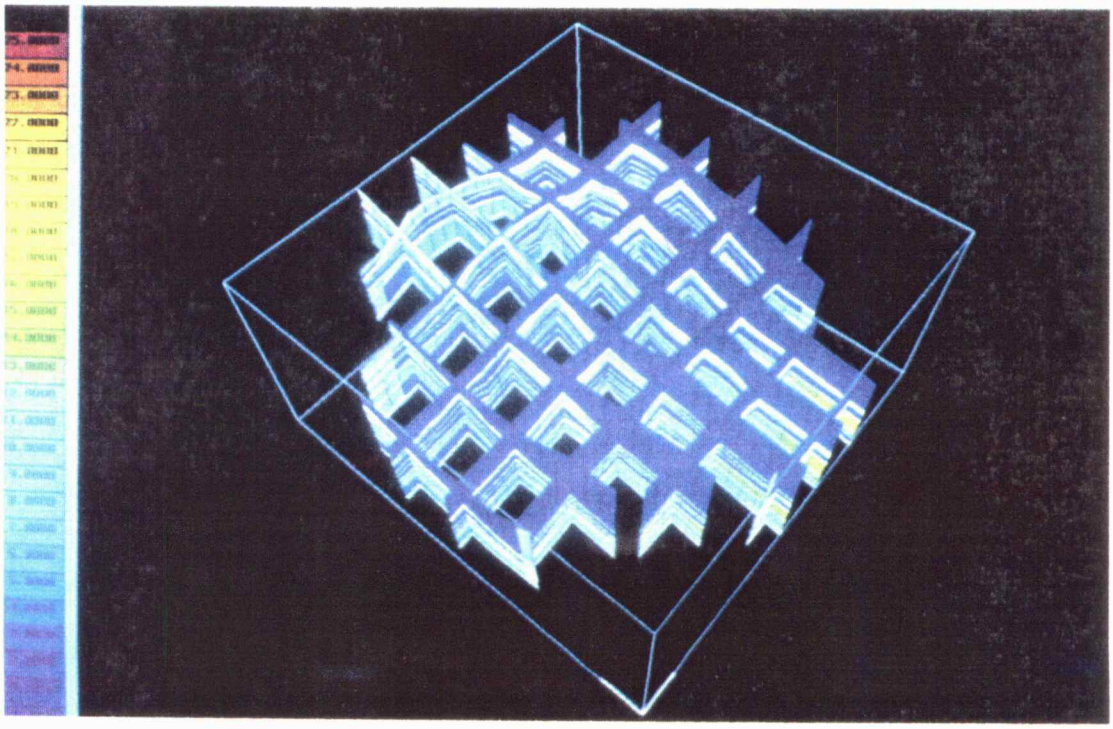

**Figure 5.6.** Permeabilities assigned to classes in three-dimensional model of the Zenith field, displayed using SGM software.

## 5.2 Subsidence Simulation for Typical Well Profiles

### 5.2.1 Theoretical Background

During basin development, many different but coupled processes occur: subsidence of the basement, deposition of sediments, compaction, flow of pore fluids, heat transport, maturation of organic material, and others. To numerically simulate these processes they must be described by partial differential equations derived from physical laws.

Physics governing movement of grains and fluid, as in sediment compaction and pore fluid flow, may be expressed in the following form (Woods *et al.*, 1988):

$$\nabla \vec{V}_D = \alpha \frac{d\sigma_T}{dt} - (\alpha + n\beta)\frac{dp}{dt} \tag{1}$$

$$\vec{V}_D = -\frac{k}{\mu}\left[\nabla p + \rho_w g \vec{z}\right] \tag{2}$$

$$\frac{d\sigma_T}{dt} = g[n\rho_w + (1-n)\rho_r]\frac{dl}{dt} \tag{3}$$

$$\nabla \vec{V}_s = -\alpha\left(\frac{d\sigma_T}{dt} - \frac{dp}{dt}\right) \tag{4}$$

where:

| | |
|---|---|
| $\vec{V}_D$ | Darcy velocity of fluids relative to grains |
| $\vec{V}_s$ | Grain velocity |
| $\sigma_T$ | Total stress |
| $\alpha$ | Compressibility of sediment |
| $\beta$ | Compressibility of water |
| $n$ | Porosity |
| $p$ | Fluid pressure |
| $k$ | Permeability |
| $\mu$ | Water viscosity |
| $\rho_w$ | Density of water |
| $\rho_r$ | Density of rock |
| $g$ | Acceleration of gravity |
| $\vec{z}$ | Unit vector in $z$ direction |
| $\frac{dl}{dt}$ | Sedimentation rate |

If the compressibility of water is ignored (*i.e.*, $\beta = 0$) and a constant water density $\rho_w$ is assumed, the concept of the hydraulic head $h$ may be introduced:

$$h = \frac{p}{\rho_w G} + z$$

This yields

$$p = \rho_w g(h - z)$$

$$\nabla p + \rho_w g\vec{z} = \rho_w g \nabla h \tag{5}$$

and the combination of equations (1), (4), (2), and (5) gives the alternative expressions

$$\nabla \vec{V}_s = \nabla \vec{V}_D$$

$$\nabla \vec{V}_s = \nabla\big(\frac{k}{\mu}(\nabla p + \rho_w g\vec{z})\big)$$

$$\nabla \vec{V}_s = \nabla(K \nabla h) \tag{6}$$

and the hydraulic conductivity,

$$K = \frac{\rho_w g h}{\mu}.$$

The combination of (3) and (4) yields the equation

$$\nabla \vec{V}_s = -\alpha g \rho_s \frac{dl}{dt} + \alpha \frac{dh}{dt},$$

with the sediment density $\rho_s = n\rho_w + (1 - n)\rho_r$. Again, replacing $p$ by $h$ gives

$$\nabla \vec{V}_s = -\alpha g \rho_s \frac{dl}{dt} + \alpha \rho_w g \frac{dh}{dt}.$$

Defining the specific storage coefficient $S$ as

$$S = \alpha \rho_w g$$

and the source term $Q$ as

$$Q = \alpha g \rho_s \frac{dl}{dt}$$

and combining with equation (6) yields a single equation for the hydraulic head $h$:

$$S\frac{dh}{dt} = \nabla(K \nabla h) + Q.$$

The subsidence velocity may be computed by equation (6), since the left-hand term reduces to $\frac{\partial V_s}{\partial z}$ if only vertical movement of the grains is considered.

### 5.2.2 Software

The system of partial equations (1) to (4) was solved numerically in one spatial dimension using the program NL.TTI (Woods *et al.*, 1988). The input file NL.TTI.IN contains the recent stratigraphy of the well to be analyzed, information on the changes in surface temperature and geothermal flow with time, rock and water properties such as compressibility, permeability, density, specific heat, and thermal conductivity, and output control commands. The program produces several output files, some of which can be processed by SURFACE III (Sampson, 1988) to produce graphical displays.

### 5.2.3 Well Data

The data necessary for subsidence simulation can be subdivided into the following parts:

- Complete time table, with absolute time values for sedimentation and erosion events,
- Thickness of sediment deposited or amount of erosion for each event,
- Details about the lithotype of each layer and the recent porosity and permeability,
- Knowledge about the diagenetic history of the sediments related to changes in porosity and permeability. "Removal" of the diagenetic processes will help estimate initial porosities and permeabilities of the sediments,
- Details about the geothermal and paleogeothermal history.

Not all of the necessary data are available for this study. Additional research has already begun to refine the diagenetic, geothermal, and paleogeothermal history of the Zenith Field area.

In this model, the absolute time scale for the epochs was taken from Haq and Eysinga (1987) and extended where necessary:

| | Time M.Y.B.P. (MA) | Abbreviation |
|---|---|---|
| Quaternary | 0–1.8 | Q |
| Tertiary | 1.8–67 | T |
| Late Cretaceous | 67–95 | LCr |
| Early Cretaceous | 95–140 | ECr |
| Jurassic | 140–210 | J |

(*Cont.*)

| | Time M.Y.B.P. (MA) | Abbreviation |
|---|---|---|
| Triassic | 210–250 | T |
| Late Permian | 250–270 | LP |
| Early Permian | 270–290 | |
| Nippewalla Group | 270–280 | NiGr |
| Sumner Group | 280–284 | SuGr |
| Chase Group | 284–287 | ChGr |
| Council Grove Group | 287–293 | CoGr |
| Pennsylvanian | 290–325 | |
| Admire Group | 293–294.8 | AdGr |
| Wabaunsee Group | 294.8–296.6 | WaGr |
| Shawnee Group | 296.6–298.4 | ShGr |
| Douglas Group | 298.4–300.2 | DoGr |
| Lansing Group | 300.2–301.8 | LaGr |
| Kansas City Group | 301.8–303.4 | KcGr |
| Pleasanton Group | 303.4–305 | PlGr |
| Marmaton Group | 305–307.5 | MaGr |
| Cherokee Group | 307.5–310 | ChGr |
| Atokan Stage | 310–314 | AtSt |
| Morrowan Stage | 314–325 | MoSt |
| Mississippian | | |
| Springerian Stage | 325–335 | SpSt |
| Meramecian Stage | 335–345 | MeSt |
| Osagian Stage | 345–355 | OsSt |
| Post-Chattanooga | 355–359 | PChat |
| Chattanooga | 359–361 | Chat |
| Misener I | 361–361.25 | MisI |
| Misener II | 361.25–361.5 | MisII |
| Misener III | 361.5–361.75 | MisIII |
| Misener IV | 361.75–362.00 | MisIV |
| Erosion Event | 362.0–388.0 | EE4 |
| Hunton Group | 388.0–440.0 | HuGr |
| Erosion Event | 440.0–457.0 | EE3 |
| Maquoketa | 457.0–460.0 | Maq |
| Erosion Event | 460.0–465.0 | EE2 |
| Post-Fernvale | 465–465.8 | PFern |
| Fernvale | 465.8–466.6 | Fern |
| Viola I | 466.6–467.4 | VioI |

(*Cont.*)

| | Time M.Y.B.P. (MA) | Abbreviation |
|---|---|---|
| "Hard Streak" | 467.4–468.2 | HStr |
| Viola II | 468.2–469.0 | VioII |
| Viola III | 469.0–470.0 | VioIII |
| Erosion Event | 470.0–475.0 | EE1 |
| Simpson Group | 475.0–480.0 | SiGr |

The detailed temporal subdivision of intervals below the Mississippian was created schematically using log data from the Zenith oil field.

This initial study uses gamma-ray and resistivity log traces from 25 wells in the Zenith field for correlating lithostratigraphic units above the Chattanooga Shale. The following tables give examples of depths of unit tops (in feet) for different parts of the field.

**North Part of the Field**

| Well Name: | ZU 24 | ZU 35 | ZU 37 |
|---|---|---|---|
| Location: | 24S 11W/1 | 24S 11W/1 | 24S 11W/2 |
| **Units/Tops (ft.):** | | | |
| NiGr | | | |
| SuGr | 490 | 480 | 492 |
| ChGr | 1592 | 1590 | 1590 |
| CoGr | 1940 | 1925 | 1935 |
| AdGr | 2320 | 2310 | 2310 |
| WaGr | 2400 | 2390 | 2390 |
| ShGr | 2840 | 2840 | 2840 |
| DoGr | 3195 | 3190 | 3175 |
| LaGr | 3305 | 3295 | 3292 |
| KcGr | 3375 | 3360 | 3362 |
| PlGr | 3612 | 3595 | 3594 |
| MaGr | 3650 | 3642 | 3628 |
| ChGr | 3676 | 3666 | 3664 |
| AtSt | 3676 | 3666 | 3664 |
| MoSt | 3676 | 3666 | 3664 |
| SpSt | 3676 | 3666 | 3664 |
| MeSt | 3676 | 3666 | 3664 |
| OsSt | 3676 | 3666 | 3664 |
| Chat | 3676 | 3666 | 3664 |

## Central Part of the Field

| Well Name: | ZU 19 | Johnsen 1–S | ZU 22 |
|---|---|---|---|
| Location: | 24S 11W/14 | 24S 11W/13 | 24S 11W/18 |
| **Units/Tops (ft.):** | | | |
| NiGr | | | |
| SuGr | 510 | 480 | 488 |
| ChGr | 1650 | 1580 | 1600 |
| CoGr | 1990 | 1940 | 1950 |
| AdGr | 2370 | 2320 | 2350 |
| WaGr | 2460 | 2400 | 2415 |
| ShGr | 2898 | 2850 | 2860 |
| DoGr | 3250 | 3190 | 3200 |
| LaGr | 3370 | 3315 | 3332 |
| KcGr | 3440 | 3390 | 3410 |
| PlGr | 3635 | 3612 | 3645 |
| MaGr | 3698 | 3666 | 3685 |
| ChGr | 3718 | 3674 | 3700 |
| AtSt | 3718 | 3674 | 3700 |
| MoSt | 3718 | 3674 | 3700 |
| SpSt | 3718 | 3674 | 3700 |
| MeSt | 3718 | 3674 | 3700 |
| OsSt | 3718 | 3674 | 3700 |
| Chat | 3718 | 3674 | 3700 |

## South Part of the Field

| Well Name: | Brownlee 2 | Maxie 3 | McComb 1 |
|---|---|---|---|
| Location: | 24S 10W/31 | 24S 11W/24 | 24S 11W/26 |
| **Units/Tops (ft.):** | | | |
| NiGr | | | |
| SuGr | 480 | 515 | 510 |
| ChGr | 1625 | 1670 | 1650 |
| CoGr | 1965 | 2010 | 1990 |
| AdGr | 2355 | 2420 | 2396 |
| WaGr | 2433 | 2480 | 2455 |
| ShGr | 2880 | 2940 | 2890 |
| DoGr | 3243 | 3240 | 3240 |
| LaGr | 3375 | 3400 | 3373 |
| KcGr | 3450 | 3470 | 3440 |

*(Cont.)*

| Units/Tops (ft.): | | | |
|---|---|---|---|
| PlGr | 3700 | 3705 | 3665 |
| MaGr | 3760 | 3740 | 3710 |
| ChGr | 3810 | 3762 | 3730 |
| AtSt | 3810 | 3762 | 3730 |
| MoSt | 3810 | 3762 | 3730 |
| SpSt | 3810 | 3762 | 3730 |
| MeSt | 3810 | 3762 | 3730 |
| OsSt | 3810 | 3762 | 3730 |
| Chat | 3810 | 3762 | 3730 |

Two points merit emphasis:

a) There are no great differences in thicknesses of the units in different parts of the Zenith oil field. The southern part of the field is only about 100 to 150 ft. deeper than the northern part of the field.

b) nearly the entire Mississippian is missing in the region of the Zenith field.

Although sedimentation undoubtedly occurred during Mississippian time, the entire section was eroded during the Late Mississippian. A realistic thickness for the eroded interval is difficult to determine. An amount of erosion between 300 and 1000 ft. may be reasonable (USGS, 1979).

Lithotypes of intervals in wells of the Zenith field were interpreted from well logs. Two previously interpreted type logs in Stafford and Reno counties were useful in this study. The following lithotypes are common in all wells: sandstones, siltstone, shale, salt, anhydrite, and limestone.

For comparison with subsidence in the Zenith field, the type log from Clark County * was used. Thicknesses (in ft.) of the units are: NiGr—945, SuGr—1415, ChGr—425, CoGr—410, AdGr—95, WaGr—470, ShGr—540, DoGr—140, LaGr—110, KcGr—510, PlGr—15, MaGr—180, ChGr—165, AtSt—70, MoSt—10, SpSt—305, MeSt—735, OsSt—510, Viola—170, Si-Gr—100. A general assumption of 50 $mW/m^2$ and a surface temperature of 20°C was used for the geothermal and paleogeothermal regime.

* Stanolind Oil & Gas Co. #1D Santee, 18–33S–23W, and Skelly Oil B.M. Gabbert No. 1, 25–34S–24W, from *Type Logs of Kansas*, Catalog No. 18–33–23W: Kansas Geol. Society, Wichita, Kansas, 1966.

### 5.2.4 Results of Modeling

Figure 5.7 shows a typical subsidence curve for the Zenith oil field. This figure represents the time between deposition of the Marmaton Group until the Nippewalla Group. The curve has the typical form of a subsidence curve connected with a foreland basin until about 280 MYBP (see also Schmoker, 1989). The model shows that with the assumption of a low paleogeothermal gradient, oil could not have been generated from the Chattanooga Shale or from Ordovician units in the area of the Zenith field. Also, assuming very high amounts of erosion during the Mississippian and Cretaceous results in no oil generation. The influence of compaction due to thickness variations seems weak in intervals above the Chattanooga Shale. The frequently occurring limestones are, for the most part, cemented.

Figure 5.8 shows modeling results for the Clark County type log (*Type Logs of Kansas*, Catalog No. 18-33-23W: Kansas Geol. Society, Wichita, Kansas, 1966). The section is nearly 7500 ft. thick. The curve indicates the strong subsidence during the Carboniferous. Erosion events were not considered as a first approximation.

The computed TTI values show the capability for oil generation. From the end of the Jurassic time until the present, the Viola and the Simpson Group are in a stage of maturation near the beginning of the oil window (TTI $>$ 10). Following Schmoker (1989), who suggested the possibility of a higher geothermal regime during foreland basin development, and considering the possible magnitude of erosion events, there is the capability for oil generation in all units below the Mississippian. In certain circumstances, the Lower Mississippian may have reached maturation and some oil generation seems to be possible also. Such a conclusion requires further work to create more reliable estimates of geologic boundary conditions. Future work should include a subsidence and maturation study of a larger area around the Central Kansas Uplift, using the available software. For working with a large number of wells, the interactive program BASIN should be used and a subsidence and maturation simulation at selected wells should be performed with the program NL.TTI. Vitrinite reflection data would provide important constraints for realistic modeling.

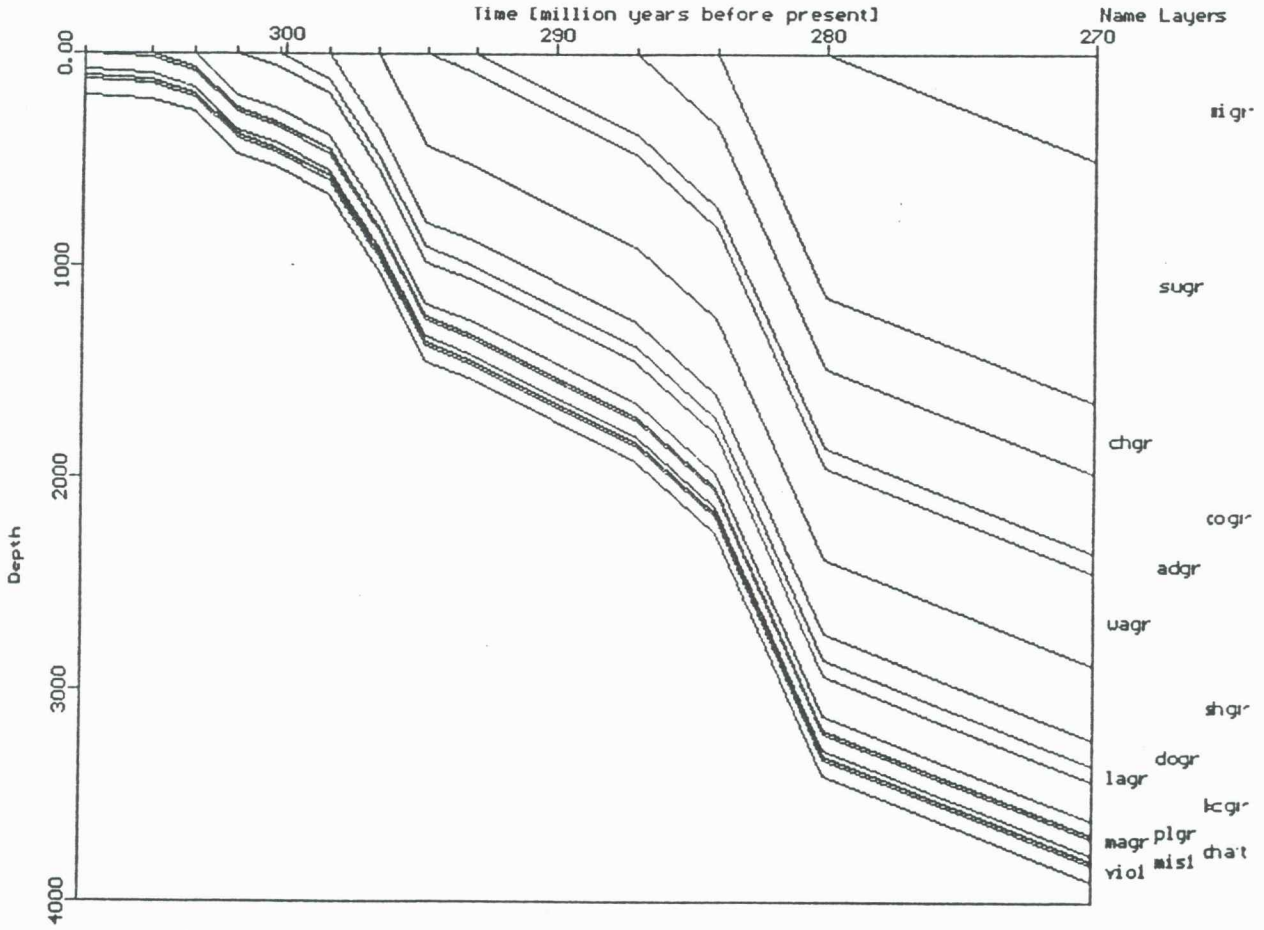


**Figure 5.7.** Subsidence history for the Zenith oil field, 310 M.Y.B.P. to 270 M.Y.B.P.

## REFERENCES

Asquith, G.B. and Gibson, C.R., 1982, Basic Well Log Analysis for Geologists: *Methods in Exploration Series*, Am. Assoc. Petroleum Geologists, Tulsa, Oklahoma, 216 pp.

Choquette, P.W. and Traut, J.D., 1963, Pennsylvanian carbonate reservoirs, Ismay Field, Utah and Colorado: *A Symposium on Shelf Carbonates of the Paradox Basin*, Four Corners Geol. Soc. 4th Field Conf., p. 157–184.

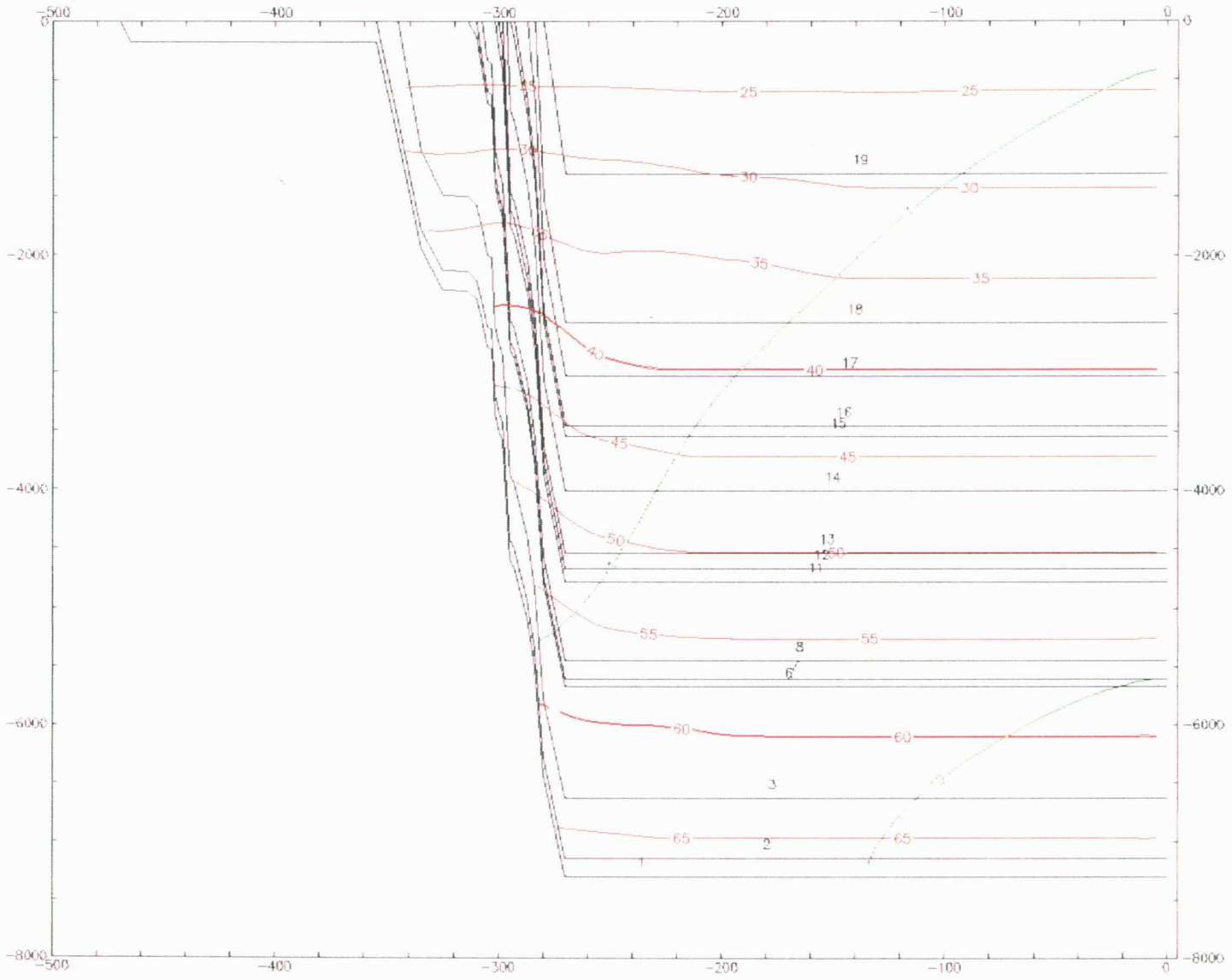


**Figure 5.8.** Subsidence and maturation history for the type log of Clark County.

Haq, B.U. and Eysinga, F.W.B., 1987, *Geological Time Table:* Fourth Revised Enlarged and Updated Ed., Elsevier Science Publishers B.V., Amsterdam [Wall Chart].

Herron, M.M., 1987, Estimating the intrinsic permeability of clastic sediments from geochemical data: *Trans. SPWLA,* Paper HH, 22 pp.

Krumbein, W.C. and Monk, G.D., 1942, Permeability as a function of the size parameters of sedimentary particles: *AIME Tech. Publ.*, 1942, p. 153–162.

Sampson, R.J., 1988, *A user's guide to SURFACE III:* Interactive Concepts Inc., Lawrence, Kansas, 277 pp.

Schmoker, J.W., 1989, Thermal maturation of the Anadarko Basin: *Oklahoma Geological Survey Circular 90,* 289 pp.

Timur, A., 1968, An investigation of permeability, porosity, and residual water saturation relationships: *SPWLA Ninth Annual Logging Symposium Transactions,* J, p. 1–18.

USGS, 1979, Paleotectonic investigations of the Mississippian System in the United States: *U.S. Geological Survey Professional Paper 1010,* GPO, Washington, 559 pp.

Woods, J.J., Bohling, G.C., McElwee, C.D., and Newell, K.D., 1988, Thermal basin modeling and analysis using the time–temperature index—An improved general basin model incorporating compaction, fluid flow and heat flow: *Kansas Geological Survey Open-file Report 88–28,* 153 pp.

# 6. SUMMARY

J. Harff and J.C. Davis

Regionalization is a statistically based procedure for subdividing a collection of spatially distributed multivariate observations into classes so that the classes lie within spatially contiguous subareas. As a consequence, these define "regions" that are as homogeneous as possible and distinct from other regions. Regionalization is derived from classification concepts expressed by Voronin (1967) and Rodionov (1981), combined with the spatial concepts propounded by Matheron (1962). Harff and Davis (1990) provide a two-dimensional demonstration of regionalization.

The motivation behind the development of regionalization is to construct a three-dimensional geometric framework that can describe the structural configuration and lithofacies relationships within the sedimentary fill of a basin. The framework derived by regionalization should be a parsimonious description whose complexity reflects the availability of observations. It would be objective in the sense that it would not depend upon a presumed genetic history of the basin, as do conventional basin models. A regionalized model of a sedimentary basin would provide the starting point for dynamic modeling of compaction, heat flow, and fluid movement.

Regionalization procedures were first applied to the North German Basin (Harff and others, 1990), using a personal computer implementation (Springer, Lewerenz, and Harff, 1990). Subsequently, through the collaborative efforts of the Central Institute for the Physics of the Earth (ZIPE) in Potsdam, DDR, and the Kansas Geological Survey, the methodology was formalized and applied in two dimensions to the Western Kansas Shelf area (Harff and others, 1989; Harff and Davis, 1990). Continued collaboration between the Kansas Geological Survey and ZIPE has focused on the problems of implementing regionalization in three dimensions in a manner that reflects the influence of stratigraphy, and on incorporating petrophysical variables from wireline logs to express lithology. The resulting three-dimensional model is to be displayed on a graphics workstation.

The general procedure for three-dimensional modeling of a sedimentary basin, using data from well logs as the primary source of data, involves a succession of steps. The first is zonation, to subdivide the basin fill into correlative layers. Then, typification is performed on each layer, followed by discrimination and interpolation of the classification probabilities to the nodes of a regular grid. The result is a layered generalized data model, which can be used for backstripping to reconstruct the geological history of the basin. The generalized data model also provides the framework for deterministic modeling of heat and fluid flow during the subsidence and

filling of the basin.

It is apparent that the procedure for three-dimensional regionalization may be useful in other contexts, such as reservoir simulation. Although the spatial dimensions of a reservoir are smaller than those of a sedimentary basin, the stratigraphic, structural, and lithologic interrelationships may be equally complex. In current petroleum engineering practice, multiphase fluid flow simulations are run to predict the future behavior of a reservoir during exploitation. The simulations are deterministic calculations of fluid movement, based on the known history of pressure changes and fluid input and removal, and a model of initial physical conditions (porosities, permeabilities, fluid saturations, etc.) at points on a regular three-dimensional grid covering the reservoir. A major problem in reservoir simulation is to create the initial three-dimensional static model, using only data from the scattered wells that have been drilled and cored or logged. Petroleum engineers rely on geologists to provide the initial model, and the geologists usually develop their models from genetic interpretations. Typically, the initial characterizations require extensive, arbitrary adjustments in order to obtain adequate history matches, a failing that has been a serious source of contention between engineers and geologists for many years.

The Kansas Geological Survey has conducted an independent investigation of the Zenith oil field in central Kansas, as part of a continuing research program to estimate the potential for enhanced recovery from older fields (Kansas Geological Survey and Tertiary Oil Recovery Project, 1991). This provided a convenient data base for testing regionalization procedures, and a way of comparing the results of regionalization against more conventional geological interpretations. The Zenith field was discovered in 1937 and has yielded over 24 million barrels of oil. However, secondary recovery attempts have been disappointing, which has led to its selection for study.

Production comes from five different reservoirs in the Zenith field: the Misener sandstone, Misener "limestone" (Upper Devonian-Lower Mississippian), Maquoketa dolomite (Upper Ordovician), and three Viola limestone reservoirs (Middle Ordovician). The lower carbonates and the Misener sequence were typified separately by cluster analysis, using three wireline-log variables: gamma-ray intensity, corrected neutron porosity, and corrected density porosity. Five rock types for the carbonates and four rock types for the Misener sequence were determined. Anomalous petrophysical properties of the Misener clastics were investigated by laboratory mineralogical determinations.

The stratigraphic interval was correlated and zoned using the CORRELATOR program, based on gamma ray and neutron porosity logs from 38 wells. Within each stratigraphic zone, wells were assigned to rock types (classes) by discriminant analysis and the probabilities of class membership

were interpolated to the nodes of a regular grid. This procedure subdivides each layer into homogeneous regions, each characterized by the class mean values of the petrophysical variables. Additional variables, such as porosity ($PORW$), were determined using deterministic models based on wireline log responses which then were averaged within classes.

Permeabilities ($k$) were calculated from a regression between core permeabilities and wireline log responses for the equivalent intervals. The regression was used to estimate a class mean permeability from the means of $IGR$ and $PORW$. The structural configurations of the individual layers were mapped using SURFACE III, creating a stack of grids that could be displayed using SGM, a modeling and display program running on a Silicon Graphics workstation. The results of regionalization of the lithologic or fluid-flow variables are displayed as color variations within this structural framework.

Additional one-dimensional models were run of subsidence, heat flow, and TTI, based on wells in the vicinity of the Zenith field and in adjacent areas to the south. These indicate that the oil contained in the Zenith reservoirs could have been generated in Lower Mississippian or older source rocks at times beginning in the Late Jurassic in areas south of the Zenith field.

The next phases of research on the Zenith field will evolve in three distinct directions:

1. The discrete programs now used for the research must be linked to form an easily usable software tool for constructing the generalized layered model and providing input to three-dimensional display programs such as SGM.
2. Further mineralogical and petrophysical investigations of logs and cores are needed to resolve remaining ambiguities in log interpretation and to specify parameters for interpretation in the Zenith field.
3. A fluid-flow simulation of the Zenith field should be run, based on input specified by regionalization. Results of this simulation should be compared to those obtained from the conventionally interpreted model of the field.

Following completion of the Zenith study, cooperative research should be refocused on basin-wide modeling and interpretation. The objectives should be to refine the earlier study of the North German Basin using the newly developed modeling tools and to extend work in Kansas to include a major portion of the Western Kansas Shelf area.

## REFERENCES


Harff, J. and Davis, J.C., 1990, Regionalization in geology by multivariate classification: *Mathematical Geology,* vol. 22, no. 5, p. 573–588.

Harff, J., Davis, J.C., Watney, L., Bohling, G. and Wong, J.C., 1989, *Regionalization of western Kansas based on multivatiate classification of stratigraphic data from oil wells:* Kansas Geol. Survey, Open-File Report 89–21, 26 pp.

Harff, J., Eiserbeck, Wolfgang, Hoth, Klaus and Springer, Jorn, 1990, Computer-assisted basin analysis and regionalization aid in search for oil and gas: *GEOBYTE,* no. 11, p. 11–15.

Kansas Geological Survey and Tertiary Oil Recovery Project, 1991, Zenith field—A field demonstration project for improved efficiency for oil and gas recovery in Kansas: *Final Report submitted to the Kansas Corporation Commission,* Topeka, Kansas, 263 pp.

Matheron, G., 1962, *Traité de Géostatistique Appliquée:* Mémoires du Bureau de Recherches Géologiques et Minières, v. 14, Editions Technip, Paris, 333 pp.

Rodionov, D.A., 1981, *Statisticĕskie resĕnija v geologii.:* —Izd. "Nedra", Moskva, 231 pp.

Springer, J., Lewerenz, B. and Harff, J., 1990, *BASIN—Modeling of Sedimentary Basins: User's Guide:* ZIPE, Potsdam, FRG, 17 pp.

Voronin, Ju. A., 1967, *Geologija i matematika:* —Izd. "Nauka", Novosibirsk, 253 pp.

# REFERENCES CITED


Asquith, G.B. and Gibson, C.R., 1982, Basic Well Log Analysis for Geologists: *Methods in Exploration Series*, Am. Assoc. Petroleum Geologists, Tulsa, Oklahoma, 216 pp.

Choquette, P.W. and Traut, J.D., 1963, Pennsylvanian carbonate reservoirs, Ismay Field, Utah and Colorado: *A Symposium on Shelf Carbonates of the Paradox Basin*, Four Corners Geol. Soc. 4th Field Conf., p. 157–184.

Davis, J.C., Harff, J., and Watney, W.L., 1990, Determination of homogeneous components of a sedimentary basin, *in* Pflug, R. and K. Bitzer (eds.), *Three-dimensional Computer Graphics in Modeling Geologic Structures and Simulat ing Geologic Processes:* Freiburger geowiss. Beitr, Band 2, Freiburg, p. 22–24.

Fisher, R.A., 1936, The use of multiple measurements in taxonomic problems: *Annals of Eugenics*, no. 67, p. 179–188.

Haq, B.U. and Eysinga, F.W.B., 1987, *Geological Time Table:* Fourth Revised Enlarged and Updated Ed., Elsevier Science Publishers B.V., Amsterdam [Wall Chart].

Harff, J. and Davis, J.C., 1990, Regionalization in geology by multivariate classification: *Mathematical Geology*, vol. 22, no. 5, p. 573–588.

Harff, J., Davis, J.C., Watney, L., Bohling, G. and Wong, J.C., 1989, *Regionalization of western Kansas based on multivatiate classification of stratigraphic data from oil wells:* Kansas Geol. Survey, Open-File Report 89–21, 26 pp.

Harff, J., Eiserbeck, Wolfgang, Hoth, Klaus and Springer, Jorn, 1990, Computer-assisted basin analysis and regionalization aid in search for oil and gas: *GEOBYTE,* no. 11, p. 11–15.

Henrion, G., Henrion, A. and Henrion, R., 1988, *Beispiele zur Datenanalyse mit BASIC-Programmen:* Dt. Verl. d. Wissenschaften, Berlin, 363 pp.

Herron, M.M., 1987, Estimating the intrinsic permeability of clastic sediments from geochemical data: *Trans. SPWLA*, Paper HH, 22 pp.

Imbt, W.C., 1941, Zenith pool, Stafford County, Kansas—An example of stratigraphic trap accumulation, *in* Levorsen, A.I. (ed.), *Stratigraphic Type Oil Fields:* Am. Assoc. Petroleum Geologists, Tulsa, Oklahoma, p. 139–165.

Journel, A.G. and Huijbregts, C.J, 1978, *Mining Geostatistics:* Academic Press, London, 600 pp.

Kansas Geological Survey and Tertiary Oil Recovery Project, 1991, Zenith field—A field demonstration project for improved efficiency for oil and gas recovery in Kansas: *Final Report submitted to the Kansas Corporation Commission,* Topeka, Kansas, 263 pp.

Krumbein, W.C. and Monk, G.D., 1942, Permeability as a function of the size parameters of sedimentary particles: *AIME Tech. Publ.,* 1942, p. 153–162.

Krumbein, W.C. and Sloss, L.L., 1963, *Stratigraphy and Sedimentation:* W.H. Freeman & Co., San Francisco, California, 660 pp.

Lee, W., 1956, Stratigraphy and structural development of the Salina basin area: *Kansas Geological Survey Bulletin 121,* 167 pp.

Matheron, G., 1962, *Traité de Géostatistique Appliquée:* Mémoires du Bureau de Recherches Géologiques et Minières, v. 14, Editions Technip, Paris, 333 pp.

Merriam, D.F., 1963, The geologic history of Kansas: *Kansas Geological Survey Bulletin 162,* 317 pp.

Newell, K.D., 1989, Distribution of Upper Devonian–Lower Mississippian Misener sandstone in Salina basin: *Kansas Geological Survey, Open-File Report 89–18,* (1:1,000,000 scale map, with discussion).

Olea, R.A., 1988, CORRELATOR: An interactive computer system for lithostratigraphic correlation of wireline logs: *Petrophysical Series 4,* Kansas Geol. Survey, Lawrence, KS, 85 pp.

Olea, R.A. and Davis, J.C., 1989, An expert system for the correlation of geophysical well logs, *in* Simaan, M. and F. Aminzadeh (eds.), *Advances in Geophysical Data Processing,* Vol. III: Jai Press, Inc., Greenwich, Connecticut, p. 279–307.

Olea, R.A., Newell, K.D., and Harff, J., 1991, Geologic modeling of the Zenith field, Kansas, using CORRELATOR: *Kansas Geological Survey, Open-File Report no. 91-39 (two vols.),* University of Kansas, Lawrence, Kansas, 456 pp.

Paddleford, J.T., 1941, The Zenith pool of Stafford and Reno counties, Kansas: *Mines Magazine,* v. 31, p. 445–448, 454, 470, 472.

Rodionov, D.A., 1981, *Statisticĕskie resĕnija v geologii.:* —Izd. "Nedra", Moskva, 231 pp.

# APPENDIX A

## Digitized Wireline Log File

```
 1  01  :SI32:HARFF:MISENER:STRIK37.DAT
 2  02  :SI32:HARFF:MISENER:STRIK37.DAT
 3  01  :SI32:HARFF:MISENER:STRIK14.DAT
 4  02  :SI32:HARFF:MISENER:STRIK14.DAT
 5  01  :SI32:HARFF:MISENER:STRIK29.DAT  3580-3770
 6  02  :SI32:HARFF:MISENER:STRIK29.DAT  3580-3770
 7  01  :SI32:HARFF:MISENER:STRIK28.DAT  3580-3770
 8  02  :SI32:HARFF:MISENER:STRIK28.DAT  3580-3770
 9  01  :SI32:HARFF:MISENER:STRIK32.DAT  gamma ray in error
10  02  :SI32:HARFF:MISENER:STRIK32.DAT
11  01  :SI32:HARFF:MISENER:NSTRIK32.DAT correct gamma ray
12  01  :SI32:HARFF:MISENER:STRIK28.DAT  3580-3820
13  02  :SI32:HARFF:MISENER:STRIK28.DAT  3580-3820
14  01  :SI32:HARFF:MISENER:STRIK29.DAT  3580-3820
15  02  :SI32:HARFF:MISENER:STRIK29.DAT  3580-3820
16  01  :SI32:HARFF:MISENER:STRIK39.DAT
17  02  :SI32:HARFF:MISENER:STRIK39.DAT
18  01  :SI32:HARFF:MISENER:BRAZE3.DAT
19  02  :SI32:HARFF:MISENER:BRAZE3.DAT
20  01  :SI32:HARFF:MISENER:STRIK25.DAT
21  02  :SI32:HARFF:MISENER:STRIK25.DAT
22  01  :SI32:HARFF:MISENER:STRIK21.DAT
23  02  :SI32:HARFF:MISENER:STRIK21.DAT
24  01  :SI32:HARFF:MISENER:STRIK30.DAT
25  02  :SI32:HARFF:MISENER:STRIK30.DAT
26  01  :SI32:HARFF:MISENER:STRIK17.DAT
27  02  :SI32:HARFF:MISENER:STRIK17.DAT
28  01  :SI32:HARFF:MISENER:STRIK18.DAT
29  02  :SI32:HARFF:MISENER:STRIK18.DAT
30  01  :SI32:HARFF:MISENER:STRIK19.DAT
31  02  :SI32:HARFF:MISENER:STRIK19.DAT
32  01  :SI32:HARFF:MISENER:BRADEN6W.DAT to 3800 ft
33  02  :SI32:HARFF:MISENER:BRADEN6W.DAT
34  01  :SI32:HARFF:MISENER:STRIK13.DAT
35  02  :SI32:HARFF:MISENER:STRIK13.DAT
36  01  :SI32:HARFF:MISENER:STRIK35.DAT
37  02  :SI32:HARFF:MISENER:STRIK35.DAT
38  01  :SI32:HARFF:MISENER:STRIK24.DAT
39  02  :SI32:HARFF:MISENER:STRIK24.DAT
42  01  :SI32:HARFF:MISENER:PAUL1.DAT
43  02  :SI32:HARFF:MISENER:PAUL1.DAT
44  01  :SI32:HARFF:MISENER:BRADEN6W.DAT to 3840 ft
45  02  :SI32:HARFF:MISENER:BRADEN6W.DAT
```

APPENDIX A—Digitized Wireline Log File (*Cont.*)

```
46  01  :SI32:HARFF:MISENER:STRIK1_5.DAT
47  02  :SI32:HARFF:MISENER:STRIK1_5.DAT
48  01  :SI32:HARFF:MISENER:STRIK_S.DAT
49  02  :SI32:HARFF:MISENER:STRIK_S.DAT
50  01  :SI32:HARFF:MISENER:BRAZE1.DAT
51  02  :SI32:HARFF:MISENER:BRAZE1.DAT
52  01  :SI32:HARFF:MISENER:BRAZE10.DAT from 3620
53  02  :SI32:HARFF:MISENER:BRAZE10.DAT
54  01  :SI32:HARFF:MISENER:BRAZE10.DAT from 3580
55  02  :SI32:HARFF:MISENER:BRAZE10.DAT
56  01  :SI32:HARFF:MISENER:CASE142.DAT
57  02  :SI32:HARFF:MISENER:CASE142.DAT
58  01  :SI32:HARFF:MISENER:STRIK15.DAT
59  02  :SI32:HARFF:MISENER:STRIK15.DAT
60  01  :SI32:HARFF:MISENER:STRIK16.DAT
61  02  :SI32:HARFF:MISENER:STRIK16.DAT
62  01  :SI32:HARFF:MISENER:CASE117.DAT
63  02  :SI32:HARFF:MISENER:CASE117.DAT
64  01  :SI32:HARFF:MISENER:STRIK27.DAT
65  02  :SI32:HARFF:MISENER:STRIK27.DAT
66  01  :SI32:HARFF:MISENER:STRIK33.DAT
67  02  :SI32:HARFF:MISENER:STRIK33.DAT
68  01  :SI32:HARFF:MISENER:STRIK23.DAT
69  02  :SI32:HARFF:MISENER:STRIK23.DAT
70  01  :SI32:HARFF:MISENER:STRIK36.DAT
71  02  :SI32:HARFF:MISENER:STRIK36.DAT
72  01  :SI32:HARFF:MISENER:STRIK22.DAT
73  02  :SI32:HARFF:MISENER:STRIK22.DAT
74  01  :SI32:HARFF:MISENER:STRIK20.DAT
75  02  :SI32:HARFF:MISENER:STRIK20.DAT
76  01  :SI32:HARFF:MISENER:MAX3.DAT
77  02  :SI32:HARFF:MISENER:MAX3.DAT    Wrong neutron
78  02  :SI32:HARFF:MISENER:MAX3.DAT    Correct log
79  01  :SI32:HARFF:MISENER:BRA2W2.DAT
80  02  :SI32:HARFF:MISENER:BRA2W2.DAT
81  01  :SI32:HARFF:MISENER:STRIK2W.DAT
82  02  :SI32:HARFF:MISENER:STRIK2W.DAT
83  01  :SI32:HARFF:MISENER:FIG5.DAT
84  02  :SI32:HARFF:MISENER:FIG5.DAT
85  01  :SI32:HARFF:MISENER:STRIK26.DAT
86  02  :SI32:HARFF:MISENER:STRIK26.DAT
87  01  :SI32:HARFF:MISENER:FIG1.DAT
88  01  :SI32:HARFF:MISENER:FIG1N.DAT  Wrong Gamma Ray
89  01  :SI32:HARFF:MISENER:FIG1.DAT   Correct
```

# APPENDIX B

## Well Data File

| | WELL M.DIG SEA LEVEL | | | | | | | 38 F | R | L |
|---|---|---|---|---|---|---|---|---|---|---|
| 1 | Zenith #37(16) | 15 | 1805.0 | GR | 1 | 130 | CNS | 2 | | |
| 2 | Zenith #14(26) | 15 | 1813.0 | GR | 3 | 105 | CNS | 4 | | |
| 3 | Zenith #29(19) | 11 | 1820.0 | GR | 14 | 120 | CNS | 15 | | |
| 4 | Zenith #28(36) | 11 | 1816.0 | GR | 12 | 130 | CNS | 13 | | |
| 5 | Zenith #32(38) | 11 | 1805.0 | GR | 11 | 120 | WEXN | 10 | | |
| 6 | Zenith #39(41) | 11 | 1808.0 | GR | 16 | 120 | WEXN | 17 | | |
| 7 | Zenith #3(13) | 11 | 1813.0 | GR | 18 | 120 | LANN | 19 | | |
| 8 | Zenith #25(34) | 11 | 1804.0 | GR | 20 | 150 | CNS | 21 | | |
| 9 | Zenith #21(44) | 11 | 1812.0 | GR | 22 | 110 | CNS | 23 | | |
| 10 | Zenith #30(37) | 11 | 1785.0 | GR | 24 | 100 | CNS | 25 | | |
| 11 | Zenith #17(9) | 15 | 1814.0 | GR | 26 | 110 | CNS | 27 | | |
| 12 | Zenith #18(28) | 15 | 1817.0 | GR | 28 | 105 | CNS | 29 | | |
| 13 | Zenith #19(1) | 11 | 1811.0 | GR | 30 | 120 | CNS | 31 | | |
| 14 | Zenith #6W(57) | 11 | 1805.0 | GR | 44 | 120 | WELN | 45 | | |
| 15 | Zenith #13(18) | 11 | 1809.0 | GR | 34 | 110 | CNS | 35 | | |
| 16 | Zenith #35(39) | 11 | 1803.0 | GR | 36 | 90 | CNS | 37 | | |
| 17 | Zenith #24(33) | 11 | 1812.0 | GR | 38 | 120 | CNS | 39 | | |
| 18 | Paulsen L #1(23) | 15 | 1804.0 | GR | 42 | 120 | WITN | 43 | | |
| 19 | Johnson #1-5(21) | 11 | 1794.0 | GR | 46 | 135 | CNS | 47 | | |
| 20 | Stewart #1S(24) | 11 | 1794.0 | GR | 48 | 130 | CNS | 49 | | |
| 21 | Zenith #1(2) | 15 | 1816.0 | GR | 50 | 110 | SNP | 51 | | |
| 22 | Zenith #10(6) | 15 | 1820.0 | GR | 54 | 150 | ELEN | 55 | | |
| 23 | McComb #1(42) | 11 | 1819.0 | GR | 56 | 110 | WITN | 57 | | |
| 24 | Zenith #15(8) | 11 | 1807.0 | GR | 58 | 110 | CNS | 59 | | |
| 25 | Zenith 16(27) | 11 | 1809.0 | GR | 60 | 110 | CNS | 61 | | |
| 26 | G. McComb #1(17) | 11 | 1801.0 | GR | 62 | 110 | WITN | 63 | | |
| 27 | Zenith #27(35) | 11 | 1791.0 | GR | 64 | 135 | CNS | 65 | | |
| 28 | Zenith #33(15) | 11 | 1808.0 | GR | 66 | 130 | CNS | 67 | | |
| 29 | Zenith #23(32) | 11 | 1807.0 | GR | 68 | 110 | CNS | 69 | | |
| 30 | Zenith #36(40) | 11 | 1807.0 | GR | 70 | 110 | CNS | 71 | | |
| 31 | Zenith #22(31) | 15 | 1811.0 | GR | 72 | 120 | CNS | 73 | | |
| 32 | Zenith #20(29) | 15 | 1796.0 | GR | 74 | 110 | CNS | 75 | | |
| 33 | Maxie #3(22) | 11 | 1813.0 | GR | 76 | 110 | CNS | 78 | | |
| 34 | Zenith #2(10) | 11 | 1813.0 | GR | 79 | 100 | SNP | 80 | | |
| 35 | Zenith #2W(11) | 15 | 1816.0 | GR | 81 | 110 | JOHN | 82 | | |
| 36 | Maxie#5(49) | 11 | 1826.0 | GR | 83 | 130 | WEXN | 84 | | |
| 37 | Zenith #26(12) | 15 | 1822.0 | GR | 85 | 120 | CNS | 86 | | |
| 38 | Figger #1(5) | 15 | 1822.0 | GR | 89 | 130 | WEXN | 88 | | |

Figures 4.6 through 4.16 of KGS OFR 91-41 are mislabelled. The figure captions are in the correct order but the order of the maps themselves is exactly the opposite of the correct order.

| Actual Figure | Currently Labelled | Appears on Page |
|---|---|---|
| 4.6 (Viola 3) | 4.16 | 58 |
| 4.7 (Viola 2) | 4.15 | 57 |
| 4.8 (Hard Streak) | 4.14 | 56 |
| 4.9 (Viola 1) | 4.13 | 54 |
| 4.10 (Fervale) | 4.12 | 53 |
| 4.11 (Maquoketa) | 4.11 | 52 |
| 4.12 (Miseneer IV) | 4.10 | 51 |
| 4.13 (Misener III) | 4.9 | 50 |
| 4.14 (Misener II) | 4.8 | 49 |
| 4.15 (Misener I) | 4.7 | 48 |
| 4.16 (Chattanooga) | 4.6 | 47 |